

ISSN number 0971 - 9709



# The Journal of Indian Geophysical Union

VOLUME 21, ISSUE 1 | JANUARY 2017

AN OPEN ACCESS BIMONTHLY JOURNAL OF IGU



| <b>Journal of Indian Geophysical Union<br/>Editorial Board</b>  | <b>Indian Geophysical Union<br/>Executive Council</b>  |
|---|--|
| <b>Chief Editor</b><br>P.R. Reddy (Geosciences), Hyderabad  | <b>President</b><br>Prof. Shailesh Nayak, Distinguished Scientist, MoES, New Delhi   |
| <b>Associate Editors</b><br>B.V.S. Murthy (Exploration Geophysics), Hyderabad<br>D. Srinagesh (Seismology), Hyderabad<br>Nandini Nagarajan (Geomagnetism & MT), Hyderabad<br>M.R.K. Prabhakara Rao (Ground Water Geophysics), Hyderabad   | <b>Vice-Presidents</b><br>Dr. Satheesh C. Shenoi, Director, INCOIS, Hyderabad<br>Prof. Talat Ahmad, VC, JMI, New Delhi<br>Dr. V.M. Tiwari, Director, CSIR-NGRI, Hyderabad<br>Director, CSIR-NIO, Goa   |
| <b>Editorial Team</b><br><b>Solid Earth Geosciences:</b><br>Vineet Gahlaut (Seismology), New Delhi<br>B. Venkateswara Rao (Water resources Management), Hyderabad<br>N.V. Chalapathi Rao (Geology, Geochemistry & Geochronology), Varanasi<br>V.V. Sessa Sai (Geology & Geochemistry), Hyderabad<br><b>Marine Geosciences:</b><br>K.S.R. Murthy (Marine Geophysics), Visakhapatnam<br>M.V. Ramana (Marine Geophysics), Goa<br>Rajiv Nigam (Marine Geology), Goa<br><b>Atmospheric and Space Sciences:</b><br>Ajit Tyagi (Atmospheric Technology), New Delhi<br>Umesh Kulshrestha (Atmospheric Sciences), New Delhi<br>P. Sanjeeva Rao (Agrometeorology & Climatoplogy), New Delhi<br>U.S. De (Meteorology), Pune<br>Archana Bhattacharya (Space Sciences), Mumbai<br><b>Editorial Advisory Committee:</b><br>Walter D Mooney (Seismology & Natural Hazards), USA<br>Manik Talwani (Marine Geosciences), USA<br>T.M. Mahadevan (Deep Continental Studies & Mineral Exploration), Ernakulum<br>D.N. Avasthi (Petroleum Geophysics), New Delhi<br>Larry D Brown (Atmospheric Sciences & Seismology), USA<br>Alfred Kroener (Geochronology & Geology), Germany<br>Irina Artemieva (Lithospheric Structure), Denmark<br>R.N. Singh (Theoretical & Environmental Geophysics), Ahmedabad<br>Rufus D Catchings (Near Surface Geophysics), USA<br>Surjalal Sharma (Atmospheric Sciences), USA<br>H.J. Kumpel (Geosciences, App. Geophysics, Theory of Poroelasticity), Germany<br>Saulwood Lin (Oceanography), Taiwan<br>Jong-Hwa Chun (Petroleum Geosciences), South Korea<br>Xiujuan Wang (Marine Geology & Environment), China<br>Jiro Nagao (Marine Energy and Environment), Japan<br><b>Information &amp; Communication:</b><br>B.M. Khanna (Library Sciences), Hyderabad | <b>Hon. Secretary</b><br>Dr. Kalachand Sain, CSIR-NGRI, Hyderabad<br><b>Joint Secretary</b><br>Dr. O.P. Mishra, MoES, New Delhi<br><b>Org. Secretary</b><br>Dr. ASSRS Prasad, CSIR-NGRI, Hyderabad<br><b>Treasurer</b><br>Mr. Rafique Attar, CSIR-NGRI, Hyderabad<br><b>Members</b><br>Prof. Rima Chatterjee, ISM, Dhanbad<br>Prof. P. Rama Rao, Andhra Univ., Visakhapatnam<br>Prof. S.S. Teotia, Kurukshetra Univ., Kurukshetra<br>Mr. V. Rama Murty, GSI, Hyderabad<br>Prof. B. Madhusudan Rao, Osmania Univ., Hyderabad<br>Prof. R.K. Mall, BHU, Varanasi<br>Dr. A.K. Chaturvedi, AMD, Hyderabad<br>Mr. Sanjay Jha, Omni Info, NOIDA<br>Mr. P.H. Mane, ONGC, Mumbai<br>Dr. Rahul Dasgupta, OIL, NOIDA<br>Dr. M. Ravi Kumar, ISR, Gujarat<br>Prof. Surjalal Sharma, Univ. of Maryland, USA<br>Dr. P. Sanjeeva Rao, Advisor, SERB, DST, New Delhi<br>Dr. N. Satyavani, CSIR-NGRI, Hyderabad<br>Prof. Devesh Walia, North Eastern Hills Univ., Shillong |
| <b>EDITORIAL OFFICE</b><br>Indian Geophysical Union, NGRI Campus, Uppal Road, Hyderabad- 500 007<br>Telephone: +91 -40-27012799; 23434631; Telefax: +91-04-27171564<br>E. mail: jigu1963@gmail.com, website: www.j-igu.in   |  |
| The Open Access Journal with six issues in a year publishes articles covering<br>Solid Earth Geosciences; Marine Geosciences; and Atmospheric, Space and Planetary Sciences.  |  |
| <b>Annual Subscription</b><br>Individual Rs. 1000 per issue and Institutional Rs. 3500 for four issues (from 2017 onwards, six issues Rs.5000/-)<br>Payments should be sent by DD drawn in favour of "The Treasurer, Indian Geophysical Union", payable at Hyderabad,<br>Money Transfer/NEFT/RTGS (Inter-Bank Transfer), Treasurer, Indian Geophysical Union, State Bank of Hyderabad,<br>Habsiguda Branch, Habsiguda, Uppal Road, Hyderabad- 500 007<br>A/C: 52191021424, IFSC Code: SBHY0020087, MICR Code: 500004020, SWIFT Code: SBHYINBB028.<br>For correspondence, please contact, Hon. Secretary, Indian Geophysical Union, NGRI Campus, Uppal Road,<br>Hyderabad - 500 007, India; Email: igu123@gmail.com; Ph: 040 27012799  |  |

## CONTENTS

Editorial

3

| S.No. | Title   | Authors   | Pg.No. |
|-------|---|---|--------|
| 1     | Sparsity- based GPR blind deconvolution and wavelet estimation  | Alaeddin Ebrahimi, Ali Gholami and Majid Nabi-Bidhendi                            | 7      |
| 2     | Edge Detection of Gravity Anomalies with Directional Hyperbolic Tilt Angles: Application to Synthetic and Field Data                  | Ahmad Alvandi and Mojtaba Babaei  | 13     |
| 3     | Gravity Anomalies and Basement Structure below Deccan Traps in Gondwana Basins of Eastern Maharashtra, India                          | K.V. Swamy, Neetha Raj, S.K.G. Krishnamacharyulu and I.V. Radhakrishna Murthy     | 17     |
| 4     | Source Characteristics of the 2012 Earthquake Swarm Activity in the Andaman Spreading Ridge   | G. Srijayanthi, M. Ravi Kumar, S. Prasanna and N. Purnachandra Rao                | 25     |
| 5     | Groundwater quality in and around Tuticorin town, Southeast coast of India  | Somvir Singh, N.C. Mondal and V.S. Singh  | 34     |
| 6     | Evaluation of shallow aquifers contamination along Cauvery River Basin using Electrical resistivity and hydro chemical investigations | K.V. Satyanarayana, M. Pradeep Kumar, M.S. Kumar, B. Balakrishna and Dinesh Gupta | 44     |
| 7     | Co-Seismic Water Level Changes in Koyna – Warna Region- A Wavelet Analysis  | D.V. Ramana and Ch. V.V. Eswari   | 52     |
| 8     | Simulation Results for Southern Indian Ocean (SIO) Using Ocean Model  | A.P. Mishra and A.C. Pandey   | 58     |
|       | News at a Glance  |   | 67     |
| 9     | Can we have an organised Sustainable agriculture System that can ensure our food security?  | P.R.Reddy   | 72     |

## Editorial

---

I wish JIGU readers, authors, editorial board members, well wishers and IGU management "A Happy and Prosperous New Year". I have included two interesting topics as the core of this issue's editorial. The first one is purely scientific, where as the second covers an important societal problem. I welcome your constructive suggestions in better structuring of future editorials.

### **We Need a New Definition for "Magma"**

Any earth scientist carrying research on structure and dynamics of crust and sub crustal lithosphere, genesis of volcanic activity, formation of kimberlite pipes, plumes/hot spots and assembly- break up and reassembly of Super continents invariably talk about presence of shallow and deep Magma/ Magma chambers .In doing so many a time the definition of Magma is subconsciously misused. To focus on this aspect a good study has been carried out by a group of scientists. I detail below their apt handling of the topic through easily understandable presentation.

Magma is a fundamental constituent of the Earth. Issues as diverse as volcanic hazard assessment and planetary evolution studies rely on knowledge of magma's properties, origin, evolution, and significance. Thus, the definition of "magma" should be simple and universally agreed upon, but the term means fundamentally different things to different people. This inconsistency has led to miscommunication between petrologists, geophysicists, the press, and the public, making the "confused or disordered" definition of the word unintentionally appropriate. It is time to agree on a clearer geologic definition of "magma". Magma should mean material that is capable of moving within the Earth and onto its surface. To the public, magma is the stuff of lava—hot, glowing red liquid that flows out of volcanoes—and such lava is unquestionably magma that has reached the surface. The point of contention is whether partially molten rock that resides below the surface and is too crystalline to flow should also be called magma. Because this distinction is critical when geologists communicate about magma, especially to the press and public, Glazner et al (2016) contend that highly

crystalline immobile material should not be called "magma." Rather, magma should mean material that is capable of moving within the Earth and onto its surface. "Magma" is commonly used to mean any rock that is at least a little bit molten. Whether rock that contains a small percentage of partial melt should be called magma is debatable. Indeed, use of the word "magma" to refer both to material that can flow across the Earth's surface and to a largely solid volume that contains a small fraction of melt is akin to using the same word to refer to a river and to an aquifer. To do so ignores and obscures fundamental differences, and broad usage of "magma" is clearly causing such conceptual problems.

A critical control on mobility in a crystal-liquid mixture is the volume ratio of crystals to liquid; the apparent viscosity of a mixture (the ratio of how much shear stress is applied to the rate at which the material deforms) depends upon the proportion of particles suspended in it. For a low percentage of solid particles, less than 20% by volume, for example, the particles are sufficiently dispersed that they scarcely interact during flow. During cooling, crystals grow onto one another and interlock to produce a welded framework that is even stronger than one produced by nonreactive particles such as pebbles in water. Such a material can only flow by processes such as crystal plasticity and solution-reprecipitation, at rates dramatically slower than those at which even highly viscous silica-rich melts can flow. Collecting melt from such a material is a slow process.

This fundamental difference in deformation and flow (rheology) between partially molten rock that is melt rich (more than about 50% melt by volume) and its melt-poor counterpart (less than about 50%) is reason to give the two materials different names. Here we suggest that the term "magma" be reserved for melt-rich materials that can flow as fluids on timescales consonant with volcanic eruptions. We suggest that more crystal-rich and largely immobile partially molten rock be referred to by another name such as "crystal mush" or "rigid sponge". By this definition, highly viscous materials such as water-poor rhyolite lavas, with viscosities that can reach  $10^{10}$  pascal seconds or greater, are magma, whereas

highly crystal rich materials are not. The former can ascend to the Earth's surface sufficiently rapidly to be erupted, whereas the latter cannot. This is consistent with the general observation that volcanic rocks with more than about 50% crystals by volume are rare.

For the press, the public and even Earth scientists who do not specialize in magmatic systems, "magma" conjures up dramatic images of lava flowing down hillsides. Using the same term to describe large rock volumes that contain small melt fractions as well as large bodies of mobile magma can engender such mistaken perceptions as a sea of potentially eruptible magma underneath Yellowstone of USA.

To solve this, intellectual debate is necessary. In the November, 2016 issue of JIGU I suggested a proper debate amongst learned specialists in fixing up onset of Anthropocene as an Epoch. Similarly it is essential to start a conversation to have a more appropriate definition of "magma". To start with as a starting point the following definition as suggested by Glazner et al (2016) can be used as a more viable definition.

**Magma:** naturally occurring, fully or partially molten rock material generated within a planetary body, consisting of melt with or without crystals and gas bubbles and containing a high enough proportion of melt to be capable of intrusion and extrusion.

This proposed definition naturally reflects our particular scientific perspective and concerns. It is opined by Glazner et al that the proposed definition will stimulate a broad-based discussion that will yield a consensus definition.

**Citation:** Glazner, A. F., J. M. Bartley, and D. S. Coleman (2016), We need a new definition for magma, *Eos*, 97, doi:10.1029/2016EO059741.

### **Good health of Surface water bodies, a basic necessity for sustenance of life**

With increased irregularity and absence of a set pattern of precipitation during monsoon, it has become a necessity to store rain water as and when rains occur for sustenance of our very existence on this planet; the only planet as of now known to have life. Storage of water has been practiced since hundreds of years through surface water bodies;

lakes, tanks and ponds. Unfortunately, due to the unchecked growth of population human needs have terribly increased and man has over exploited our natural resources. He has also produced material that helped him to ease day to day activities (essential to lead a physically less stressed life). In this process he has created mounds of waste, which polluted significantly our life saving water, air and food. In addition to pollution, improper maintenance of our water storage facilities led to insufficient availability of quality water for drinking, irrigation and industrial purposes. A time has come for a radical change in our outlook. We cannot afford to postpone rehabilitation and revitalization of our surface water bodies. In the recent times both the central and state governments have taken up rehabilitation measures, through mega projects spending thousands of crores of rupees. Since these initiatives are time bound, some execution lapses creep in.

After viewing at the type of rehabilitation measures presently in vogue (in different parts of our country, including the newly formed Telangana State), experts have carried out area specific monitoring studies and arrived at the conclusion that "de-silting" of the surface water bodies is more dangerous and hazardous as it disturbs the original lake/ tank/ pond bed and increases losses through heavy seepage. While this could be true where significant number of fractures and fissures exist it may help better storage in areas that are devoid of fractures. As such it is essential to go through the satellite imageries of a lake or pond, to initiate appropriate rehabilitation measures. Sediments from agricultural areas often contain high levels of nutrients. These can be carried by streams and deposited in the still water areas of lakes. Nutrient-enriched sediments can be trapped before they reach the lakes. In the Indian Lakes, there are several channels which act as natural sediment deposition areas. Sediments accumulated there can be dredged out periodically and returned to the land as fill or fertilizer. To avoid random and disorganised removal of sediments it is essential to identify all the sites which contain nutrient-enriched sediments. These sites should have easy access for heavy equipment. Such a provision helps in not building additional structures.

Now a days, desilting is becoming a major component of any Lake Conservation Project. The basic reasons

given for necessity of desilting are - increasing the storage capacity and checking eutrophication conditions (the process of physical, chemical, and biological changes ("aging") associated with nutrient, organic matter, and silt enrichment of a lake). It is not practicable to reverse the slow process of silting in the bed of lakes through which only silt can be removed. What we are doing in the name of 'desilting' is practically 'digging' or 'excavation' of lake bed. By so called desilting, the original lake bed is disturbed, which has far reaching adverse effects on the performance of the lake. Most visible effect is the increase in percolation rate resulting in heavy seepage losses through the lake bed as observed after massive desilting at Pushkar lake in 2009. Increasing storage capacity by digging lake bed is the most costly proposal when compared to other alternatives and therefore needs study of alternatives as well as detailed hydrological investigations considering available yield, existing storage capacity, down-stream needs, etc. As overflowing of a lake is necessary to keep the river alive in the downstream and to flush out the static water of the lake, if a lake does not overflow at least once in four years on an average, there is no need to increase the storage capacity. Instead of desilting, the long term solution is to treat the catchment area so that silt load in the incoming flow is permanently reduced. This can be done by contour bunding, check dams, massive plantation, etc. (PS: Their location and quality in execution, however, is paramount to ensure the benefits) which will be less costly and will have far reaching positive effects of permanent nature. Desilting, if not done in a planned way, creates isolated pits of considerable size in the submergence area, which may have lower bottom levels than the main storage. Because of this isolation, water collected in these pits never reach to the main storage, it only seeps or evaporates. Thus, desilting said to be carried out for increasing storage capacity, practically reduces the actual utilizable storage in most of the cases. Removing surface soil to check eutrophication, is like giving treatment for

symptoms instead of the disease. Unless we check the inflow of untreated sewage in lakes, it is not possible to reduce the nitrate or phosphate contents. Therefore, it is better to invest funds on checking of sewage inflow than on removing surface soil for the purpose so as to have permanent solution of the problem.

**Sources:**

- 1) (<http://www.solitudelakemanagement.com/blog/improving-pond-water-quality-through-phosphorus-reduction#sthash.Iub78F9r.dpuf>).
- 2) P.Cullen; Hydrobiologia; December 1988, Volume 170, Issue 1, pp 321-336 (<http://link.springer.com/article/10.1007/BF00024912>).
- 3) (<http://www.indiawaterportal.org/articles/conservation-lakes-myths-and-realities-desilting>).

**In this issue:**

I am happy to mention that JIGU is catering to the needs of students and young researchers by encouraging them to contribute manuscripts covering their research pursuits. The support extended by young researchers and their guides is very encouraging. This positive development has made us to forget the hardships in maintaining the quality of the journal, as the basic aim of JIGU in providing a viable medium to young researchers is realised. I thank the young authors and experienced experts who carry out constructive review for this positive development.

In this issue we have 8 research articles, News at a Glance and a research note. I do hope our readers enjoy reading these well presented articles.

I earnestly solicit your co-operation, support and guidance in making JIGU a premier earth system science journal.

**P.R.Reddy**

# Sparsity- based GPR blind deconvolution and wavelet estimation

Alaeddin Ebrahimi\*, Ali Gholami and Majid Nabi-Bidhendi

Institute of Geophysics, university of Tehran, Tehran, Iran

\*Corresponding author: ala\_ebrahimi@ut.ac.ir

---

## ABSTRACT

Improving the vertical resolution of Ground Penetrating Radar (GPR) data by blind deconvolution technique is an approach we target here. Sometimes geologic situations such as presence of clay or humidity lead to blurred sections. Advanced processing steps, that are so common in seismic reflection, such as deconvolution are needed. In this approach the sparse deconvolution algorithm on GPR data has been used in a novel way. It is often assumed that reflectivity series are sparse and noise is random. Generalized Cross Validation (GCV) method has been used to estimate the desired wavelet and to find the optimum iteration in the deconvolution algorithm. To examine the efficacy of the method, it is applied to synthetic data. The GCV and MSE curves versus iteration are then plotted in order to determine the optimal point. The final deconvolved section shows a satisfying result for GPR field data and the speed and accuracy of this robust algorithm to reconstruct reflectivity series is considerable.

**Key words:** Ground Penetrating Radar (GPR), Blind deconvolution, Sparsity, Generalized Cross Validation(GCV) and Reflectivity series.

---

## INTRODUCTION

Ground penetrating radar (GPR), amongst all near-surface geophysical techniques, is one of the most commonly applied non-invasive subsurface characterization tools for engineers (Benedetto, 2002; Hugenschmidt, 2002), archeologists (Goodman, 1994; Sternberg and McGill, 1995), geologists (Bano et al., 2000; Bednarczyk and Szykiewicz, 2015) and other related tasks. A GPR tool has different parts, each of which is responsible for some function. The transmitter and the receiver are the main ones. A transmitter sends electromagnetic waves into the earth in the frequency range of 10 MHz to 2 GHz and a receiver detects them after travelling back from the earth (Jol, 2008).

The basic processing steps are the same as seismic processing and significant insights into GPR processing can be gained from developments of the period (Jol and Bristow, 2003). However, there are some key differences between them, which are important for validity of more advanced processing methods (Baker et al., 2001). Attenuation and dispersion effects are more extreme with GPR, and therefore, the frequency component (and phase equations) of signals can change markedly with recorded time and depth (Jol, 2008). Unfortunately, many of the advanced signal processing and analysis methods used in GPR data interpretation are poorly suited for use in near-surface environments, primarily because of the limiting assumptions inherent in their mathematical descriptions (e.g. high frequency, uniform half-space sub-surfaces, etc.) (Daniels, 2004).

Deconvolution is a temporal inverse filtering technique that improves resolution of data (Yilmaz, 2001) by

compressing the measured GPR wavelet into a distinct form. On the other hand, it is applicable to remove effect of source wavelet from acquired data (Neves et al., 1995) and just leaves an impulse response of underground layers. While deconvolution is considered to be a key step in seismic processing (e.g. Yilmaz, 2001), in GPR data, these are very restricting conditions as the subsurface is more complex and propagating GPR wavelet is totally vectored with non-planar, spatially complex fields (Conyers and Goodman, 1997). This has led to a debate on the usefulness of casual deconvolution techniques.

The features and considerations of GPR reflection data closely depend on optimized temporal resolution of sections. However, unprocessed GPR data appears blurred and incorrectly images true reflectivity series due to real characteristic of the GPR wavelet (Van Dam and Schlager, 2000).

Deterministic deconvolution has been applied to GPR data by Xia et al., (2003, 2004) and approximately 50 % improvement in the temporal resolution of the section has been presented (Xia et al., 2003). The wavelet in deterministic deconvolution has been earned by measuring the signal traveling through the air while keeping the source and receiver antennas in front of each other (Economou and Vafidis, 2011). There are some techniques to estimate source wavelet, published in literatures (Amundsen, 2001). Air wave that has occurred because of antenna separation and especially first waveform status could be used as a GPR wavelet (Gottsche et al., 1994). In another way, a plate sends electromagnetic pulse and another plate that has faced it, records a wavelet (Xia et al., 2004) while measured wavelet is not available every time as it is time consuming and difficult technically.

A type of blind deconvolution method has been applied to GPR data by Schmelzbach et al., (2011) where parameterization of wavelet has been designed as convolution of a wavelet with a dispersive all pass filter, including prior information about wavelet to be estimated in a Bayesian framework and linked with the assumption of a sparse reflectivity. This method has earned increased temporal resolution compared to the results of standard processing (Schmelzbach et al., 2011). Chahine et al., (2009) cast the convolution model as multidimensional data which accomplishes blind deconvolution through independent component analysis. They carried out the GPR for pavement evaluation. According to Chahine et al., (2009), the blind deconvolution technique could be used as a method to retrieve the latter reflectivity series and recover time resolution without reliance on prior information. Clearly, a nonlinear contrast function has been selected which fits to the sparse quiddity (the inherent nature) of the reflectivity series. Moreover, Li (2014) extends the classical minimum entropy deconvolution strategy and forms a general-purpose framework of blind deconvolution of GPR data, according to which the formulation of sparsity-promoted optimization problem in a scale-invariant regularizer has been suggested. The substituted iterative method is defined to solve the by-product, non-convex optimization issue. Rudimentary consequences show that by applying this method to GPR data, vertical resolution will be improved. Recently, Schmelzbach, and Huber (2015) presented a method of GPR deconvolution wherein, first a signal-by-signal minimum-phase deconvolution was applied and then, a global phase rotation was applied to maximize the sparseness of the minimum-phase deconvolved data where as some series have needed for a better sparseness estimation and steady phase rotation.

In this paper, the blind deconvolution scheme is used to estimate the wavelet and reflectivity series in an alternating fashion using sparse analysis tools. The solution procedure is fully automated so that the regularization parameter is determined by the generalized cross validation (GCV) score. In what follows, we first present the theory of our blind deconvolution and then the synthetic data examples are tested and the method is applied to GPR field data.

### Theory of blind deconvolution

GPR trace can be represented as a convolution of source wavelet with the earth reflectivity series and additive noise (Daniels, 2004; Giannopoulos, 2005; Irvin and knight, 2006)

$$w * r + e = y \quad (1)$$

where  $r$  is the reflectivity series, a column vector of length  $N$ ,  $w$  is the source wavelet of length  $M$ ,  $*$  denotes convolution operator,  $y$  is the GPR trace which is

contaminated by additive random noise  $e$ . Equation (1) can be rewritten in matrix form as

$$y = Wr + e = Rw + e \quad (2)$$

Where  $R, W \in \mathbb{R}^{m \times n}$  are square Toeplitz matrices with kernels  $r$  and  $w$  respectively.

Since both  $W$  and  $R$  are unknown, we solve Equation (2) in a sequential form by first estimating  $w$  and then using the estimated wavelet to solve the problem for  $r$ . In the following sections each step is described in details.

### Wavelet and reflectivity series estimation

A wavelet can be recovered from equations (3) and (4).

$$\hat{w} = \operatorname{argmin} \|Fy - w\|_2^2 + \lambda \|D^{(2)}w\|_2^2 \quad (3)$$

Where  $D^{(2)}$  is the second order differential operator,  $F$  is the Fourier transform matrix,  $\hat{s} = Fs$  for a given vector  $s$ ,  $\|s\|_p = \sum |s_i|^p$  and  $\lambda > 0$  is a regularization parameter. Solving

$$\hat{w} = F^T (I + \lambda D^{(2)T} + D^{(2)})^{-1} Fy \quad (4)$$

Where  $I$  is the identity matrix.

Using the initial wavelet  $w^{(l)}$  estimated by equation (4), averaged over all traces, and setting  $l = 1$ , a sparse reflectivity section can be obtained by nonlinear optimization (5) which is applied for each trace separately

$$r^{(t)} := \operatorname{argmin}_r \|r\|_1 \text{ subject to } \|y - w^{(t-1)} * r\|_2^2 \leq \gamma \quad (5)$$

Then the estimated section is used to update the source wavelet in a least square form while fixing the support of the wavelet. The process is repeated until convergence. Equation (5) is solved via the Bregman iteration summarized below (see Gholami and Sacchi (2012) for more details about the algorithm).

$$\text{Set: } D = \operatorname{diag} \left( \frac{1}{|a|\hat{w}|^2 + \beta} \right)$$

$$\text{Initialize: } k = 0, d^0 = b^0 = 0$$

$$\text{while } \|W\hat{x}^k - \hat{y}\|_2^2 > \gamma$$

$$\hat{x}^{k+1} = D(\alpha W * \hat{y}^k + \beta F[d^k - b^k])$$

$$d^{k+1} = \operatorname{prox}_{1/\beta}^1 (F^{-1}\hat{x}^{k+1} + b^k)$$

$$b^{k+1} = b^k - [d^{k+1} - F^{-1}\hat{x}^{k+1}]$$

$$\hat{y}^{k+1} = \hat{y}^k + \hat{y} - w\hat{x}^{k+1}$$

$$k = k + 1$$

End while

$$r = d^k$$

In the algorithm, we have tested numerous values of  $\alpha$  and  $\beta$  and finally  $\alpha=0.5$ ,  $\beta=1$  derived successfully which meet suggested values by Gholami and Sacchi (2012). Defined Prox function is

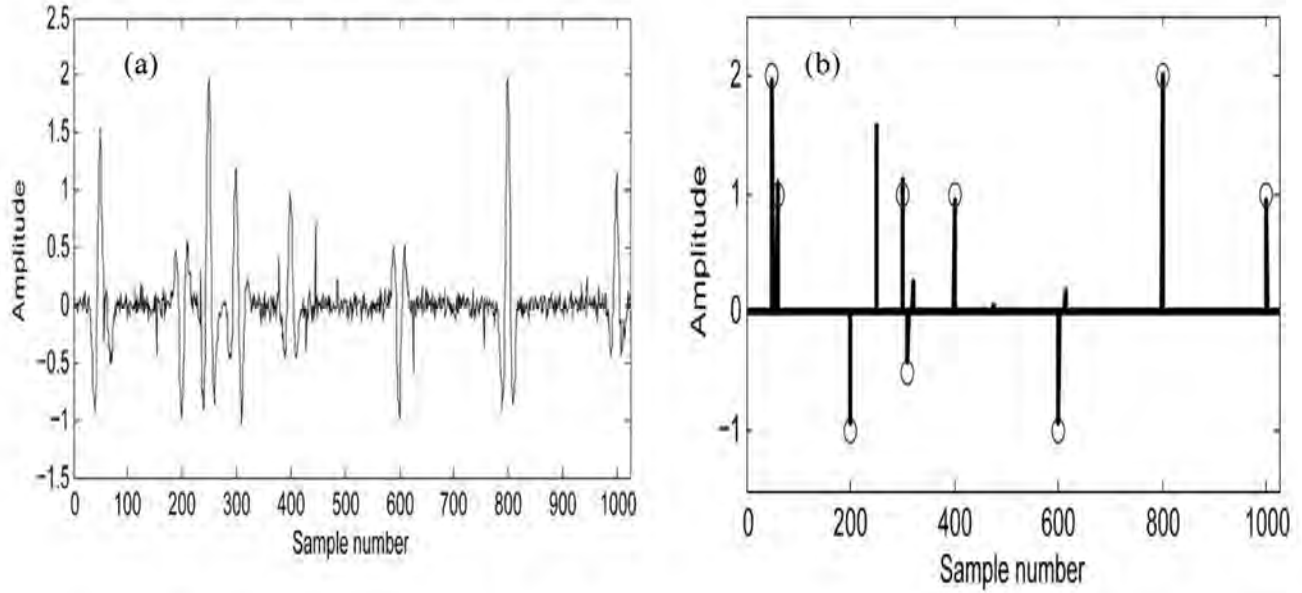


**Figure 1.** (a)Synthetic trace , (b)estimated and original reflectivity series showed with circles.

$$\text{prox}_\tau^1 = \text{sign}(y) \max(|y| - \tau, 0) \quad (6)$$

Generalized Cross Validation (GCV) score is used (Golub et al., 1979) to find the optimum number of iterations (Gholami and Sacchi, 2012)

$$\text{GCV}(k) = \frac{\|y - wd^k\|_2^2}{[N - c \cdot \text{nnz}(d^k)]^2} \quad (7)$$

Where N is number of data in each trace, c is stabilizing parameter and nnz is non-zero elements of a vector.

### Numerical Examples

Accepted waveform for GPR signals was mainly supposed to be a Ricker wavelet (Daniels, 2004; Giannopoulos, 2005; Irvin and knight, 2006). The Ricker wavelet (Ricker, 1953) has been defined as the second differential of a Gaussian function and is the general form of a waveform that results from the application of a Gaussian impulse to an impulse radiating antenna or transducer system (Daniels, 2004).

### Synthetic Data

In this part, GPR wavelet is assumed to be a Ricker wavelet with 1024 samples and center frequency of 200 MHz. The synthetic trace shown in Figure 1(a) is obtained by convolution of reflectivity model that consists of 10 spikes with the Ricker wavelet. The noise vector includes a signal with Gaussian random distribution signal-to-noise-ratio (SNR) of 15 db and some outliers have also been included. First spike in the model represents ground reflection by strength amplitude and other spikes are indicative of different layers.

To test the functionality of GCV score, the generated trace has been deconvolved by assuming the original wavelet to be known. The GCV curve and the Mean Square Error (MSE) as functions of iteration have been calculated and shown in Figure 2. The estimated reflectivity series (minimizer of the GCV score) are shown in Figure 1(b).

### Field data and Computations

The GPR data was acquired near Talesh city and Caspian Sea coast (Iran) with antenna frequency of 250 MHz in one traverse with length of 50 m. Local information indicated that some excavation has occurred at the end of the profile (Figure 3).

The final estimated wavelet has been illustrated in figure 4. Now, with estimated wavelet the desired deconvolved is achievable.

The resulting GCV curves as a function of iteration for all GPR traces together are shown in figure 5. It is now to be seen if this selection could result in achieving a suitable deconvolved section or not.

It shows that average optimum iteration number for this data set is 46. By choosing outputs in proportion with iteration 46, deconvolved trace for input traces would be provided and then, the final section would be illustrated by considering all traces together. In acquisition fields, overburdened and underneath layer shows high damping because of clayey material and humidity. In 20 ns, ground reflection is clearly visible and the event above it, which has been removed, indicates the presence of direct wave, a linear phenomenon, the effects of which are deleted by algorithms. From 40 ns up to 80 ns, the presence of another

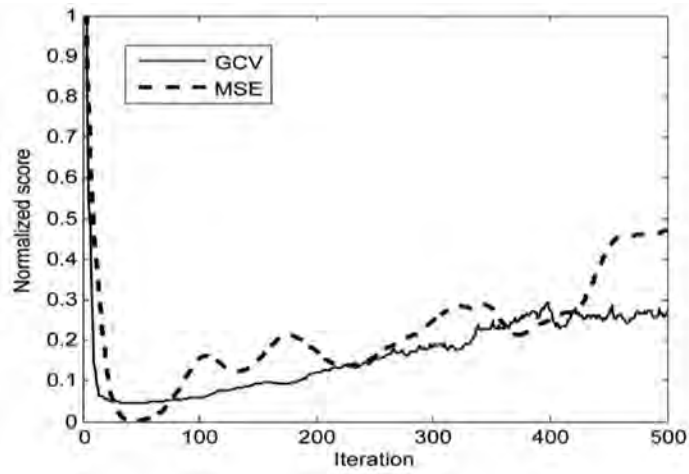


Figure 2. Calculated GCV and MSE diagrams for synthetic trace.

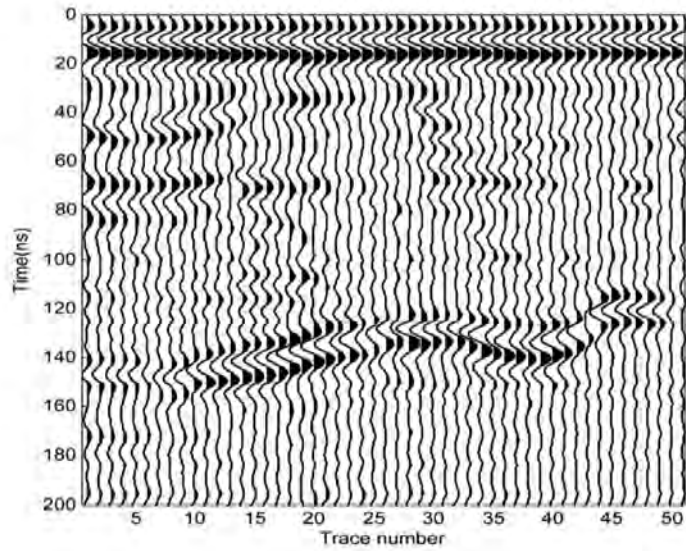


Figure 3. GPR section.

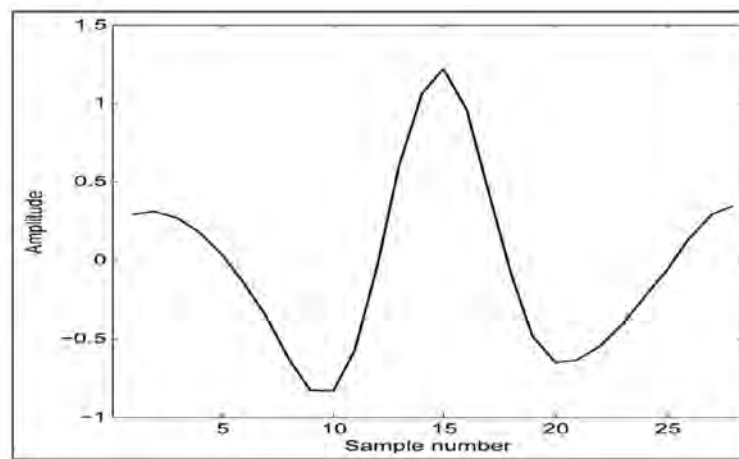
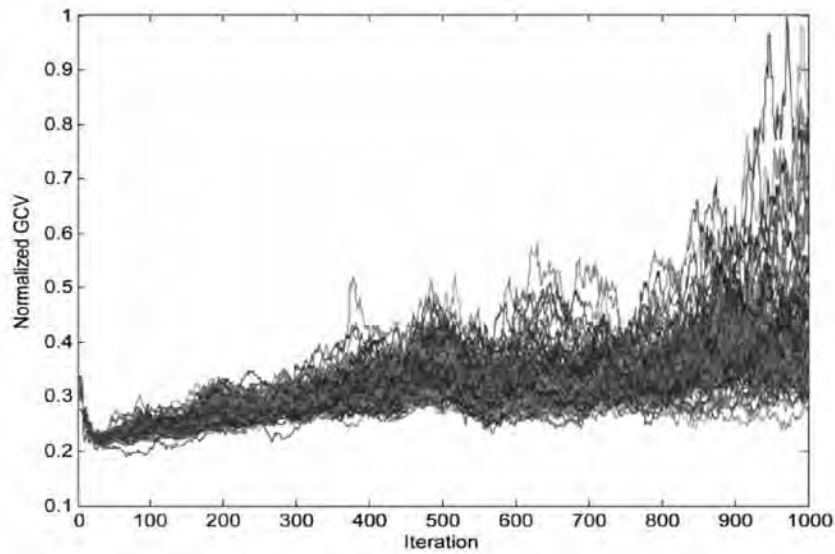
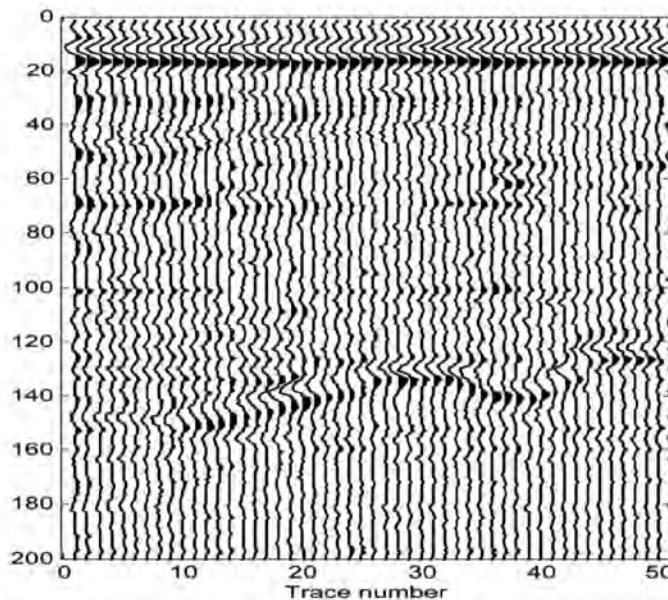


Figure 4. The final estimated wavelet.



**Figure 5.** The resulting GCV curves with iteration corresponding to deconvolution of the GPR section shown in Figure 3.



**Figure 6.** Deconvolved data section.

layer which seems to be narrower (tighter) deconvolved section is observed (Figure 6) compared to the raw section (Figure 3). Moreover, in 120 ns up to 160 ns of the section, a reflection has occurred which is due to the excavation of multiple effects on top of it. The results show that the multiple effects have been suppressed. So, it appears that part of diffraction is reduced as shown in the last section in Figure 6 and the processed, compressed, signals compared to raw data (Figure 3).

## CONCLUSIONS

Numerical experiments with synthetic and field GPR data confirmed that the proposed automatic deconvolution generates high-resolution estimators of the reflectivity in only a few iterations. It is thus recommended to be applied on similar GPR data. Moreover, the speed and quickness of achieving optimal results through the application of this algorithm makes it an efficient and accurate method for

delineation of very thin layers in GPR volumes. Attention must be paid to the fact that the algorithm is on the whole automatic without any requirement for selecting parameters.

## ACKNOWLEDGEMENTS

The authors highly appreciate the reviewers for their helpful comments. They extend their thanks to the funding agencies for carrying out this study. We extend our thanks to the Jarfkav Company for all their supports. We also thank Dr. Nandini Nagarajan and Chief Editor for editing the manuscript.

## Compliance with Ethical Standards

The authors declare that they have no conflict of interest and adhere to copyright norms.

## REFERENCES

- Amundsen, L., 2001. Elimination of free-surface related multiples without need of the source wavelet, *Geophys.*, v.66, no.1, pp: 327-341.
- Baker, G. S., Steeples, D. W., Schmeissner, C., Pavlovic, M., and Plumb, R., 2001. Near surface imaging using coincident seismic and GPR data, *Geophys. R. L.*, v.28, no.4, pp: 627-630.
- Bano, M., Marquis, G., Niviere, B., Maurin, J., and Cushing, M., 2000. Investigating alluvial and tectonic features with ground-penetrating radar and analyzing diffractions patterns, *Jour. of A.G.*, v.43, no.1, pp: 33-41.
- Bednarczyk, Z., and Szykiewicz, A., 2015. Applied Engineering Geology Methods for Exemplar Infrastructure Projects in Malopolskie and Podkarpackie Provinces. Springer International Publishing In Engineering Geology for Society and Territory, v.6, pp: 203-210.
- Benedetto, A., Manacorda, G., Simi, A., and Tosti, F., 2002. Novel perspectives in bridges inspection using GPR, *Nondestructive Testing and Evaluation*, v.27, no.3, pp: 239-251.
- Chahine, K., Baltazart, V., Dérobert, X., and Wang, Y., 2009. Blind deconvolution via independent component analysis for thin-pavement thickness estimation using GPR, Paper presented at the Radar Conference-Surveillance for a Safer World, 2009. RAD. Int.
- Conyers, L.B., and Goodman, D., 1997. Ground-penetrating radar . An Introduction for Archaeologist. *Alta. P.*, pp: 149-194.
- Daniels, D.J., 2004. Ground penetrating radar, *Iet.*, v.1.
- Economou, N., and Vafidis, A., 2011. Deterministic deconvolution for GPR data in the tf domain, *Near. S. G.*, v.9, no.5, pp: 427-433.
- Gholami, A., and Sacchi, M. D., 2012. A fast and automatic sparse deconvolution in the presence of outliers, *Geoscience and Remote Sensing, IEEE. T.O.*, v.50, no.10, pp: 4105-4116.
- Giannopoulos, A., 2005. Modelling ground penetrating radar by GprMax, *Construc. and B.M.*, v.19, no.10, pp: 755-762.
- Golub, G. H., Heath, M., and Wahba, G., 1979. Generalized cross-validation as a method for choosing a good ridge parameter, *Techno.*, v.21, no.2, pp: 215-223.
- Goodman, D., 1994. Ground-penetrating radar simulation in engineering and archaeology, *Geophys.*, v.59, no.2, pp: 224-232.
- Gottsche, F.-M., Stolte, C., and Nick, K.-P., 1994. Two-sided deconvolution-A Method to improve the temporal resolution in radar data, Paper presented at the 56th EAEG Meeting.
- Hugenschmidt, J., 2002. Concrete bridge inspection with a mobile GPR system, *Const. and B. M.*, v.16, no.3, pp: 147-154.
- Irving, J., and Knight, R., 2006. Numerical modeling of ground-penetrating radar in 2-D using MATLAB. *Comp. and Geosciences*, v.32, no.9, pp: 1247-1258.
- Jol, H.M. ed., 2008. Ground penetrating radar theory and applications. elsevier.
- Jol, H. M., and Bristow, C. S., 2003. GPR in sediments: advice on data collection, basic processing and interpretation, a good practice guide, *Geolog. S., London, Special Publications.*, v.211, no.1, pp: 9-27.
- Li, L., 2014. Sparsity-promoted blind deconvolution of ground-penetrating radar (GPR) data, *Geoscience and Remote Sensing Letters, IEEE.*, v.11, no.8, pp: 1330-1334.
- Neves, F., Roulston, M., and Miller, J., 1995. Source signature deconvolution of ground penetrating radar data, *Revis. B. G.*, v.13, no.2, pp: 143-153.
- Ricker, N., 1953. The form and laws of propagation of seismic wavelets, *Geophys.*, v.18, no.1, pp: 10-40.
- Schmelzbach, C., Scherbaum, F., Tronicke, J., and Dietrich, P., 2011. Bayesian frequency-domain blind deconvolution of ground-penetrating radar data, *Jour. of A.G.*, v.75, no.4, pp: 615-630.
- Schmelzbach, C., and Huber, E., 2015. Efficient Deconvolution of Ground-Penetrating Radar Data, *Geosc. and R. S., IEEE. T. O.*, v.53, no.9, pp: 5209-5217.
- Sternberg, B. K., and McGill, J. W., 1995. Archaeology studies in southern Arizona using ground penetrating radar, *Jour. of A. G.*, v.33, no.1, pp: 209-225.
- Van Dam, R. L., and Schlager, W., 2000. Identifying causes of ground-penetrating radar reflections using time-domain reflectometry and sedimentological analyses, *Sedimen.*, v.47, no.2, pp: 435-449.
- Xia, J., Franseen, E. K., Miller, R. D., and Weis, T. V., 2004. Application of deterministic deconvolution of ground-penetrating radar data in a study of carbonate strata, *Jour. of A.G.*, v.56, no.3, pp: 213-229.
- Xia, J., Franseen, E. K., Miller, R. D., Weis, T. V., and Byrnes, A. P., 2003. Improving ground-penetrating radar data in sedimentary rocks using deterministic deconvolution, *Jour. of A.G.*, v.54, no.1, pp: 15-33.
- Yilmaz, Ö., 2001. Seismic data analysis . Tulsa, Soc. of Exploration Geophysicists, v.1, pp: 74170-2740.

# Edge Detection of Gravity Anomalies with Directional Hyperbolic Tilt Angles: Application to Synthetic and Field Data

Ahmad Alvandi\*<sup>1</sup> and Mojtaba Babaei<sup>2</sup>

<sup>1</sup>University of Applied Science and Technology, Hamedan Province Branch, Iran

<sup>2</sup>Department of Physics, Tuyserkan Branch, Islamic Azad University, Tuyserkan, Iran

\*Corresponding Author: sim.alvandi@gmail.com

## ABSTRACT

Edge detection is an image processing method for finding the boundaries of anomalies. Local phase filters have been widely used to detect the edges of the anomalies. There are various filters that are employed to attain edge detection, for example, Analytic signal, tilt angle, directional tilt angle and hyperbolic tilt angle. The tilt angle is a widely used edge detection filter. We make some improvement to tilt angle filter, so that it can process the gravity data. We describe a new filter based on the first order directional hyperbolic tilt angle. Directional hyperbolic tilt angle is used for edge detection of the gravity anomalies by a calculation program based on MATLAB. This filter is applied to synthetic data with and without random noise. Finally, the validity of the filter is tested on a real case from Iran.

**Key words:** Edge Detection, Gravity Anomalies, Hyperbolic Tilt Angle, Salt Dome and Iran.

## INTRODUCTION

Potential field data, especially gravity and magnetic anomalies are generally used to map geological boundaries such as faults and contacts between intrusions and their host rocks. Edge detection is a requested task in the interpretation of potential-field data, which has been widely used as a tool in exploration technologies for mineral resources and engineering targets (Blakely and Simpson, 1986; Ardestani, 2005; Ardestani and Motavalli, 2007; Yuan et al., 2014). The measurement of the local phase of potential fields can be useful for their magnetic and gravity interpretation (Cooper and Cowan, 2006 and 2011). There are various local phase filters that have been employed to achieve edge detection, for example, Analytic signal, tilt angle, directional tilt angle, and hyperbolic tilt angle (Pilkington and Keating, 2004; Hoseini et al., 2013; Alvandi and HoseiniAsil, 2014). The tilt angle is a useful form of local phase filter for enhancing subtle detail in gravity data (Cooper and Cowan, 2006). The hyperbolic tilt angle is also less sensitive to noise than the tilt angle but their result is better and clearer than the tilt angle filter (Cooper and Cowan, 2006). In this paper, we define the first order direction hyperbolic tilt angle, and propose a new filter based on it. The method is tested by using synthetic data created for prism models at different depths. In addition, practical utility of the method is demonstrated for a salt dome in Iran.

## METHODOLOGY

Cooper and Cowan (2006) defined the directional tilt angle to delineate the edge. In order to increase the resolution of the edges, we propose another method using the first order derivatives to form the hyperbolic tilt angle, called

first order directional hyperbolic tilt angle (DHT). The first order directional hyperbolic tilt angle can be rewritten as

$$HT_x = \tanh^{-1} \left( \frac{\partial f / \partial x}{\sqrt{((\partial f / \partial z)^2 + (\partial f / \partial y)^2)}} \right) \quad (1)$$

and

$$HT_y = \tanh^{-1} \left( \frac{\partial f / \partial y}{\sqrt{((\partial f / \partial z)^2 + (\partial f / \partial x)^2)}} \right) \quad (2)$$

Here the subscripts x and y denote the directions. We combine  $HT_x$  and  $HT_y$  to define an edge detector as follow:

$$HT_{tot} = \sqrt{(HT_x)^2 + (HT_y)^2}$$

Using equations (1) and (2), a normalized version of this filter is established as follow:

$$DHT = \tanh^{-1} \left( \frac{\sqrt{((\partial f / \partial x)^2 + (\partial f / \partial y)^2)}}{|\partial f / \partial z|} \right) \quad (3)$$

## SYNTHETIC MODEL

Firstly, we constructed three prism shaped gravity sources with top depths of 3m, 5m and 8m. Figure 1(a) shows the gravity anomalies. Figure 1(b) shows the hyperbolic tilt angle of the data in figure 1(a). Figure 1(c) shows

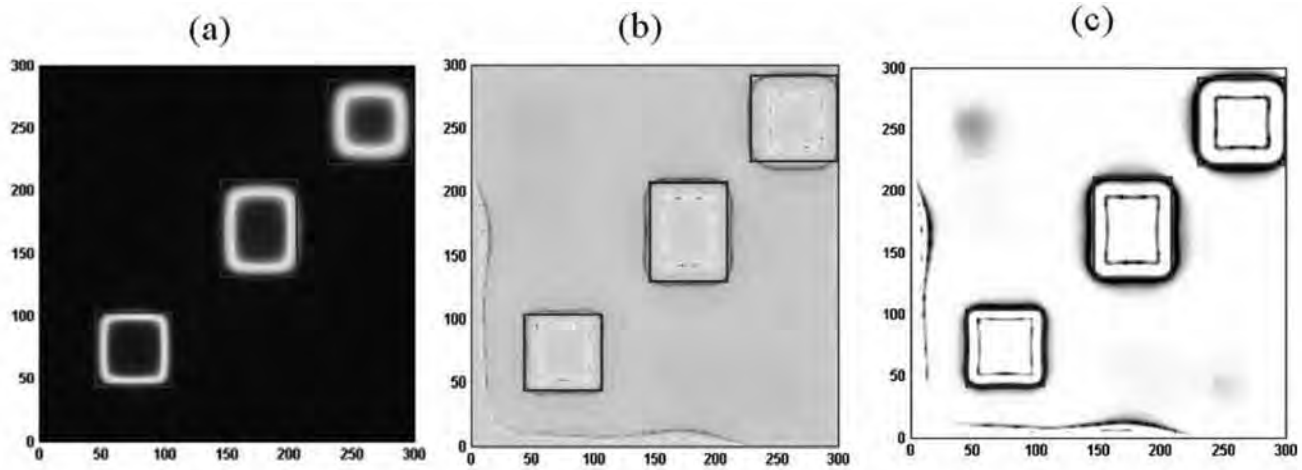


**Figure 1.** (a) Gravity anomaly (mGal), (b) Hyperbolic tilt angle of the data in 1a, (c) Directional hyperbolic tilt angle of the data in 1a.

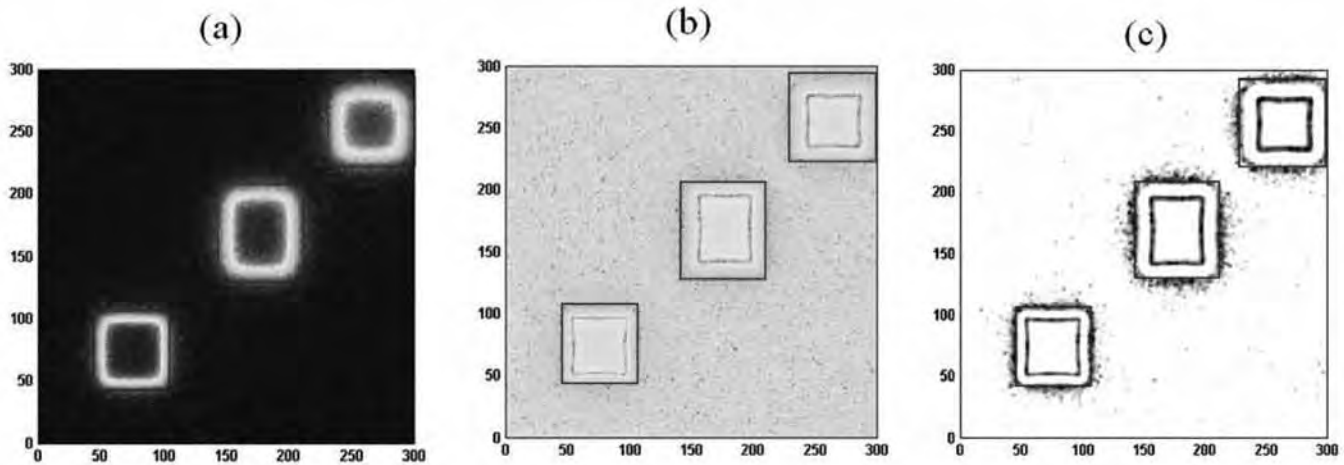


**Figure 2.** (a) Noisy anomaly map (mGal), (b) Hyperbolic tilt angle of the data in 2a, (c) Directional hyperbolic tilt angle of the data in 2a.

the directional hyperbolic tilt angle of the data in figure 1(a). By comparison among the results in figure 1, the edges detected by DHT are clearer than that obtained by hyperbolic tilt angle filter.

To demonstrate how this method works, the data should be contaminated by random noise. With amplitude equal to 5% of the maximum data amplitude random noise was added to the gravity data set shown in figure 2(a). Figures 2(b) and 2(c) show, respectively, hyperbolic tilt angle map and the outputs of the proposed method. In the case of noisy data, it is seen that the DHT technique produces better result than that from the hyperbolic tilt angle method.

### Field Model

In this section, the real data edge detection is studied. The case study taken up for applying the presently proposed method is the gravity data over a salt dome in Qom province (Aghashahi and Zomorrodian, 1981; Motasharrei et al., 2010). The map of geographic location of Qom area is shown in figure 3a and geological scheme of the study area is shown in figure 3b. Residual gravity anomalies measured over salt dome of Qom is shown in figure 4a. Figure 4b shows the hyperbolic tilt angle of the data in figure 4a. Figure 4c shows the directional hyperbolic tilt angle of the data in figure 4a.

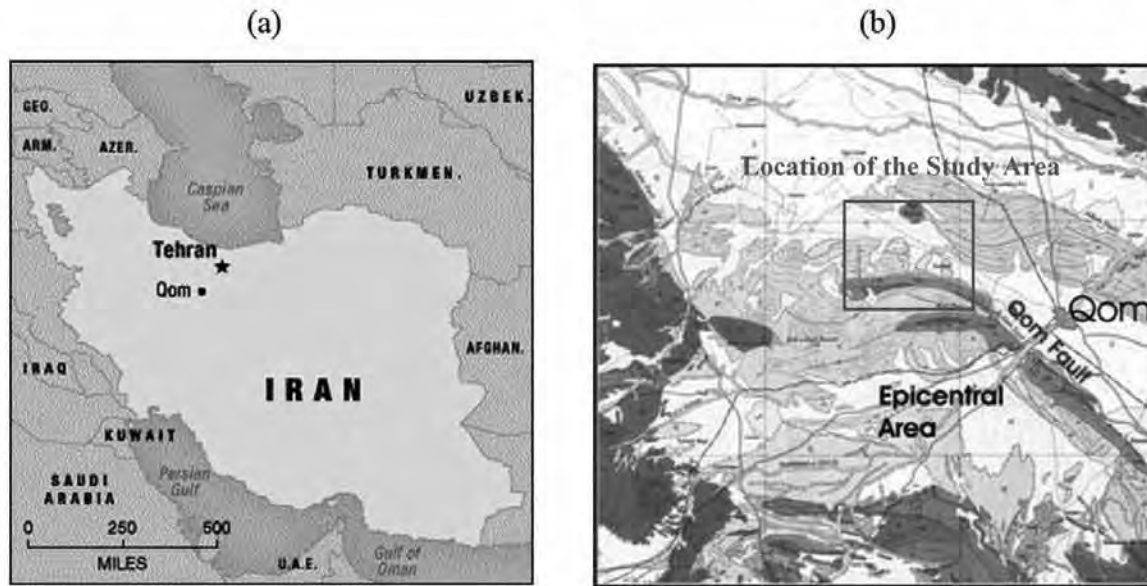


Figure 3. (a) Geographic location of Qom area in the map of Iran, (b) geological scheme of the study area.

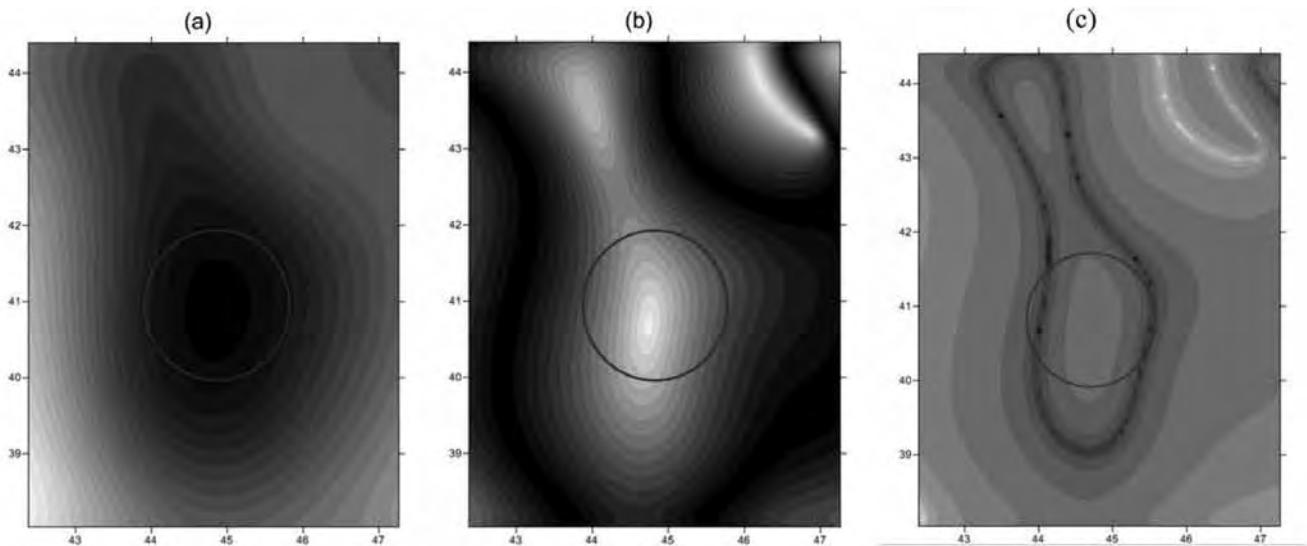


Figure 4. (a) gravity anomaly (mGal), (b) Hyperbolic tilt angle of the data in 4a, (c) Directional hyperbolic tilt angle of the data in 4a.

## CONCLUSIONS

This paper defines the first order directional tilt angle. We use the first order directional tilt angle to define a new edge detector to process the gravity data. This method has been tested by using synthetic data created for prism models at different depths and also real data from a salt dome. The Directional hyperbolic tilt angle proposed and demonstrated in the present paper can reveal the edges more clearly than the hyperbolic tilt angle.

## ACKNOWLEDGEMENTS

Authors thank Prof.D.Bhaskar Rao for constructive suggestions and evaluation of the manuscript. They also thank Prof.B.V.S.Murthy and Chief Editor for apt editing and useful suggestions to enhance the quality of the manuscript.

## Compliance with Ethical Standards

The authors declare that they have no conflict of interest and adhere to copyright norms.

## REFERENCES

- Aghashahi, E., and Zomorrodian, H., 1981. Gravity study of Qom salt dome in Iran, *Journal of Earth and Space Physics*, v.10, pp: 21-24.
- Alvandi, Ahmad and HoseiniAsil, Rasoul, 2014. Edge detection process of Qom salt dome gravity anomalies using hyperbolic tilt angle, *International Journal of Geomatics and Geosciences*, v.5, no.2, pp: 209-224.
- Ardestani, V. E., 2005. Gravity interpretation via gravity gradients and analytic signal, *Journal of Earth sciences*, v.12, no.54.
- Ardestani, V. E., and Motavalli, S. H., 2007. Constraints of Analytic Signal to determine the depth of gravity anomalies: *J. Earth Space Phys.*, v.33, no.2.
- Blakely, R. J., and Simpson, R. W., 1986. Approximating edges of source bodies from magnetic or gravity anomalies. *Geophysics*, v.51, pp: 1494-1498.
- Cooper, G.R.J., and Cowan, D.R., 2006. Enhancing potential field data using filters based on the local phase, *Computers & Geosciences*, v.32, pp: 1585-1591.
- Cooper, G.R.J., and Cowan, D.R., 2011. A generalized derivative operator for potential field data, *Computers & Geosciences, Geophysical Prospecting*, v.59, pp: 188-194.
- Hoseini, Ali Akbar., DoulatiArdejani, Faramarz., Tabatabaie, SeyedHashem., and Hezarkhani,Ardeshir., 2013. Edge detection in gravity field of the Gheshm sedimentary basin, *International journal of Min & Geo-Eng (IJMGE)*, v.47, no.1, pp: 41-50.
- Motasharrie, A., Zomorodian, H., SiahKoochi, H. R., and Mirzaei, M., 2010. Inversion of gravity data in wavelet domain using normalized forward models, *Journal of Earth &space physics*, v.36, no.1, pp: 29-38.
- Pilkington, M., and Keating, P., 2004. Contact mapping from gridded magnetic data—a comparison.Extended abstracts, ASEG 17th Geophysical Conference and Exhibition, Sydney.
- Yuan, Y., Yu, Q.L., and Geng, M., 2014. Edge Detection of Potential Field Gradient Tensor Data with Horizontal Second Order Directional Analytic Signal, 76th EAGE Conference & Exhibition, Amsterdam RAI, the Netherlands.

# Gravity Anomalies and Basement Structure below Deccan Traps in Gondwana Basins of Eastern Maharashtra, India

K.V. Swamy<sup>1</sup>, Neetha Raj<sup>1</sup>, S. K. G. Krishnamacharyulu\*<sup>2</sup> and I. V. Radhakrishna Murthy<sup>3</sup>

<sup>1</sup>Department of Geology, Adikavi Nannaya University, NH-16, Rajamahendravaram, Andhra Pradesh

<sup>2</sup>School of Earth Sciences, SRTM University, Nanded, Maharashtra

<sup>3</sup>Professor (Retd) of Geophysics, Andhra University, Vishakhapatnam, Andhra Pradesh

\*Corresponding Author: skgkchary@gmail.com

---

## ABSTRACT

The Gondwana basins with their complex tectonics and high hydrocarbon potential have become targets of serious geophysical investigations in the last decade. It is increasingly concluded that the Deccan Syncline (DS) in the west and central regions of India is underlain by highly prospective hydrocarbon bearing Gondwana basins. However, the nature and thickness of sedimentary basins and the associated basement structure are yet to be geophysically ascertained. In this paper, the Bouguer gravity anomalies of Gondwana basins of Eastern Maharashtra are modelled to infer the thickness and structure of the basins beneath the Deccan trap cover. The modelling studies along six profiles indicate the depth to the basement and thickness of sediments is gradually decreasing from N to S. The study also indicates that the basement undulates with alternative highs and lows with concealed sub-trappean rift basins at the eastern extremity of Deccan Syncline (DS).

**Key words:** Deccan Traps, Gondwana basins, Gravity anomalies, Modelling and Basement structure.

---

## INTRODUCTION

With the discovery of commercial grade oil and gas fields and Coal Bed Methane in the Gondwana sediments of the Krishna–Godavari sub basins and in the northern part of the Godavari basin in 1978, Gondwana basins of India are being increasingly subjected to intensive geophysical exploration (Subramanian, 2003). The prime objective of geophysical investigations by different investigative agencies is to estimate the thickness of the Gondwana sediments underneath the Deccan trap cover. The initial geophysical investigation by ONGC in Nagpur-Pusad-Betul area brought out the thickness of sediments as about 2.1 Km in the West of Wardha town and 4.17 to 5.74 Km near Katol (Ghildyal, 1985). Ramakrishna et al., (1999) brought out a comprehensive Bouguer gravity anomaly map (on 1:250,000 scale) based on the regional gravity surveys conducted by GSI in different blocks of DS for Gondwana basins of eastern Maharashtra region covering parts of Nagpur, Wardha, Yeotmal and Chandrapur districts. They also attempted for a qualitative and quantitative interpretation of residual gravity anomalies along two profiles constructed from this map. They estimated the thickness of sediments (the Gondwana and Vindhyan put together) as varying between 3 and 4 km for a constant density contrast of -0.3gm/cc between the sediments and the Archean basement. However, their profiles did not cover all the possible depositional areas. Serious efforts were made by several other investigators (Sarma et al., 2004; Jitendra Kumar et al., 2004; Yash Rastogi et al., 2014) to press into service deep electromagnetic and

magnetotelluric (MT) techniques to understand the nature of the hidden sediments beneath the Deccan traps. Of the two, MT has proven to be the effective technique in identifying the sediments below volcanic rocks like basalts as demonstrated by the results obtained from Saurashtra Peninsula, India (Sarma et al., 1992; Srinivasan and Khar, 1995), Columbia River Basaltic areas in USA (Corine Prieto et al., 1985) and Parana basin in Brazil (Stanley et al., 1985; Padilha et al., 1992). The success has been attributed to the higher conductivity of the sediments in relation to the overlying volcanic rocks and the underlying Archean basement. Chakravarti et al., (2007) attempted 3D modelling of Katol gravity low in the Gondwana basins of eastern Maharashtra region after calculating and removing the effect of the basalts from the gravity anomalies and deep resistivity values. According to them the thickness of basalts around Katol varies between 100 and 400 m with an average of 300 m and the maximum depth to the basement is in excess of 3.2 km. Considering the MT and Gravity data modelling, Jitendra Kumar et al., (2004) and Sarma et al., (2004) have indicated that the basement depth is of the order of 5 km in Katol low. However, most of these studies are either limited to only Katol gravity low or qualitatively interpreted.

In this paper an attempt is made to model the gravity anomalies along six profiles covering all possible depositional areas constructed from the gravity anomaly map of Ramakrishna et al., (1999) to identify nature and structure of the basement and thickness of sediments below trap cover. The objective is to understand the broad architecture of Nagpur-Wardha sub basin which is believed

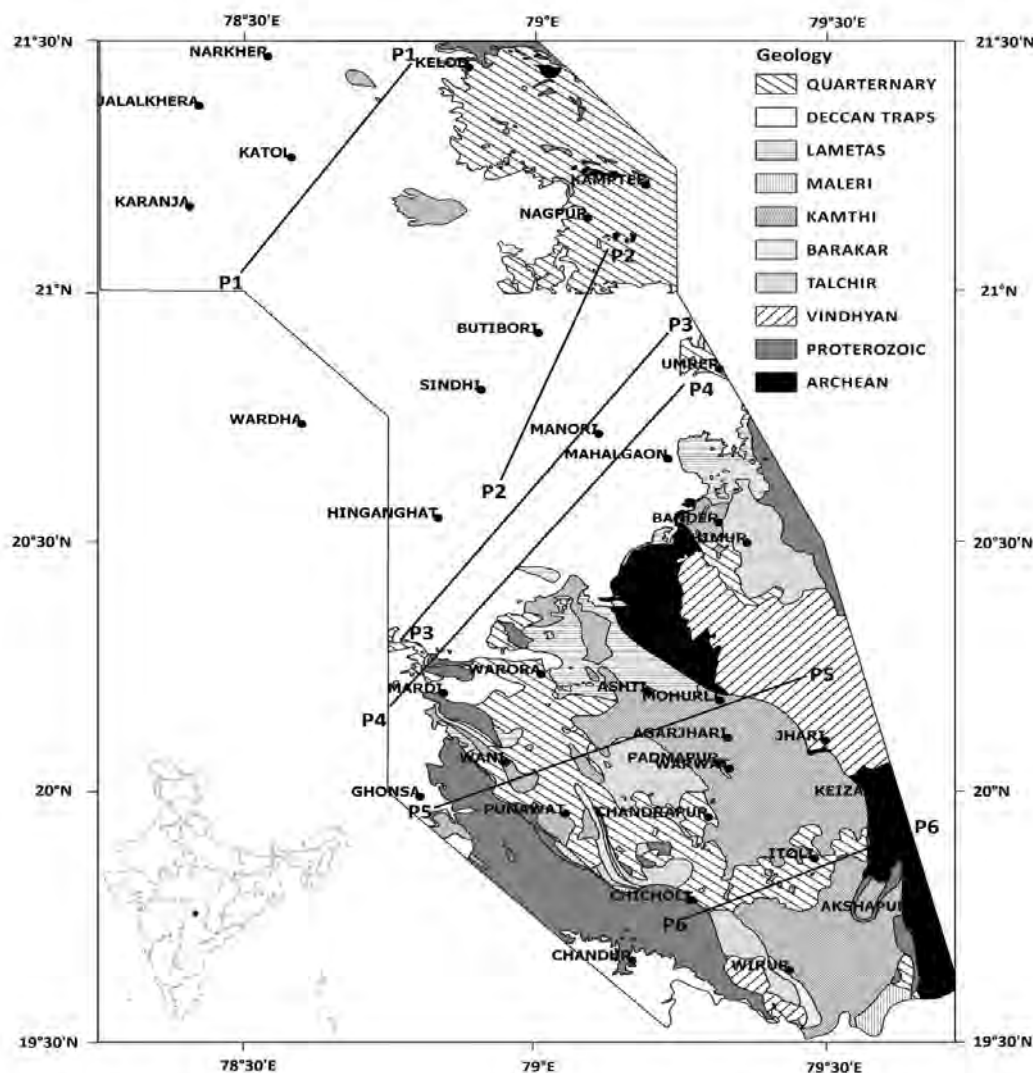


Figure1. Study area with geology.

to be a concealed subtrapean rift basin at the eastern extremity of DS.

**Study area, its geology and tectonics**

The study area forms a part of the DS measuring about 13,000 km<sup>2</sup> and it is bounded by 19°30'N to 21°30'N latitudes and 78°15'E to 79°45'E longitudes. Its outcrops range from Archean gneisses to Quarternary sediments (Figure 1). Its northern part is dominantly covered by the Deccan traps of Cretaceous-Paleocene age, whereas its southern part has exposures of Archean gneisses and sediments including post- syn- and pre-Gondwanas.

Tectonically, the Gondwana basins of peninsular India correspond to linear zones of structural weakness in the craton (Chatterjee and Ghosh, 1991) and are believed to have been formed under accumulated stress conditions

due to tensional and gravitational forces without the involvement of orogenic tectonics. They are considered to be irregular, elongated intracratonic depressions, trough-like rags and rift basins having graben/half graben structures marked by a major normal fault on one side making them highly asymmetric. Mukhopadhyaya (1994) opined that these basins underwent multiple phases of faulting, mostly aligned in E-W, ENE-WSW, N-S and ESE-WNW directions. Padhi and Ramakrishna (1999) based on Landsat (MSS) imagery of the Gondwana basins, geology, geomorphology and Bouguer gravity map of the area concluded that the tectonics of Katol region is controlled by two major NW-SE trending crustal faults, a two stage crustal subsidence and few other sub-basinal faults. Such faults identified geologically, are marked as solid circles in Figure 2 and most of these faults are correlated with gravity anomaly flexures.

### Gravity anomaly map and its qualitative analysis

The Bouguer gravity anomaly map (Figure 2) interpreted in the present study was compiled by the Geological Survey of India on 1:250,000 scale (Ramakrishna et al., 1999). The Bouguer gravity map exhibits distinct anomaly variations from -20 mGal to about -85 mGal with contours following a general NW to SE trend. E-W trending contours can also be observed at places locally. From the gravity map, several anomaly closures having distinct anomaly variations could be identified. These are marked as A1, A2, A3, A4, A5, A6, A7, A8, A9 and A10 respectively in Figure 2. Several NE-SW trending faults can be identified in the area based on the termination of these anomaly closures as marked. All these observed closures are anomaly lows - each having a limited areal extent- and hence may be attributed to individual basin-like structures bounded by faults.

The observed gravity lows distinctly occur along three axes named as northern gravity low axis (NGL), central gravity low axis (CGL) and the southern gravity low axis (SGL). The NGL with a clear SE-NW trend, extends to about 150 km length between Chimur and Jalalkhera. This axis is composed of few gravity lows viz., A10 around Katol (-85 mGal) in the NW, A8 around Butibori (-70 mGal), A7 around Mahalgaon (-65 mGal), A6 around Bander (-60 mGal) and A5 around Chimur (-55 mGal) in the SE. Each of these gravity low features can be explained by an individual basinal structure filled with sediments. Butibori, Mahalgaon, Bander and Chimur anomalies are bounded on their western side by a steep linear gradient anomaly indicating the presence of faulted contact.

The CGL axis initially runs roughly about 55 km in NNW-SSE direction between Wirur and Warwat and can be considered to be the northward extension of Godavari graben. Beyond Warwat this axis swings towards the west and runs in a SE-NW direction for about 80 km upto Hinganghat from where it appears to swing further towards the west making gravity contours align almost E-W. This central axis of depositional basin appears to be consisting of three sub areas/ basins of deposition characterized by three gravity lows, one lying between Wirur and Warwat towards the south i.e., A1, another lying around Ashti in its central portion i.e., A2 and the third towards north lying south of Hinganghat i.e., A4. Relatively high gravity anomalies observed between Padmapur and Jhari appear to indicate the presence of a ridge- like feature separating the sub-basins characterized by anomalies A1 and A2.

The SGL is comparatively a smaller one and extends for about 40 km from Warora in the North to Punawat in the south. This axis is characterized by a single gravity low of -55 mGal. The trend of this anomaly axis is almost N-S and swings towards NW to the west of Warora. Interestingly these three linear axes of gravity lows viz., NGL, SGL and CGL are separated by intervening gravity

highs of the order -35 to -20 mGal, indicating the presence of horst and graben structures in the area. This horst and graben structural setup can also be explained by the rift related tectonic activity as inferred in the following lines. One such important relative gravity high characterized by broad anomalies lies between Chimur in the East and Hinganghat in the West following the trend of the CGL of deposition. It runs initially in a NW-SE direction for about 80 km between Jhari and Manori and then takes an E-W trend to join Wardha. Either side of this relative gravity high is bounded by steep gradients indicating the presence of faulted contacts. This is to imply that the deposition of Gondwana sediments had taken place along the three sub-parallel axes along which characteristic low gravity anomalies are observed. Several researchers earlier have also indicated the presence of Gondwana sediments and pre-trappean tectonic settings concealed below the Deccan traps (Jitendra Kumar et al., (2004), Sarma et al., (2004), Ramakrishna et al., (1999), Yash Rastogi et al., 2014).

### Quantitative interpretation of anomalies

To understand the nature and configuration of basement underlying the Gondwanas buried below the trap rocks, six representative profiles namely P1-P1, P2-P2, P3-P3, P4-P4, P5-P5 and P6-P6 are constructed by digitizing the anomalies at an interval of 4 km across various gravity lows and modelled employing the program GR2DMODE (Radhakrishna Murthy, 1998) which is equally applicable for a submerged basin and an undulating topography over an assumed mean depth. This program works out to get the thickness of the basin at each point of observation along the profile. The program starts with determining the initial depths to the interface at various points and modifies them iteratively. These determined depths are constrained to be not less than ZTLT and not greater than ZBLT. These limiting depths- ZTLT may be the thickness of the Deccan trap and ZBLT the depth to the basement. At the end of the each iteration, an error function called the objective function, being the sum of squares of differences between the observed and calculated anomaly values, is calculated. The program is terminated either when the objective function tends to exceed or fall below a tolerance level, or when the specified number of iterations, 50 in this case, are completed.

Gravity modelling in the present case was carried out for different values of density contrast between sediments and basement rocks. The interpreted model that does not contradict the known geology is taken as the final solution to the modelling. In the present case the modelling of gravity anomalies is carried out for different values of density contrasts varying from -0.3 gm/cc to -0.5 gm/cc. Taking an average density of 2.30 gm/cc for the sediments (post-Gondwanas, Gondwanas and pre-Gondwanas put together) and 2.75 gm/cc for the

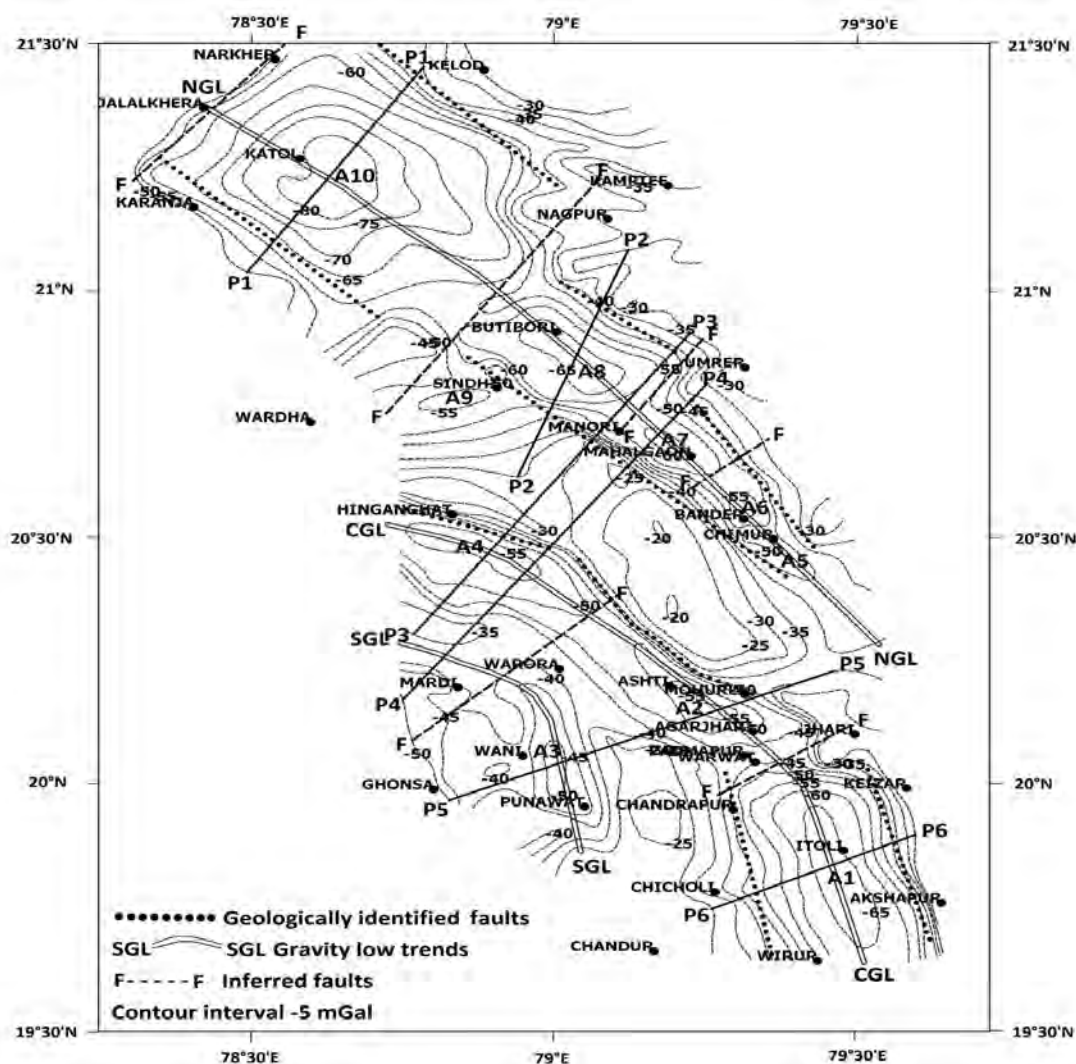


Figure 2. Bouguer anomaly map of the study area.

Archeans a value of  $-0.45 \text{ gm/cc}$  for the density contrast between the sediments and the basement rocks was found appropriate in the present study. The intrinsic assumption in the present interpretation is that the effect of trap rocks that is present in the observed anomalies is removed by the regional-residual separation.

**Profile P1-P1:** Observed gravity anomalies along P1-P1 are shown in the Figure 3. This profile runs through the major Katol gravity low (A10) which is nearly a circular feature. The profile starts from the SE of Karanja, passes through Katol towards west of Kelod with its entire length occupied by the trap rocks on the surface and showing a broad low of  $-85 \text{ mGals}$ . The modelling of residual anomalies along this profile shows a maximum of  $5.63 \text{ km}$  as depth to the basement at the center of the profile which is decreasing towards the periphery. Interestingly the structure on the basement shows that the basin had formed due to a series of step faults and existence of several

sub basins separated by horst like structures as seen that below  $56 \text{ km}$  point on the profile. A maximum of  $3.2 \text{ km}$  was estimated for the basement depth by Chakravarti et al., (2007) through 3D modelling for a density contrast of  $-0.5 \text{ gm/cc}$ . A basement depth of the order of  $5 \text{ km}$  and a thick sequence of Gondwana sediments are predicted by Jitendra Kumar et al., (2004) and Ghildyal, 1985 using MT surveys and gravity studies.

**Profile P2-P2:** The profile P2-P2 (Figure 4) covers the Butibori low (A8) and runs from the NE of Hinganghat, through Butibori towards south of Nagpur. The modelling of residual anomalies along this profile gives the maximum depth to the basement as about  $3.93 \text{ km}$  and shows presence of two grabens separated by a horst in the centre of the profile. Earlier Murty et al., (1985) had estimated  $4 \text{ to } 5 \text{ km}$  thick sediments around Butibori. However, Ramakrishna et al., (1999) estimated a basement depth of  $2.8 \text{ km}$  below Butibori low and opined that the sediment

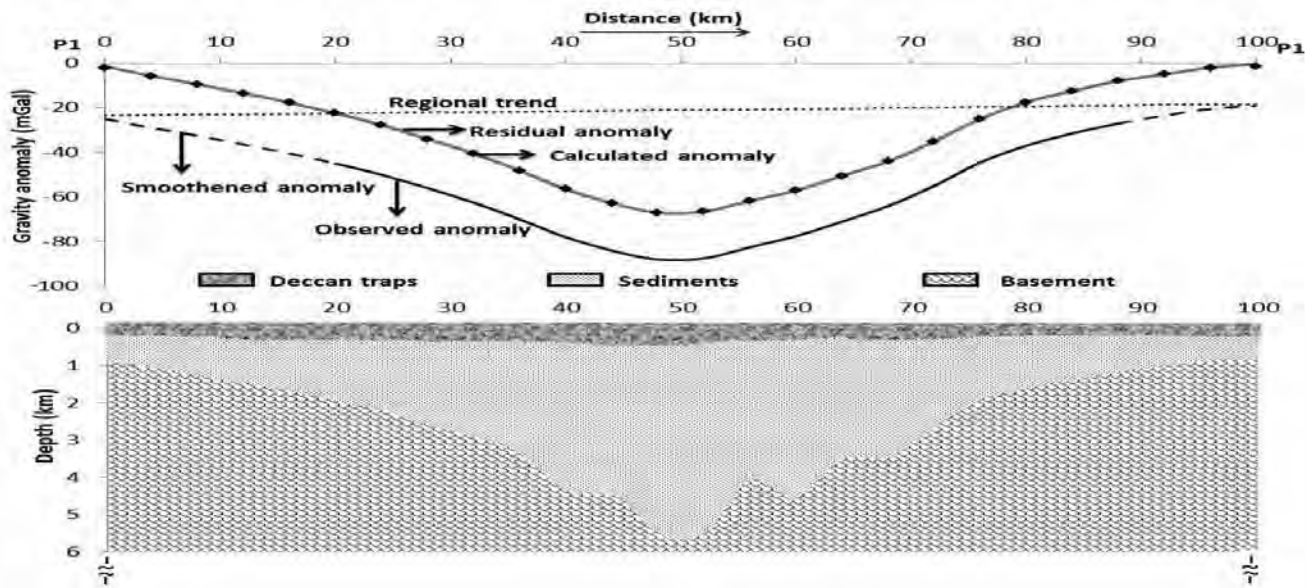


Figure 3. Gravity anomalies along profile P1-P1 and its interpretation.

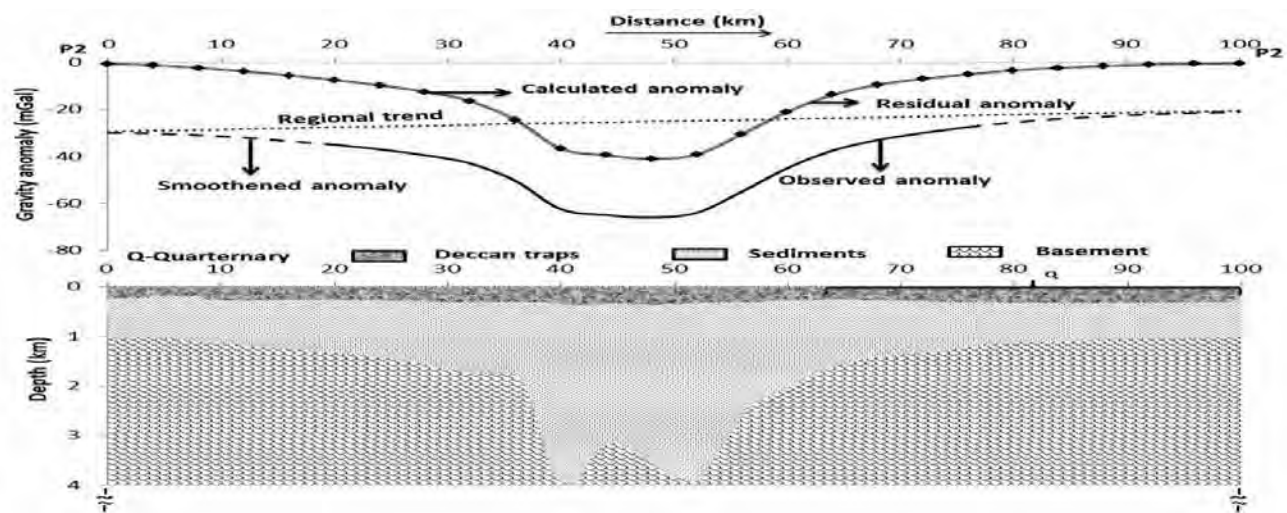


Figure 4. Gravity anomalies along profile P2-P2 and its interpretation.

thicknesses estimated by Murthy et al., (1985) are on the higher side as the low gravity anomaly may not be entirely due to only Gondwanas.

**Profile P3-P3:** This profile (Figure 5) is drawn to cover the main Hinganghat low (A4). The profile starts from the SW of Hinganghat passing through the major Hinganghat low up to the west of Butibori. The modelling of residual gravity anomalies shows that this profile covers two basins, one in the SW corner and the other in the NE corner characterized respectively by gravity lows A4 and A8 of magnitudes -60 and -65 mGal and a central broad basinal structure with a depth about 1.3 to 1.4 km. The modelling puts a maximum depth to the basement at 3.58 km below the SW low showing the role of step faulting in its formation and 3.6 km below the NE low. Ramakrishna

et al., (1999) have estimated a maximum depth of 2.7 km to the basement below Hinganghat low.

**Profile P4-P4:** Profile P4-P4 (Figure 6) runs almost parallel to the profile P3-P3. It starts from the west of Mardi, runs through NE of Hinganghat and ends SW of Umrer. Major length of the profile is occupied by trap rocks on the surface except between 15 km and 20 km distances where small patches of Quaternaries and Proterozoics are exposed. Modelling of the residual anomalies along this profile suggests three basins corresponding to the three gravity lows which the profile crosses. The maximum depth to the basement obtained with the present modelling below the SW low anomaly is 1.74 km, that below the central gravity low is 2.89 km and below the NE end gravity low the maximum depth of basement is 4.67 km. Interestingly,

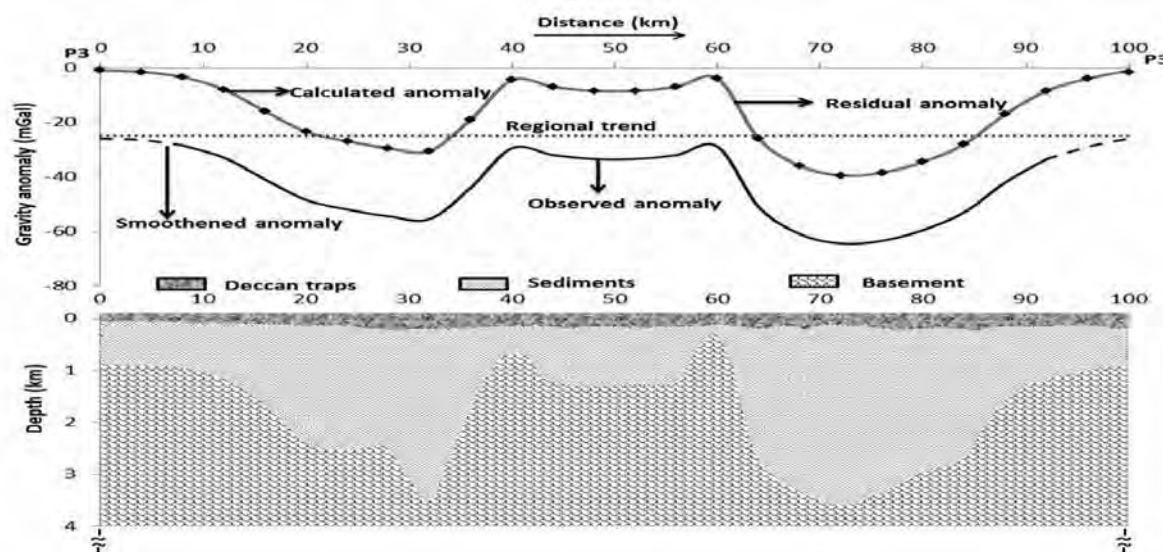


Figure 5. Gravity anomalies along profile P3-P3 and its interpretation.

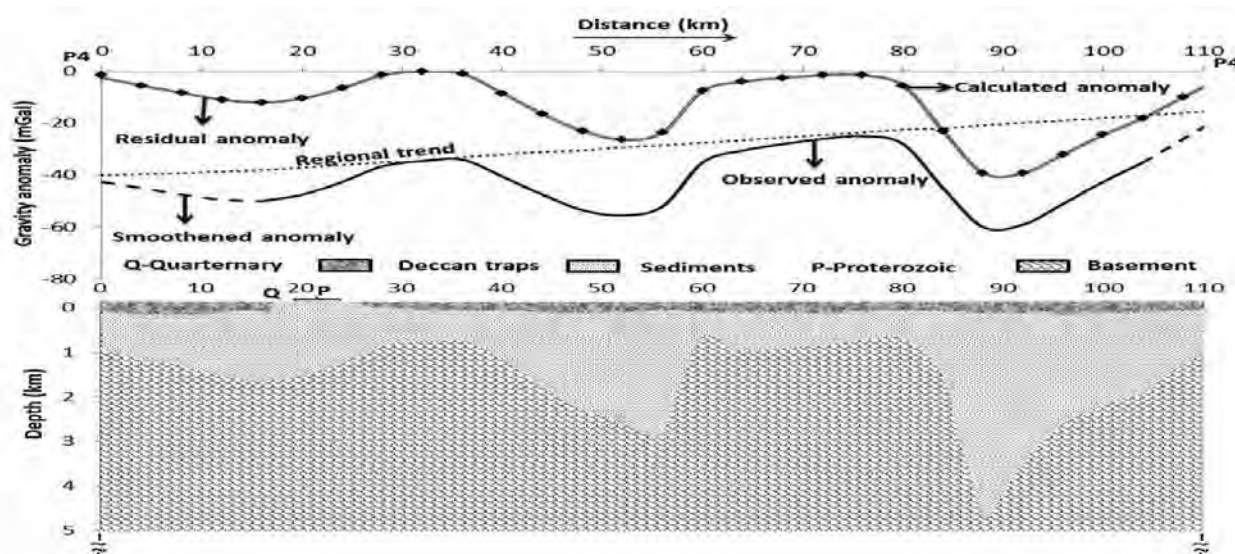


Figure 6. Gravity anomalies along profile P4-P4 and its interpretation.

modelling scheme brings the basement to a level of around 1.2 km where Proterozoic sediments are exposed at the surface. Jitendra Kumar et al., (2004) had estimated a maximum thickness of 1000 m to Proterozoic rocks in DS area. The profile passes through the conspicuous gravity high of -25 mGal where the basement comes to a level of 0.86 km showing that the two major basement lows are separated by a ridge-like feature.

**Profile P5-P5:** This profile (Figure 7) runs from the south of Ghonsa through the south of Wani and north of Agarjhari to the west of Mohurli. This profile covers the Wani (A3) and Agarjhari (A2) lows characterized by anomalies -50 and -55 mGal respectively. The modelling of the residual anomalies along this profile places the maximum depth to the basement at 2.74 km below the

Wani low and at 3.45 km below the Agarjhari low bringing it to a minimum depth of 0.6 km at the ends of the profile. The reduced depths to the basement along this profile may be explained by the occurrence of pre-Gondwana sediments (Vindhyan & Proterozoic) on the surface and the absence of Gondwanas and younger sediments along the profile.

**Profile P6-P6:** Profile P6-P6 (Figure 8), starting from the south of Chicholi and extending to the south of Keizar runs across Itoli anomaly low (A1). Modelling of residual anomalies along this profile with the assumed density contrast brings the basement close to the surface towards the periphery of the profile from its maximum depth of 3.07 km at the center, which can be explained by the exposure of Proterozoic and Archean formations at either end of the profile.

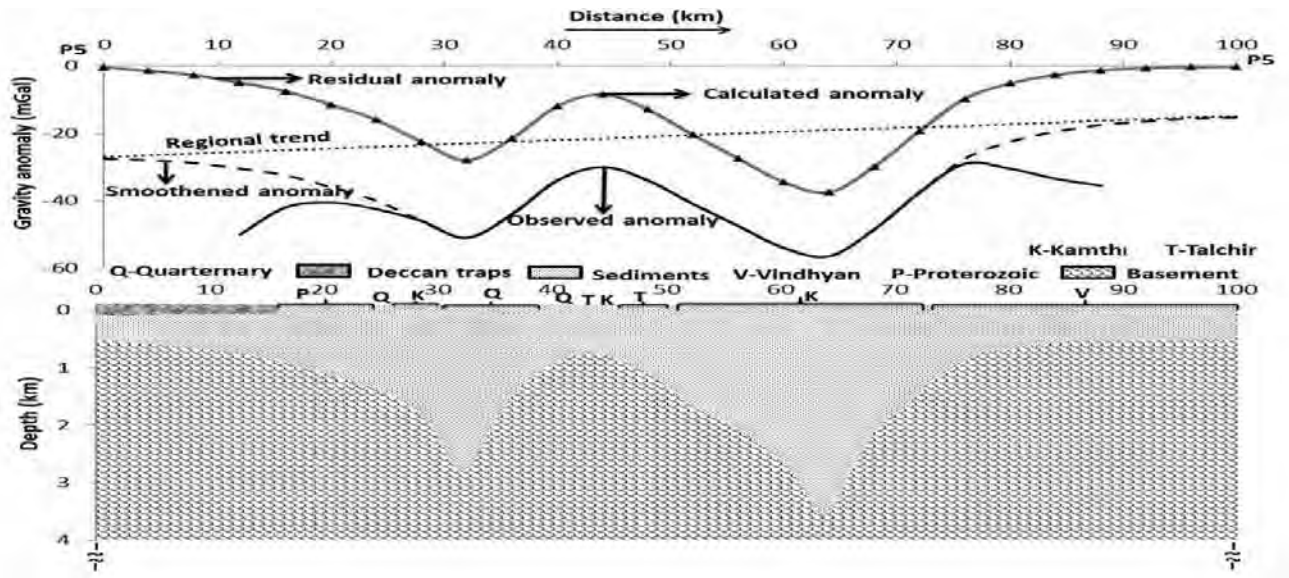


Figure 7. Gravity anomalies along profile P5-P5 and its interpretation.

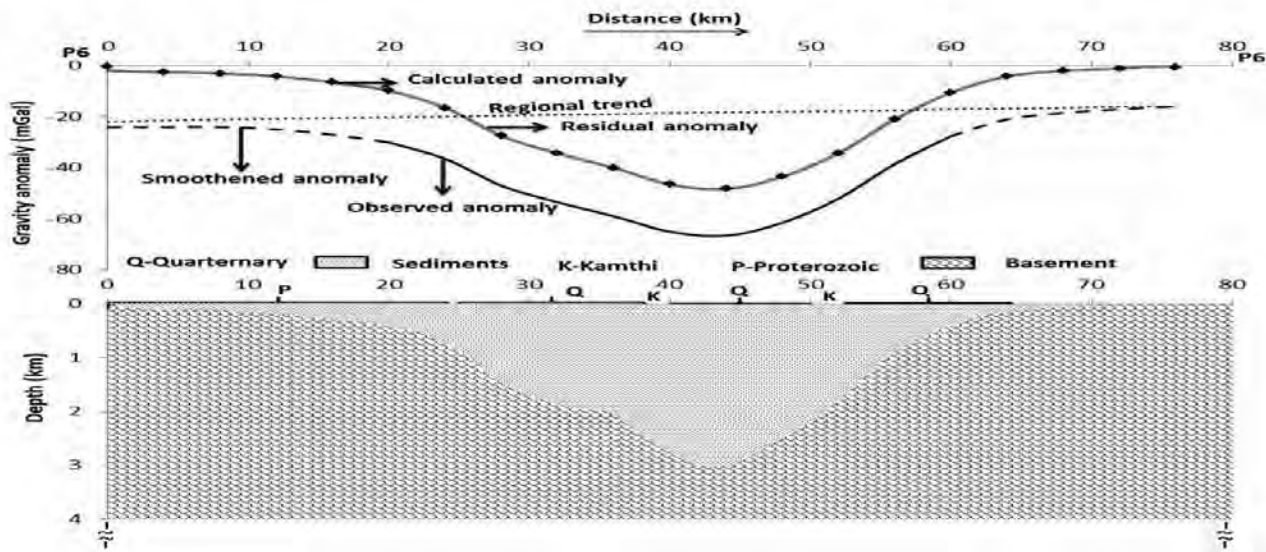


Figure 8. Gravity anomalies along profile P6-P6 and its interpretation.

## CONCLUSIONS

Modelling of Bouguer gravity anomalies indicates the presence of two sub-parallel NW-SE trending basinal features below the Deccan traps in parts of Eastern Maharashtra. The gravity anomaly map also indicates presence of few more smaller basinal features- one between Punawat and Warora almost trending in the N-S direction parallel to 79° E longitude and the other almost trending E-W around Sindhi.

Gravity modelling along the six profiles indicates the presence of a ridge-like feature between the two NW-SE trending long basins viz., NGL and CGL. It also indicates

that these basins are filled with a thick pile of sediments varying between 5.33 km near Katol in the NW corner to 1.44 km near Mardi in the SW corner. All the faults identified above indicate that the basement is highly faulted and show alternate horst and graben structures or relay ramps. There is a gradual decrease in the basement depth from NE to SW and also from NW to SE which indicates an en-echelon pattern of faults. The NW-SE faults appear to be more prominent and associated with horst and graben-like structures as evidenced by the interpreted basement depths and inferred faults (Figure 2). Padhi and Ramakrishna (1999) also came out with almost similar results in the Gondwana basins of Maharashtra. Relay

ramps, normal fault planes and transfer fault zones are typical in an extensional environment and play a major role in the development of rift basins (Morley et al., 1990; Nelson et al., 1992 and Peacock and Sanderson, 1994).

Therefore the present interpretation supports that this part of the study area in DS is a concealed sub-trappean rift basin at the eastern extremity of DS. The Katol basin was identified as one of the 26 potential hydrocarbon Gondwana basins of India by Singh (2013) along with others. As such the present results are of value in the context of searching for hydrocarbon reserves in India.

## ACKNOWLEDGEMENTS

The first two authors are grateful to the Adikavi Nannaya University for providing research facilities. Mrs. Neetha Raj is thankful to the Department of Science and Technology for the INSPIRE fellowship to carry out the research. Authors are grateful to Prof. B. V. S. Murthy for constructive review and editing. We thank the Chief Editor for his support.

## Compliance with Ethical Standards

The authors declare that they have no conflict of interest and adhere to copyright norms.

## REFERENCES

- Chakravarti, V., Shankar, G. B. K., Muralidharan, D., Harinarayana, T., and Sundararajan, N., 2007. An integrated geophysical approach for imaging sub-basalt sedimentary basins: Case study of Jam river basin, India, *Geophysics*, v.72, no.6, pp: B141-B147.
- Chatterjee, G. C., and Ghosh, P. K., 1991. Tectonic frame work of the Peninsular Gondwanas of India, *Memoir no.21*, Geol. Soc. Ind.
- Corine Prieto, Carolyn Perkins, and Ernest Berkman, 1985. Columbia River Basalt Plateau- An integrated approach to interpretation of basalt-covered areas, *Geophysics*, v.50, no.12, pp: 2709-2719.
- Ghildyal, N.D., 1985. Report of Gravity-Magnetic Survey in Nagpur, Betul, Akola, Pusad, Yeotmal area of Maharashtra and Madhya Pradesh (Field session 1984-85), ONGC unpublished Report.
- Jitendra Kumar, Paramjit Singh, and Dipankar Dutta, 2004. Infra trappean modelling of Deccan syncline, 5<sup>th</sup> Conference and Exposition on Petroleum Geophysics, Hyderabad, pp: 65-68.
- Morley, C. K., Nelson, R. A., Patton, T. L., and Muss, S. G., 1990. Transfer zones in the East African rift system., *Bull. Am. Ass. Petr. Geol.*, v.74, pp: 1234-1253.
- Mukhopadhyaya, A., 1994. Tectonic evolutionary history of peninsular Gondwana basins, *Proc. 9<sup>th</sup> Int. Gondwana Sym.* Hyderabad (Abs).
- Murthy, B. G. K., Raghunath Rao, K., and Puneekar, D. V., 1985. Report on geophysical investigation for delineating Gondwanas below traps in Umrer, Bander, Kamptee and Katol trough in Nagpur district, under deep geology project, *Unpub.Rep.Geo.Surv. Ind.*
- Nelson, R. A., Patton T. L., and Morley C. K., 1992. Rift Segment Interaction and Its Relation to Hydrocarbon Exploration in Continental Rift Systems, *Bull. Am. Ass. Petr. Geol.*, v.76, no.8, pp: 1153-1169.
- Padhi, R. N., and Ramakrishna T. S., 1999. Tectonic History Deduced From A Combined Study Of Bouguer Gravity And Lineaments of Gondwana Basins In Maharashtra, *Jour. of Geophysics*, v.20 no.2.
- Padilha, Trivedi, B. N., Vittorelli, I., and De Costa, J. M., 1992. Upper continental structure of N.E. Parana Basin, Brazil from integrated MT and gravity measurements, *J. Geophys. Res.* v.97, pp: 3351-3355.
- Peacock, D.C.P., and Sanderson, D.J., 1994. Geometry and Development of Relay Ramps in Normal Fault Systems, *Bull. Am. Ass. Petr. Geol.*, v.78, no.2, pp: 147-165.
- Radhakrishna Murthy, I. V., 1998. Gravity and magnetic interpretation in exploration geophysics, *Memoir, Geol. Soc. Ind.* v.40, pp: 154.
- Ramakrishna, T. S., Rama Rao, M. S. V., Bhaskara Rao, K. V. S., and Puneekar, D. V., 1999. Geophysical study of the Gondwana basins of Eastern Maharashtra, *Geological Survey of India, Special publication No. 47.*
- Sarma, S. V. S., Virupakshi, G., Murthy, D. N., Harinarayana, T., Sastry, T. S., Someswara Rao, M., Nagarajan N., Sarma, M. S., Veeraswamy, K., Prabhakar Rao, S. P. E., and Gupta, K. R. B., 1992. Magnetotelluric studies for oil exploration over Deccan traps, Saurashtra, Gujarat, India, *Tech. Report No. 92-Lithos-125*, unpublished report, pp: 80.
- Sarma, S. V. S., Harinarayana, T., Virupakshi, G., Someswara Rao, M., Madhusudan Rao, Nandini Nagarajan, Sastry T. S., and Prabhakar E Rao S., 2004. Magnetotelluric investigations in Deccan trap covered areas of Nagpur-Wardha region, India, *Journal of Geophysics*, v.25, no.4, pp: 87-91.
- Singh, D.N., 2013. Petroleum Exploration in Frontier basins, 9<sup>th</sup> Seminar on "Modern Practices in Petroleum Exploration" from 9<sup>th</sup> – 12<sup>th</sup> September 2013 organized by ONGC at KDMIPE ONGC, Kaulagarh Road, Dehradun.
- Srinivasan, R., and Khar, B. M., 1995. Exploration of frontier basins and hydrocarbon prospects, *Petrotech 95*, New Delhi, v.1, pp: 3-19.
- Stanley, W. D., Saad, A. R., and Ohofugi, W., 1985. Regional magnetotelluric surveys in hydrocarbon exploration, Parana Basin, Brazil, *AAPG Bull.* v.69, pp: 1344-1360.
- Subramanian T. S., 2003. A unique and lucrative basin, *Frontline*, v.20, no.3.
- Yash Rastogi, Abhishek Sharma and Ashish Sahu, 2014. Hydrocarbon prospects in Deccan traps, *International Journal of Scientific and Engineering Research*, v.5, no.5, pp: 127-144.

# Source Characteristics of the 2012 Earthquake Swarm Activity in the Andaman Spreading Ridge

G. Srijyanthi\*, M. Ravi Kumar, S. Prasanna, and N. Purnachandra Rao

CSIR-National Geophysical Research Institute, Hyderabad-500007, India

\*Corresponding Author email: srijyanthi.india@gmail.com

---

## ABSTRACT

Earthquake swarms are a sequence of events clustered in space and time, with no single earthquake dominating in size. Such swarms were observed in the Andaman sea region during the years 1983-1984, 1994, 2005 and 2012. The recent one in 2012 occurred to the north of the Nicobar Islands (9° N, 94° E) within the Andaman spreading ridge, starting on 16 April, 2012. Interestingly, the swarm followed the  $M_w$ 8.6 Indian Ocean earthquake of 11 April, 2012, the largest strike-slip earthquake ever. This activity lasted for nine days and comprised about 27 earthquakes in the local magnitude ( $M_L$ ) range of 2.2 to 4.4, whose focal depth varied from 4 to 51 km. In the present study, we first analysed the phase data of these earthquakes recorded by a nine station broadband seismological network established by the CSIR-National Geophysical Research Institute (CSIR-NGRI), together with the data from three stations of the India Meteorological Department (IMD), to constrain the hypocentre locations of the swarm events using the double difference method. Further, we determined the moment tensor solutions of the three largest events using the full waveform inversion technique, to understand their source characteristics. Interestingly, all the three mechanisms showed a high non-double-couple component of over 70%, comprising both isotropic and CLVD components. Therefore, it is inferred from the present study that the mechanism of swarm earthquakes can be explained by ascension of magma at the spreading ridge coupled with inflation or deflation of magma chambers in the volcanic source region. In contrast, moment tensor solutions of four tectonic earthquakes that occurred to the north of the Andaman Islands away from the spreading center and the swarm, show a very high double couple percentage as expected for a normal tectonic earthquake, validating our interpretation.

**Key words:** Andaman Nicobar, Swarm earthquakes, Earthquake relocation and Moment tensor solutions.

---

## INTRODUCTION

The Andaman arc along with the Burma arc to its north forms the eastern margin of the Indian plate. The Andaman Sea adjoining the Andaman subduction complex falls in the back arc region (Figure 1). However, it is categorized as a rip-off or pull-apart basin rather than a typical back arc basin and is considered as an active extensional margin (Curry, 1989). Evidence for active extension comes from a synthesis of the results from many geophysical studies including bathymetry, magnetic, gravity and heat flow (Rodolfo, 1969; Curry et al., 1979). The structure of the Andaman back arc mapped by Kamesh Raju et al., (2004) identified three major SW-NE spreading segments offset by several kilometers having a step like structure. The spreading in this region was initially attributed to leaky transform or trench roll back, similar to the back arc basins in the Pacific (Uyeda and Kanamori, 1979). However, the most important reason for the active extension or spreading is the oblique subduction of the Indo-Australian plate beneath the Sunda plate. The complex accommodation of the strain along this oblique subduction is evidenced in the form of arc-parallel strike-slip faulting along the Western Andaman Fault and also formation of a sliver plate moving northward (Fitch, 1972; McCaffrey, 1992; 2009). The boundary between the Burma plate (Sliver), and

the Sunda plate is inferred from a system of arc-parallel transform faults and arc-normal ridges (Alock and Sewell ridges) in the back arc of the Andaman Sea.

The NW-SE extension of the Andaman Sea corresponding to the pull-apart basin along the plate boundary is due to the northward drag of the Burma Plate with respect to the Sunda plate by the underthrusting Indo-Australian plate (Curry, 2005; McCaffrey, 2009). Studies of magnetic anomalies indicate that the sea floor spreading was initiated ~4 Ma ago, much younger than in the Sunda arc, with the initial spreading rate increasing from 1.6 cm/yr to 3.8 cm/yr from ~2-2.5 Ma to the present (Kamesh Raju et al., 2004). The spreading ridge falls under the category of slow-spreading ridges. The neotectonic extension in this region is manifested in terms of normal faulting mechanisms in the northern part of the Andaman Sea whose extension is along the NW direction (Fitch, 1972). The dominance of normal earthquakes at latitudes 10° N and 14° N indicates the presence of two spreading centres, separated by N-S transform faults experiencing right-lateral strike-slip as revealed by the source mechanisms of earthquakes (Eguchi et al., 1979).

The Andaman Sea region hosted several earthquake clusters or swarms in the past, during the years 1983-1984, 1993 and 2005 (Figure 1), with an interesting periodicity of about 10 years. An earthquake swarm can

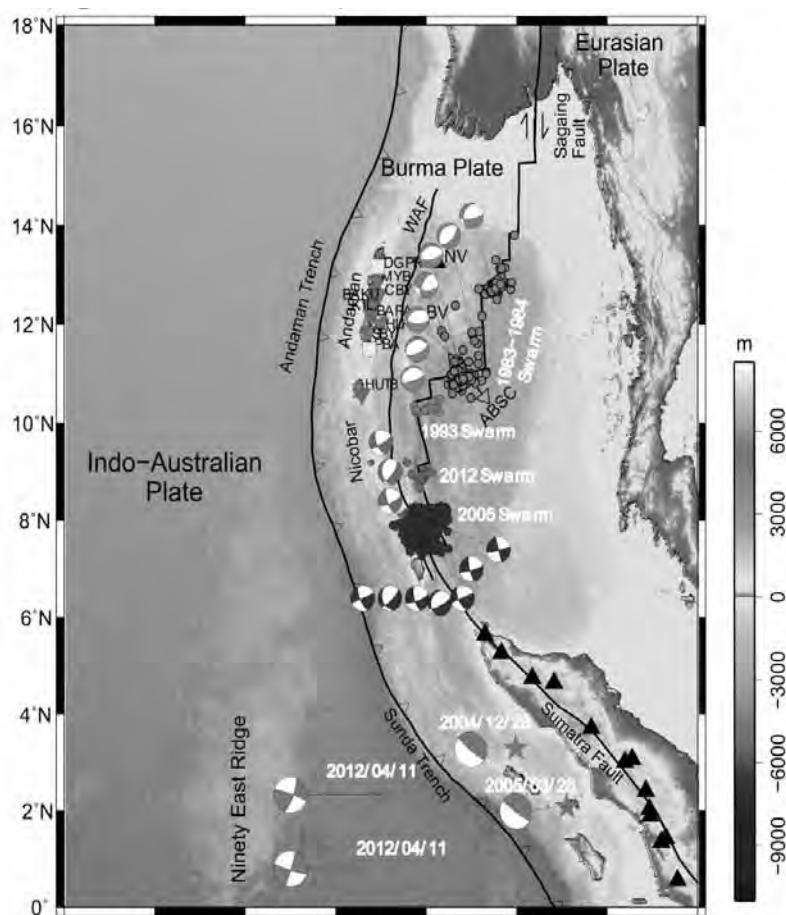


**Figure 1.** Tectonic map of the Sumatra-Andaman region with active faults indicated by solid lines and inactive faults marked as dashed black lines. Triangles correspond to volcanic arc, BV: Barren Volcano, NV: Narcondam Volcano. AB: Aceh Basin, ABSC: Andaman Back-Arc Spreading Centre, AR: Alcock Rise, SR: Sewell Rise, SFS: Sumatra fault system, SEU: Seulimeum strand of the SFS, WAF: West Andaman fault.

be defined as a sequence of earthquakes clustered in space and time with no distinct main shock (Mukhopadhyay and Dasgupta, 2008; Roland and McGuire, 2009). Among known swarms in the Andaman region, the 2005 swarm is globally considered as the most energetic one that occurred exactly a month after the  $M_w$  9.2 December 2004 Sumatra earthquake. Kundu et al., (2012) suggested that the 2005 swarm is due to a combination of both tectonic and volcanic sources. Recently, in the year 2012, after the great twin strike-slip earthquakes of  $M_w$  8.6 and 8.2 in the Indian Ocean, an earthquake swarm occurred in the Andaman Spreading region. The occurrence of swarm earthquakes not only indicates episodes of rifting, but also seems to be associated with a major or great earthquake in the proximity. Thus, understanding the source characteristics of these earthquakes would shed light on resolving the enigma associated with the complex history of swarm seismicity. In the present study, we attempt to decipher the source processes of earthquakes in the 2012 swarm using the moment tensor inversion approach. The results are

also compared with those of the 2005 swarm using the moment tensor elements of earthquakes from the global CMT catalog (Figure 2). A full moment tensor includes all mechanisms of the source process namely the Double Couple (DC), Compensated Linear Vector Dipole (CLVD) and Isotropic (ISO) (Frohlich and Apperson, 1992). The ISO component is generally associated with an explosive or implosive source where the energy is equally radiated in all directions. On the other hand, earthquakes in general tend to exhibit a combination of all these three types, with a general predominance of DC. The DC component describes equivalent forces acting on a planar fault causing a simple shear whereas the non-DC component including CLVD and ISO-describes more complex processes like landslides (Hasegawa and Kanamori, 1987), inflation or deflation of magma chambers in volcanic areas (Mori and McKee, 1987), tensile faulting caused by high fluid pressure in geothermal and volcanic areas (Ross et al., 1996; Julian et al., 1997, 1998), or shear faulting in an anisotropic medium (Kawasaki and Tanimoto, 1981). A high non-DC

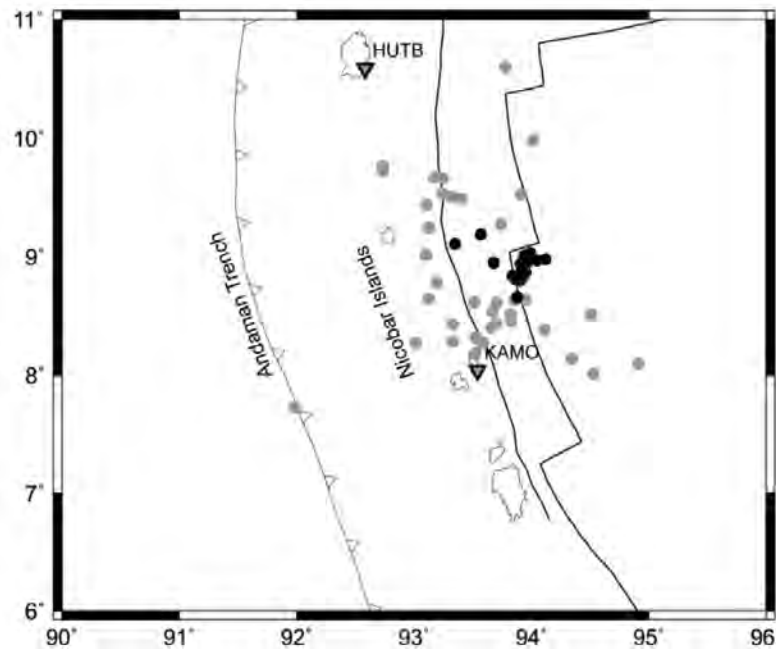


**Figure 2.** Seismicity in the vicinity of the observed 2012 swarm from 2010 January to March 2012 (ISC catalog (gray circles) and 2012 swarm (black circles)).

component may also be associated with deep earthquakes on slabs in subduction zones. The actual distribution of these components in the moment tensor is used in this study to characterize the complete earthquake source process.

### Data and Methodology

The seismic waveform data recorded by the seismic network comprising nine broadband seismological stations established by the CSIR-NGRI and two stations established by the IMD in the Andaman-Nicobar Islands are used in this study (Figure 1). The nine broadband stations are equipped with REFTEK sensors while the other two are equipped with Trillium-240, both connected to data loggers sampling the data at a frequency of 100 Hz. During the routine analysis for earthquake locations, a group of clustered events was observed to the north of Nicobar Islands (9°N, 94°E), within the Andaman spreading ridge, hitherto referred as the 2012 swarm. The background seismicity in the vicinity of the observed 2012 swarm from January 2010 to March 2012 (3 years before the swarm) clearly indicates the absence of clustering of events in the region (Figure 2). This swarm activity consisting of 27 events in the local magnitude ( $M_L$ ) range of 2.2 to 4.4, started on 16 April 2012, following the  $M_w$  8.6 Indian Ocean earthquake of 11 April 2012 and lasted until 25 April 2012. The vertical component of an event from the 2012 swarm recorded at six stations is shown in Figure 3b. For comparison, the vertical component of a non-swarm

event closer to the arc is also shown in figure 3a. The hypocentral parameters of the swarm events are obtained by an iterative least-squares technique based on the Geiger method (Geiger, 1910; 1912). Even with high precision digital data, it is difficult to precisely locate the earthquakes from the station geometry restricted to a few azimuths due to geographical constraints. Therefore, to get improved locations, events are relocated using the double difference (HypoDD) algorithm of Waldhauser and Ellsworth (2000).

**Relocation:** HypoDD technique assumes that the ray paths between the source region and a common station are similar along almost the entire ray path and the difference in travel times for two events observed at one station is attributed to the spatial offset between the events. The residual between the observed and calculated travel-time difference (or double-difference) between two events at a common station is related to the adjustments in the relative position of the hypocenters and origin times through the partial derivatives of the travel times for each event with respect to the unknown. The double-difference residuals for pairs of earthquakes at each station are minimized by weighted least squares using the method of singular value decomposition (SVD) or the conjugate gradient method (LSQR) (Paige and Saunders, 1982). In the present study, a total of 226 P and 120 S travel times are used to relocate the 27 swarm earthquakes using the LSQR method (Figure 4). The following criteria are adopted for relocating earthquakes: (i) the maximum distance between an event pair and the corresponding station is 600 km; (ii) the maximum hypocentral separation between a pair of events

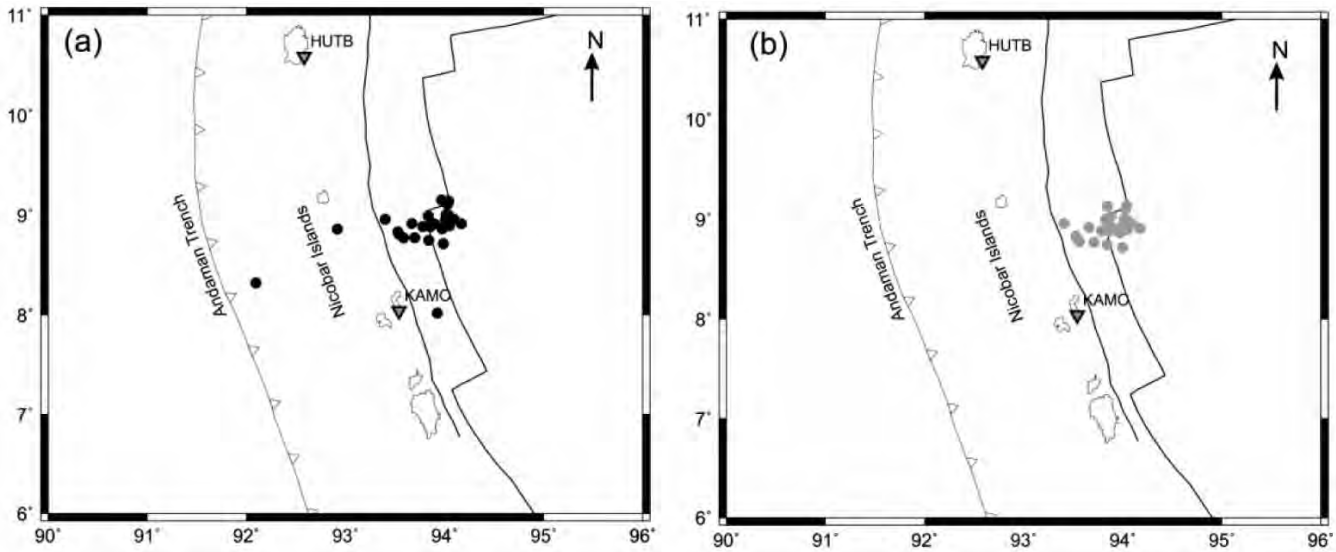


Figure 4. Epicentral map of swarm earthquakes (a) Initial, (b) relocated.

is 60 km; (iii) maximum number of neighbours per event is eight; and (iv) the definition of a neighbour involves a minimum number of three links.

**Moment Tensor Inversion:** A moment tensor provides a general description of a point source using a pair of couples representing equivalent body forces. A moment tensor solution describes not only the general earthquake faulting or shear mechanisms, but also other models of seismic sources like explosions and implosions or rock falls, landslides, meteorite terminal explosions (e.g. atmospheric), and mixed mode ruptures driven by fluid and gas injections. Thus, the moment tensor inversion is a very important tool in seismic source characterization. In general, a moment tensor is a combination of the three components: (i) Double Couple (DC) which describes equivalent forces acting on a planar fault causing shear faulting, (ii) Compensated Linear Vector Dipole (CLVD) which describes equivalent forces acting on a non-planar fault and (iii) Isotropic (ISO) which represents forces acting radially in all directions. The percentage of each component can be used to distinguish the earthquake process indicating the type of source.

The focal mechanism solution of an earthquake can be derived from the moment tensor elements. The DC component is described by the fault plane parameters: strike, dip and slip. The moment tensors can be obtained from various inversion schemes: (i) Polarity of P phase, (ii) Amplitude inversion of P, SH and SV waves, (iii) Waveform inversion. In the present study, full waveform inversion is used to obtain the moment tensor solution, including the seismic moment and moment magnitude using ISOLA code (Sokos and Zahradník 2008, 2013). An iterative deconvolution based on the approach of Kikuchi and Kanamori (1991) is used to obtain the moment tensor solutions. Synthetic waveforms are generated by

using the discrete wave number summation method of Bouchon (1981) and Coutant (1989). The core inputs used to calculate the moment tensor solution are the station coordinates, hypocentral parameters, 1D velocity model (Rao et al., 2011), waveform data and the number of iterations.

The best moment tensor solution that yields a good match between the synthetic and observed waveforms is obtained through an iterative process. A good correlation and overall variance reduction indicates the reliability of the fit between the observed and synthetic waveforms. A full moment tensor solution is a combination of DC, CLVD and ISO components which can be isolated as follows:

$$ISO = \frac{1}{3} \frac{\text{Tr}(M)}{|M|_{\max}} (100\%) \quad \text{----- (1)}$$

$$CLVD = -2 \frac{M^*_{\min}}{|M^*_{\max}|} (100 - |ISO|) \quad \text{----- (2)}$$

$$DC = (100 - |ISO| - |CLVD|) \quad \text{----- (3)}$$

where,  $\text{Tr}(M)$  represents the trace of the seismic moment tensor  $M$ ,  $M|_{\max}$  denotes the eigenvalue of  $M$  that has the maximum absolute value, and  $M^*|_{\max}$  and  $M^*|_{\min}$  are the eigenvalues of the deviatoric moment tensor with the maximum and minimum absolute values, respectively.

## RESULTS AND DISCUSSION

During the year 2012 an interesting phenomenon of earthquake clustering both in time and space, which characterizes a swarm, is observed to the north of the Nicobar Islands. The cluster of 27 earthquakes which is referred as the 2012 swarm started just 5 days after the

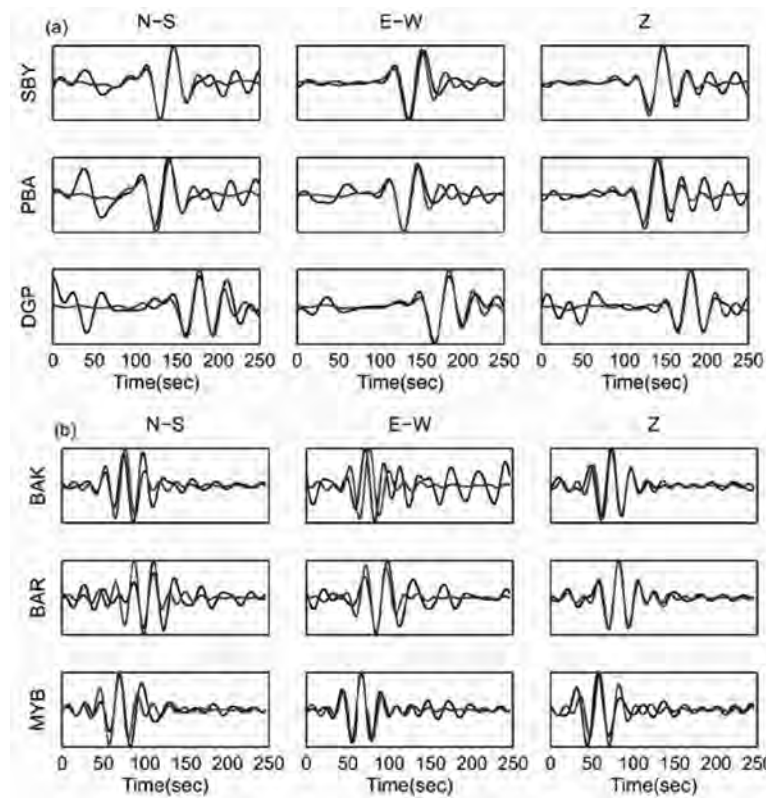


**Figure 5.** Matching of the observed (black) and synthetic (gray) 3-component displacement seismograms corresponding to (a) swarm (b) non-swarm events.

**Table 1.** Epicentral parameters and focal mechanism solutions of the 2012 swarm events in the Andaman spreading ridge, including the distribution of DC and non-DC components of the moment tensor solutions.

| S. No. | Date       | Origin Time | Lat  | Lon   | Depth (km) | $M_w$ | Centroid Depth (km) | Strike | Dip | Rake | DC   | Non-DC |      |       |
|--------|------------|-------------|------|-------|------------|-------|---------------------|--------|-----|------|------|--------|------|-------|
|        |            |             |      |       |            |       |                     |        |     |      |      | CLVD   | ISO  | Total |
| 1      | 2012/04/24 | 14:57:14    | 8.9  | 93.9  | 23         | 4.4   | 29                  | 76     | 60  | 14   | 20.1 | 33.2   | 46.7 | 79.9  |
| 2      | 2012/04/25 | 7:42:24.5   | 9.15 | 93.9  | 12.56      | 4.4   | 7                   | 135    | 50  | 150  | 27   | 22.4   | 50.6 | 73    |
| 3      | 2012/04/25 | 12:58:16.6  | 8.9  | 94.07 | 14.7       | 3.8   | 52                  | 325    | 44  | -112 | 22.5 | 71.0   | 6.5  | 77.5  |

twin ( $M > 8$ ) earthquakes in the Indian Ocean. The origin of the 2012 swarm was speculative due to its spatial proximity to the Andaman back arc spreading center, the site of the most energetic swarm in 2005 and proximity in time to the Indian Ocean earthquakes. Although the swarm consists of 23 moderate earthquakes ( $M_t$  2.2 to 4.4), focal mechanism solutions could not be obtained for most of them due to poor signal to noise ratios. In the present study, only three focal mechanism solutions that show a good correlation ( $\geq 0.5$ ) between the synthetic and observed waveforms (Figure 5) could be obtained. Out of these three focal mechanism solutions, two earthquakes have a predominantly strike-slip component with a slight normal component and the third earthquake is dominated by the normal component (Figure 6). The obtained solutions are listed in Table 1.

The combination of normal and strike-slip mechanisms can be attributed to the spreading activity and transform faulting in the Andaman Sea region as evident from the matching fault plane and slip directions. Further, the DC and non-DC components are calculated to distinguish between the tectonic and non-tectonic causes of the earthquake source. Interestingly, a significant percentage of non-DC component ( $> 70\%$ ) is observed for the swarm events which may indicate the role of tensile faulting at high fluid pressure or dyke intrusion (Julian, 1983; Aki, 1984; Julian and Sipkin, 1985). The non-DC component can often be misleading due to improper earthquake source modelling resulting from limited data, inaccurate Greens functions or oversimplified source processes (Vavrycuk, 2002). Therefore, to verify the correctness of the obtained

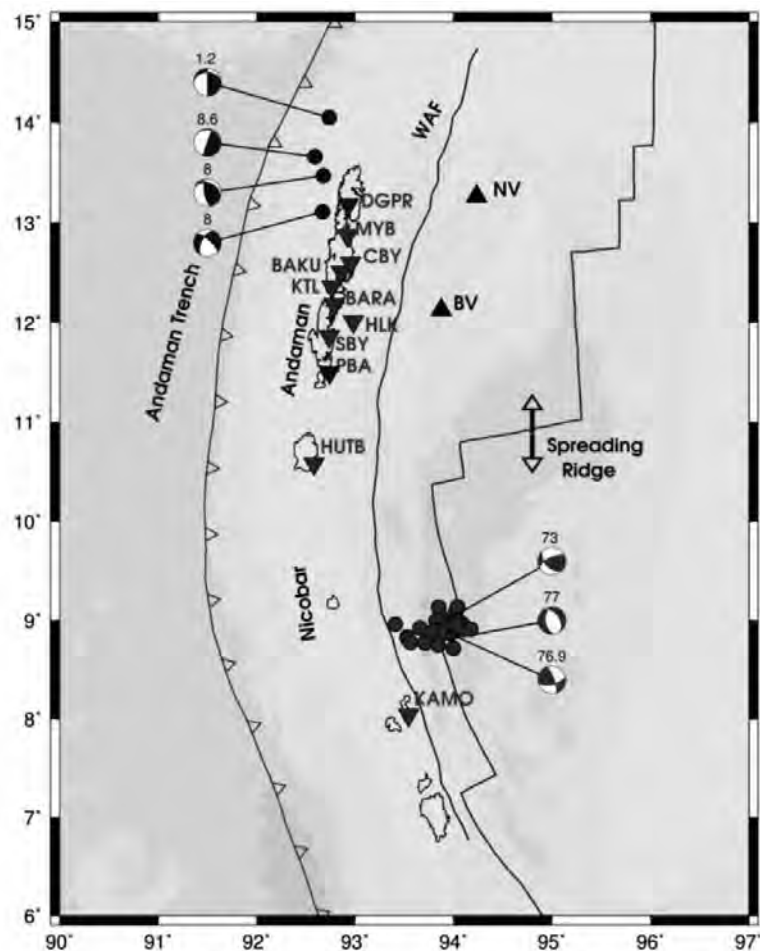


**Figure 6.** Focal mechanism solutions of swarm (near Nicobar) and non swarm (north Andaman) earthquakes obtained by moment tensor inversion. The black colour lines are the plate boundaries and faults. The numbers above the focal mechanisms indicate the values of the non-DC component.

**Table 2.** Epicentral parameters and focal mechanism solutions of the non-swarm events north of the 2012 swarm, including the distribution of DC and non-DC components of the moment tensor solutions.

| S. No. | Date       | Origin time | Lat   | Lon   | Depth (km) | M <sub>w</sub> | Centroid Depth (km) | Strike | Dip | Rake | DC   | Non-DC |      |       |
|--------|------------|-------------|-------|-------|------------|----------------|---------------------|--------|-----|------|------|--------|------|-------|
|        |            |             |       |       |            |                |                     |        |     |      |      | CLVD   | ISO  | Total |
| 1      | 2009/08/13 | 09:21:35    | 14.05 | 92.74 | 26         | 5.8            | 35                  | 180    | 90  | 119  | 98.8 | 0.5    | 0.7  | 1.2   |
| 2      | 2010/05/01 | 21:18:58    | 13.66 | 92.59 | 10         | 4.8            | 7                   | 180    | 89  | 100  | 91.4 | 1.7    | 6.9  | 8.6   |
| 3      | 2010/05/02 | 05:53:46    | 13.47 | 92.68 | 29.2       | 4.0            | 61                  | 173    | 72  | 113  | 91   | 7.1    | 1.9  | 9     |
| 4      | 2011/03/19 | 12:42:34    | 13.11 | 92.67 | 41.6       | 4.8            | 49                  | 209    | 55  | -22  | 79.3 | 0.1    | 20.6 | 20.7  |

non-DC components, a set of four earthquakes far from the 2012 swarm are chosen from the north Andaman region to calculate the moment tensor solutions. A clear match between synthetic and observed waveforms for the non-swarm events is observed, indicating a good correlation. A significantly low non-DC (or a high DC) percentage is observed for these events as expected (Table 2). The high DC (>90%) for the non-swarm events from the North Andaman indicates a pure tectonic origin in contrast to

the swarm events. On the contrary, a significant non-DC component in the 2012 swarm events indicates a non tectonic origin of the source.

For a comparison of swarm characteristics in the Andaman region, the moment tensor components of the 2005 swarm, about 100 km south of the 2012 swarm were computed from the Global CMT catalog data. The focal mechanism solutions of the strongest events of the 2005 swarm vary from a pure strike-slip to pure normal and a

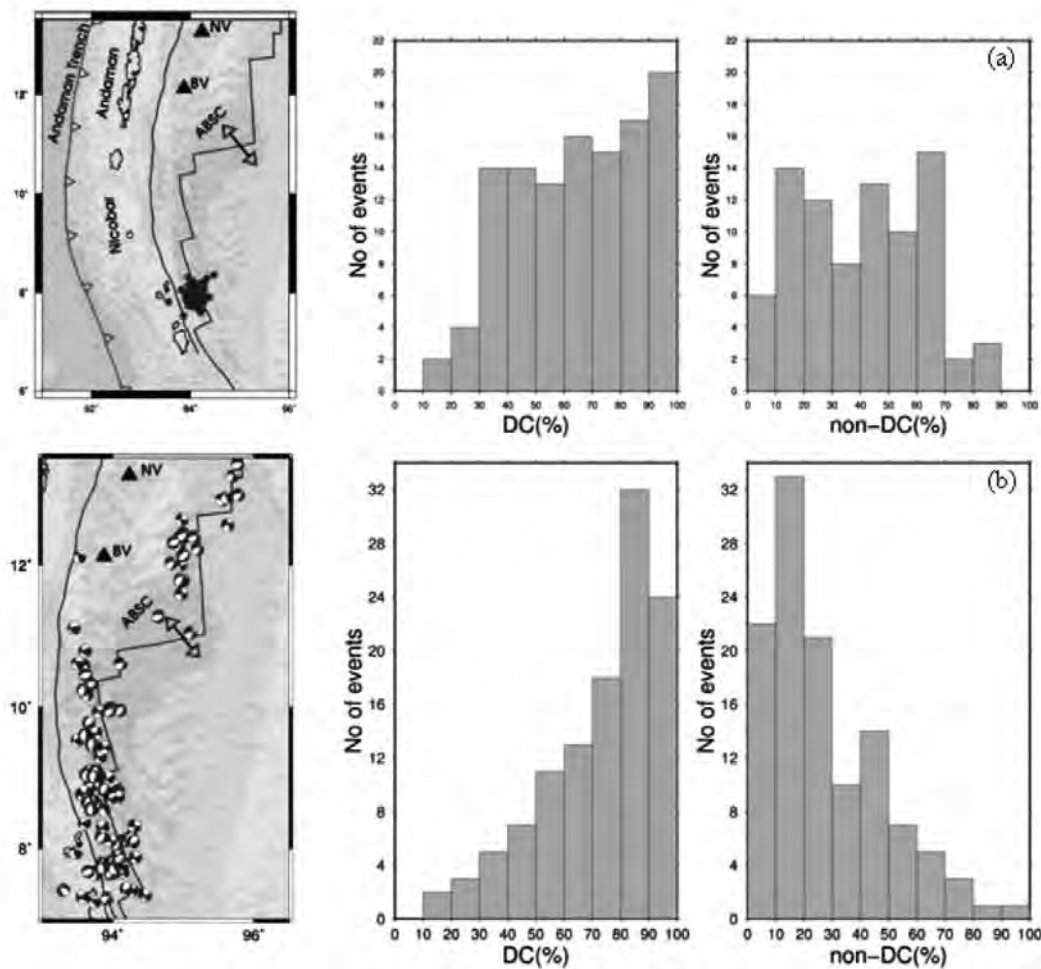


**Figure 7(a).** DC and non-DC percentages of (a) 2005 earthquake swarm calculated using the solutions from the CMT catalog, (b) earthquakes along the Andaman Back-Arc Spreading Centre calculated from the CMT catalog.

combination of both. Further, the ratio of the DC to non-DC moment tensor components is sometimes high and other times low (Figure 7a). This indicates an overlapping of both tectonic and volcanic source processes for the 2005 swarm, attributable to the mega thrust earthquake of December 2004, as also suggested by Kundu et al., (2012). In other words, the swarms originating in the ABSC seem to have a blend of tectonic and volcanic origin. Further, to understand whether all the non-swarm earthquakes in the ABSC also have a high non-DC component, we examined the moment tensor components of all the earthquakes within  $\pm 10$  km along the Andaman spreading centre from 1976 to 2013 (Figure 7b). Though the ABSC is only 300 km away from the Andaman trench, one of the most active subduction zones, interestingly a significant non-DC component is observed. This confirms that the earthquakes in the spreading centre are largely influenced by the magmatic/volcanic activity and not only the tectonic movements.

## CONCLUSIONS

The high non-DC component, comprising both CLVD and ISO, in the moment tensor solutions of the 2012 swarm earthquakes in the Andaman spreading ridge is attributed to ascension of magma at the spreading ridge coupled with inflation or deflation of magma chambers in the volcanic source region.

The 2005 swarm earthquakes on the other hand, show a predominance of both DC and non-DC components, indicating a mixture of tectonic as well as non-tectonic origin.

It is concluded that the 2012 swarm activity is linked to the magmatic activity at the Andaman spreading ridge.

## ACKNOWLEDGMENTS

The seismic networks operated by NGRI and IMD in the Andaman and Nicobar regions are supported by INCOIS,

Ministry of Earth Sciences, Government of India. We are grateful to Wessel and Smith, for the Generic Mapping Tools software (Wessel and Smith, 1998). It has been used for preparation of the figures. We are thankful to the two reviewers Dr. A. P. Singh and Dr. M. R. K. Prabhakar Rao, for their useful suggestions and comments. We are grateful to Dr.(Mrs.)Nandini Nagarajan for useful suggestions. Thanks are due to Dr.M.R.K.Prabhakar Rao for constructive editing. We thank the Chief Editor for his support and encouragement.

### Compliance with Ethical Standards

The authors declare that they have no conflict of interest and adhere to copyright norms.

### REFERENCES

- Aki, K., 1984. Evidence for magma intrusion during the Mammoth Lakes earthquakes of May 1980 and implications of the absence of volcanic (harmonic) tremor, *J. Geophys. Res.*, v.89, pp: 7689-7696.
- Bouchon, M., 1981. A Simple Method to Calculate Green's Functions for Elastic Layered Media, *Bull. Seism. Soc. Am.*, v.71, pp: 959-971.
- Coutant, O., 1989. *Programme de Simulation Numérique AXITRA*. Rapport LGIT, Université Joseph. Fourier, Grenoble, France.
- Curry, R. J., 1989. The Sunda arc: A model for oblique plate convergence, *Neth. J. Sea Res.*, v.24, pp: 131-140.
- Curry, J. R., 2005. Tectonics and history of the Andaman Sea region, *J. Asian Earth Sci.*, v.25, pp: 187-232.
- Curry, J. R., and Moore, D. G., 1974. Sedimentary and tectonic processes in the Bengal deep sea fan and geosynclines, in *The Geology of Continental Margins*, C. A. Burke and C. L. Drake (Editors), Springer Verlag, New York, pp: 617-627.
- Curry, J. R., Moore, D. G., Lawver, L. A., Emmel, F. J., Raitt, R. W., Henry, M., and Kieckhefer, R., 1979. Tectonics of the Andaman Sea and Burma, in *Geological and Geophysical Investigations of Continental Margins*, American Association of Petrochemical Geology, Memoir 29, pp: 189-198.
- Eguchi, T., Uyeda, S., and Maki, T., 1979. Seismotectonics and tectonic history of the Andaman Sea. In: S. Uyeda (Editor), *Processes at Subduction Zones*. *Tectonophysics*, v.57, pp: 35-51.
- Fitch, T. J., 1972. Plate convergence, transcurrent faults, and internal deformation adjacent to southeast Asia and western Pacific, *J. Geophys. Res.*, doi:10.1029/JB077i023p04432., v.77, no.23, pp: 4432-4460.
- Frohlich, C., and Apperson, K. D., 1992. Earthquake focal mechanisms, moment tensors and the consistency of seismic activity near plate boundaries. *Tectonics*, v.11, no.2, pp: 279-296.
- Geiger, L., 1910. Herbsbetimmung bei Erdbeben aus den Ankunftszeiten, K. Gessell. Wiss. Goett., v.4, pp: 331-349
- Geiger, L., 1912. Probability method for the determination of earthquake epicenters from the arrival time only, *Bull. St. Louis Univ.*, v.8, pp: 60-71.
- Hasegawa, H.S., and Kanamori, H., 1987. Source mechanism of the magnitude 7.2 Grand Banks earthquake of November 1929: double couple or submarine landslide?, *Bull. Seism. Soc. Am.*, v.77, pp: 1984-2004.
- Jochen, H. K., Thomas Jahr and Gerhard Jentzsch, 2004. Earthquake swarm examples and a look at the generation mechanism of the Vogtland/Western Bohemia earthquake swarms, *Physics of the Earth and Planetary Interiors*, v.142, pp: 75-88.
- Julian, B. R., 1983. Evidence for dyke intrusion earthquake mechanisms near Long Valley aldera, California, *Nature*, v.303, pp: 323-325.
- Julian, B.R., Miller A. D., and Foulger, G. R., 1997. Non-double-couple earthquake mechanisms at the Hengill-Grensdalur volcanic complex, southwest Iceland, *Geophys. Res. Lett.*, v.24, pp: 743-746.
- Julian, B.R., A. D. Miller and Foulger, G. R., 1998. Non-double-couple earthquakes 1: Theory, *Rev. Geophys.*, v.36, pp: 525-549.
- Julian, B. R., and Sipkin S. A., 1985. Earthquake processes in the Long Valley Caldera area, California, *J. Geophys. Res.*, v.90, pp: 11:155-11:169.
- Kamesh Raju, K. A., Ramprasad, T., Rao, P. S., Rao, B. R., and Varghese, J., 2004. New insights into the tectonic evolution of the Andaman basin, northeast Indian Ocean, *Earth Planet Sci. Lett.* doi:10.1016/S0012-821X(04)00075-5., v.221, no.1-4, pp:145-162.
- Kamesh Raju, K. A., Murty, G. P. S., Amarnath, D., and Kumar, M. L. M., 2007. The west Andaman fault and its influence on the aftershock pattern of the recent megathrust earthquakes in the Andaman-Sumatra region, *Geophys. Res. Lett.* L03305, doi:10.1029/2006GL028730., v.34, no.3.
- Kawasaki, I., and Tanimoto, T., 1981. Radiation patterns of body waves due to the seismic dislocation occurring in an anisotropic source medium, *Bull. Seism. Soc. Am.* v.71, pp: 37-50.
- Kikuchi, M., and Kanamori, H., 1991. Inversion of complex body waves, III, *Bull. Seism. Soc. Am.* v.81, no.6, pp: 2335-2350.
- Kundu, B., Legrand, D., Gahalaut, K., Gahalaut, V. K., Mahesh, P., Kamesh Raju, K. A., Catherine, J. K., Ambikapathy, A., and Chadha, R. K., 2012. The 2005 volcano-tectonic earthquake swarm in the Andaman Sea: Triggered by the 2004 great Sumatra-Andaman earthquake, *Tectonics*, 31, TC5009, doi:10.1029/2012TC003138.
- McCaffrey, R., 1992. Oblique plate convergence, slip vectors, and forearc deformation, *J. Geophys. Res.* doi:10.1029/92JB00483., v.97, no.B6, pp: 8905-8915.
- McCaffrey, R., 2009. The tectonic framework of the Sumatran subduction zone, *Annu. Rev. Earth Planet. Sci.*, doi:10.1146/annurev.earth.031208.100212., v.37, pp: 345-366

## Source Characteristics of the 2012 Earthquake Swarm Activity in the Andaman Spreading Ridge

- Mori, J., and McKee, C., 1987. Outward-dipping ring-fault structure at Rabaul caldera as shown by earthquake locations, *Science*, v.235, pp: 193–195.
- Mukhopadhyay, B., and Dasgupta, S., 2008. Swarms in Andaman Sea, India – a seismotectonic analysis. *ActaGeophys.*, doi: 10.2478/s11600-008-0039-5., v.56, pp: 1000-1014.
- Paige, C.C., and Saunders, M.A., 1982. LSQR: Sparse linear equations and least squares problems, *ACM Transactions on Mathematical Software* 8/2, pp: 195-209.
- Rodolfo, K. S., 1969. Bathymetry and Marine Geology of the Andaman Basin, and Tectonic Implications for Southeast Asia., doi: 10.1130/0016-7606(1969)80., v.80, pp: 1203-1230.
- Rao, N. P., Rao, C. N., Hazarika, P., Tiwari, V. M., Kumar, M. R., and Singh, A., 2011. Structure and tectonics of the Andaman subduction zone from modeling of seismological and gravity data, in *New Frontiers in Tectonic Research—General Problems, Sedimentary Basins and Island Arcs*, Evgenii V. Sharkov (Editor), InTech Publications, Janeza Trdine 9, 51000 Rijeka, Croatia, 978-953-307-595-2., pp: 249–268.
- Roland, E., and McGuire, J. J., 2009. Earthquake swarms on transform faults. *Geophysical Journal International.*, doi: 10.1111/j.1365-246X.2009.04214.x., v.178, pp: 1677–1690.
- Ross, A.G., Foulger, G.R., and Julian, B. R., 1996. Non-double-couple earthquake mechanisms at the Geysers geothermal area, California, *Geophys. Res. Lett.* v.23, pp: 877–880.
- Sokos, E., and Zahradník, J., 2008. ISOLA a Fortran code and a Matlab GUI to perform multiple-point source inversion of seismic data. *Compt. Rendus Geosci.*, [http://dx.doi.org/10.1016/j.cageo.2007.07.005.](http://dx.doi.org/10.1016/j.cageo.2007.07.005), v.34, no.8, pp: 967–977.
- Sokos, E., and Zahradník, J., 2013. Evaluating centroid-moment-tensor uncertainty in the new version of ISOLA software. *Seismological Research Letters*, v.84, no.4, pp: 656-665.
- Uyeda, S., and Kanamori, H., 1979. Back-arc opening and the mode of subduction. *J. Geophys. Res.*, v.84, pp: 1049-1061.
- Vavrycuk, V., 2002. Non-double-couple earthquakes of 1997 January in West Bohemia, Czech Republic: evidence of tensile faulting, *Geophys. J. Int.*, v.149, pp: 364–373.
- Waldhauser, F., and Ellsworth, W. L., 2000. A double-difference earthquake location algorithm: Method and application to the northern Hayward fault, *Bull. Seism. Soc. Am.*, v.90, pp: 1353-1368.
- Wessel, P., and Smith, W. H. F., 1998. New, improved version of Generic Mapping Tools released, *Eos Trans. AGU*, v.79, pp: 579.

# Groundwater quality in and around Tuticorin town, Southeast coast of India

Somvir Singh<sup>\*1</sup>, N.C. Mondal<sup>2</sup> and V.S. Singh<sup>2</sup>

<sup>1</sup>Central Ground Water Board (MoWR, River Development & Ganga Rejuvenation), Dehradun, India

<sup>2</sup>CSIR-National Geophysical Research Institute, Uppal Road, Hyderabad-500 007, India

\*Corresponding Author: somvirngri@gmail.com

---

## ABSTRACT

Rapid urbanization coupled with growth in agriculture and industries has led to deterioration of groundwater quality. The problem is severe in the coastal tracts due to salinity ingress since the last few decades. The present paper deals with a systematic hydrogeochemical study carried out in and around Tuticorin town covering an area of about 120 km<sup>2</sup> to assess groundwater quality. A total of 29 groundwater samples were collected and analyzed. Analysis of major ions has shown the anomalous values for total dissolved solids (TDS), sodium (Na<sup>+</sup>), magnesium (Mg<sup>2+</sup>), chloride (Cl<sup>-</sup>), and sulphate (SO<sub>4</sub><sup>2-</sup>) resulting in degradation of groundwater quality. Only 21% of samples are potable based on the TDS values. The order of major cations and anions obtained are Na<sup>+</sup> > Mg<sup>2+</sup> > Ca<sup>2+</sup> > K<sup>+</sup> and Cl<sup>-</sup> > SO<sub>4</sub><sup>2-</sup> > HCO<sub>3</sub><sup>-</sup> > NO<sub>3</sub><sup>-</sup> > F<sup>-</sup>, respectively. The results of these parameters were interpreted with the help of Piper, Wilcox and Gibbs diagrams apart from correlation matrix analysis. Cross plot of HCO<sub>3</sub><sup>-</sup>/Cl<sup>-</sup> (molar ratios) versus TDS indicated that about 72% of the analyzed samples are brackish and saline in nature. Out of them, about 42% samples are NaCl-type. On the basis of interpretation of US Salinity diagram, it is found that majority of the samples have very high salinity hazard and sodium hazard, and represent evaporation dominance.

**Key words:** Hydrochemistry, Drinking and Irrigation, Groundwater salinity, Coastal aquifer, Tuticorin town, Tamil Nadu and India.

---

## INTRODUCTION

Groundwater in a coastal tract is relatively vulnerable to contamination by sea water (Todd, 1980). It is of paramount importance to assess the suitability of groundwater for drinking, domestic and irrigation purposes. Saline water intrusion in coastal aquifers is a common global problem (Saxena et al., 2003; Batayneh, 2006; Singh et al., 2009; Mondal et al., 2010a; Antony Ravindran et al., 2015). This phenomenon can be attributed to a variety of factors like gentle coastal hydraulic gradients, tidal and estuarine environments, sea level rise, excessive groundwater withdrawal and local hydrogeological conditions (Rajmohan et al., 2000, Saxena et al., 2004, Sherif and Kacimov, 2007; Mondal et al., 2008; Kim et al., 2009). However, natural hazards like tidal waves and tsunami engulfing the coastal regions also result in the percolation of seawater into shallow and unconfined aquifers (Villholth et al., 2006). One of the most common methods for assessing the extent of saline water ingress in coastal aquifers is through periodic analysis of groundwater chemistry (Sukhija et al., 1996; Saxena et al., 2003; Sarwade et al., 2007; Kim et al., 2009). In case of seawater intrusion, groundwater generally exhibits high concentrations not only in total dissolved solids and major ions (Richter and Kreitler, 1993) but also enrichment of selective trace elements (Saxena et al., 2004; Mondal et al., 2010b).

Tuticorin town, a part of the southeastern coast of Tamil Nadu, is chosen as the study area which is affected by seawater ingress as well as in-situ salinity in the geological past. The objective of this paper is to characterize groundwater quality of shallow coastal aquifers by identifying hydrogeochemical facies. This will help in providing a better understanding of possible changes in groundwater quality with the rapidly developing coastal belt in and around Tuticorin town. In order to understand the pollution, it is essential to have knowledge of the natural baseline quality so that the imposed environmental change can be measured with an acceptable degree of confidence (Edmunds et al., 2003).

## The Study Area

The study area, Sterlite Industries India Ltd. (SIIL) watershed, covering an area of about 112 km<sup>2</sup> lies between 78.04 to 78.17°E longitudes and 8.77 to 8.85°N latitudes. It is situated in the eastern part of Tuticorin district along the eastern coastal belt of Tamil Nadu, India. (Figure 1). The topographic elevation varies from 26.22 m above mean sea level (amsl) in the east near Tuticorin town to the sea level near sea. The study area receives a good amount of rainfall (average 568 mm) during the northeast monsoon season between October and December of each year. The long-term average annual rainfall at Tuticorin

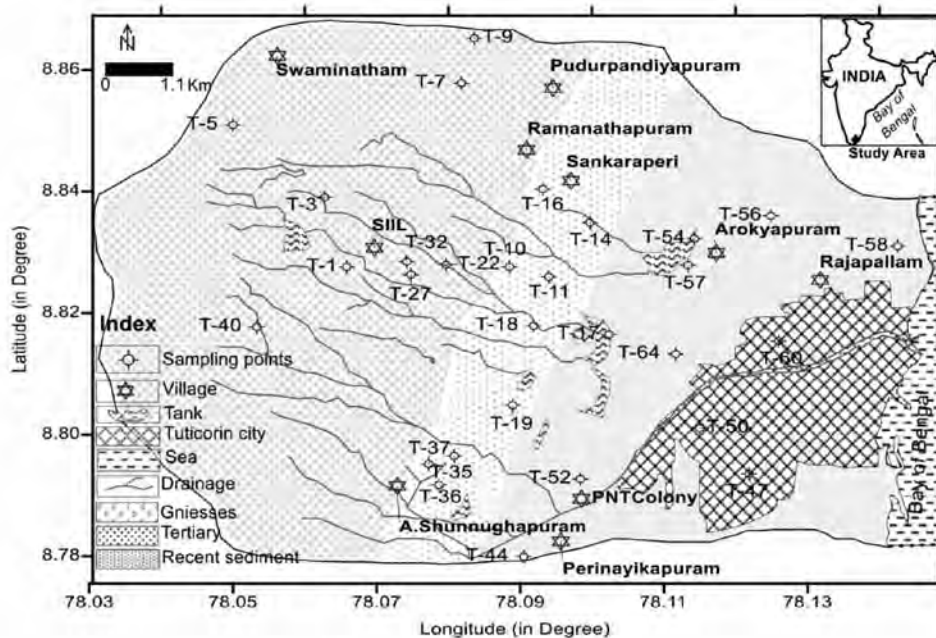


Figure 1. Location of the study area along with monitoring wells.

town is about 568 mm (IMD data) (Singh et al., 2006; Rangarajan et al., 2009).

Geomorphologically, the study area consists of flood plains, deltaic plain and natural levees. The slope of the topography is gentle in the western and central parts, but nearly flat in the eastern part of the watershed. Geologically, the area is underlain by rocks of Archaean age and recent alluvium. The Archaean rocks are mainly foliated crystalline igneous and metamorphic rocks trending in NW–SE direction (Balasubramanian et al., 1993). The quartzite ridges in the western part are weathered, jointed and fractured. Sub-recent alluvium sands characterize the coastal areas along with coarse and calcareous grits, sandstones, shales and limestones. The watershed area is covered with black soil in the western part (in and around the SIIL Plant), red soil (sandy loam to sandy soil) in the central part and alluvial sandy soil in the eastern part. The maximum soil thickness is about 3.0 m. The sandy soil derived from sandstones has low soil moisture content. The alluvial soil is windblown, derived mainly from sands and shales including the beach sand and coastal dunes, which has low soil moisture content.

Systematic hydrogeological survey was also carried out during the year 2007 covering a number of hand pumps, dug wells and boreholes tapping shallow unconfined alluvial and fractured aquifer systems. The depth of dug wells ranges from 7 to 12 m, while the borehole depth varies from a few metres to a maximum of 70 m (bgl) (Singh et al., 2006). The sandy zone constitutes the main aquifer system in the alluvium areas while the fractured rocks too are water yielders (Mondal et al., 2009). The depth to

groundwater level during the pre-monsoon season varies from 1.8 to 14.4 m bgl whereas in the post-monsoon season, it varies from 0.9 to 12.9 m bgl (Rangarajan et al., 2009).

## MATERIALS AND METHODS

The analysis of water samples was carried out following Brown et al. (1983) and APHA (1985) methodologies. pH, TDS and EC were measured in in-situ condition by using portable EC and pH meters. Sodium ( $\text{Na}^+$ ) and potassium ( $\text{K}^+$ ) were determined by atomic absorption spectrophotometer (AAS). Total hardness (TH) as  $\text{CaCO}_3$ , calcium ( $\text{Ca}^{2+}$ ), hydrogen carbonate ( $\text{HCO}_3^-$ ), and chloride ( $\text{Cl}^-$ ) were analyzed by volumetric methods. Magnesium ( $\text{Mg}^{2+}$ ) was calculated from TH and  $\text{Ca}^{2+}$  contents. Sulfate ( $\text{SO}_4^{2-}$ ) was estimated adopting the spectrophotometric technique, whereas nitrate ( $\text{NO}_3^-$ ) was determined by ion chromatography and fluoride ( $\text{F}^-$ ) by fluoride meter. All concentrations were expressed in milligrams per litre (mg/l), except pH and EC.

## RESULTS AND DISCUSSION

### General groundwater chemistry

The results of chemical analysis (carried out at CSIR-NGRI) are summarized in Table 1. The pH in the groundwater samples varies from 7.10–8.67. Comparison of hydrogeochemical data with drinking water standards of WHO (1993) shows that about 82.8% (N = 24), 75.9%

**Table 1.** Results of hydrogeochemical parameters collected in and around Tuticorin town, Southern India.

| Sl. No. | Well code | Village Name                  | Longitude | Latitude | pH   | EC    | TDS   | TH   | Ca <sup>2+</sup> | Mg <sup>2+</sup> | Na <sup>+</sup> | K <sup>+</sup> | Cl <sup>-</sup> | SO <sub>4</sub> <sup>2-</sup> | HCO <sub>3</sub> <sup>-</sup> | NO <sub>3</sub> <sup>-</sup> | F <sup>-</sup> |
|---------|-----------|-------------------------------|-----------|----------|------|-------|-------|------|------------------|------------------|-----------------|----------------|-----------------|-------------------------------|-------------------------------|------------------------------|----------------|
| 1       | T-1       | Terku Virapadiyapuram         | 78.066    | 8.828    | 7.60 | 3850  | 2464  | 280  | 64               | 29               | 288             | 10             | 103             | 385                           | 268                           | 8                            | 0.88           |
| 2       | T-3       | Kumargiri                     | 78.063    | 8.839    | 7.70 | 3370  | 2157  | 1032 | 275              | 83               | 271             | 8              | 220             | 914                           | 293                           | 25                           | 0.43           |
| 3       | T-5       | Swaminatham (S)               | 78.050    | 8.851    | 7.42 | 6000  | 3840  | 1800 | 400              | 192              | 478             | 16             | 1029            | 1142                          | 180                           | 40                           | 1.30           |
| 4       | T-7       | Nayinapuram                   | 78.082    | 8.858    | 7.80 | 500   | 320   | 96   | 16               | 13               | 76              | 2              | 14              | 5                             | 293                           | 1                            | 0.91           |
| 5       | T-9       | Pudur Pandiyapuram            | 78.084    | 8.865    | 7.70 | 400   | 256   | 112  | 22               | 13               | 52              | 2              | 21              | 17                            | 220                           | 1                            | 1.12           |
| 6       | T-10      | Pandarampatti                 | 78.088    | 8.828    | 7.80 | 7900  | 5056  | 1600 | 256              | 230              | 1260            | 151            | 1136            | 2439                          | 415                           | 54                           | 2.59           |
| 7       | T-11      | Pandarampatti (W)             | 78.094    | 8.826    | 7.40 | 2230  | 1427  | 736  | 170              | 75               | 134             | 6              | 355             | 384                           | 146                           | 15                           | 0.50           |
| 8       | T-14      | Sankarapereri (E)             | 78.100    | 8.835    | 7.10 | 6300  | 4032  | 4880 | 816              | 681              | 28              | 140            | 4082            | 1089                          | 265                           | 27                           | 0.79           |
| 9       | T-16      | Ramanathampuram               | 78.093    | 8.840    | 7.37 | 1846  | 1181  | 4320 | 832              | 538              | 267             | 16             | 2840            | 476                           | 488                           | 26                           | 0.25           |
| 10      | T-17      | Silverpuram                   | 78.102    | 8.816    | 7.32 | 10380 | 6643  | 1080 | 192              | 144              | 5.6             | 41             | 1065            | 492                           | 244                           | 20                           | 7.23           |
| 11      | T-18      | Milavittam                    | 78.092    | 8.818    | 7.39 | 4600  | 2944  | 1600 | 368              | 163              | 557             | 30             | 1526            | 397                           | 317                           | 25                           | 0.99           |
| 12      | T-19      | Madathur (N)                  | 78.089    | 8.805    | 7.44 | 2200  | 1408  | 800  | 128              | 115              | 175             | 11             | 532             | 222                           | 244                           | 13                           | 0.65           |
| 13      | T-22      | SIIL-II (N, PZ-11)            | 78.080    | 8.828    | 7.76 | 12290 | 7866  | 2360 | 464              | 288              | 1317            | 126            | 1171            | 2856                          | 854                           | 63                           | 0.60           |
| 14      | T-27      | SIIL-VII (W, PZ-2)            | 78.075    | 8.826    | 7.68 | 5300  | 3392  | 1800 | 608              | 67               | 166             | 5              | 390             | 1346                          | 220                           | 35                           | 6.76           |
| 15      | T-32      | SIIL-XI (N)                   | 78.074    | 8.828    | 7.46 | 7300  | 4672  | 2480 | 448              | 326              | 1575            | 140            | 923             | 4226                          | 415                           | 45                           | 5.33           |
| 16      | T-35      | Aynaduppu                     | 78.081    | 8.797    | 8.10 | 5230  | 3347  | 1840 | 368              | 221              | 382             | 21             | 568             | 1577                          | 293                           | 15                           | 0.68           |
| 17      | T-36      | Shunmughapura                 | 78.079    | 8.792    | 7.87 | 3100  | 1984  | 1880 | 304              | 269              | 103             | 3              | 568             | 1016                          | 268                           | 30                           | 0.92           |
| 18      | T-37      | Kailashpuram                  | 78.077    | 8.795    | 8.08 | 200   | 128   | 88   | 22               | 8                | 6               | ND             | 7               | 10                            | 98                            | ND                           | 0.32           |
| 19      | T-40      | Vadakka Silukkanpatti (E)     | 78.053    | 8.818    | 8.57 | 3300  | 2112  | 80   | 10               | 13               | 131             | 2              | 28              | 101                           | 268                           | 3                            | 0.67           |
| 20      | T-44      | Periyanayakapuram             | 78.090    | 8.780    | 8.12 | 4800  | 3072  | 880  | 128              | 134              | 808             | 45             | 1420            | 432                           | 293                           | 14                           | 1.67           |
| 21      | T-47      | Levinipuram                   | 78.122    | 8.794    | 7.77 | 4500  | 2880  | 800  | 128              | 115              | 839             | 24             | 923             | 517                           | 634                           | 15                           | 0.44           |
| 22      | T-50      | Seetapuram Nagar              | 78.115    | 8.801    | 8.10 | 1700  | 1088  | 560  | 144              | 48               | 355             | 17             | 355             | 440                           | 464                           | 16                           | 0.74           |
| 23      | T-52      | PNT Colony (S)                | 78.098    | 8.793    | 7.32 | 900   | 576   | 240  | 67               | 17               | 23              | 0.78           | 21              | 77                            | 220                           | 2                            | 0.21           |
| 24      | T-54      | Mappali Urani                 | 78.114    | 8.832    | 7.33 | 12600 | 8064  | 920  | 192              | 106              | 1960            | 103            | 1775            | 480                           | 244                           | 14                           | 0.38           |
| 25      | T-56      | Davishpuram                   | 78.125    | 8.836    | 7.46 | 9100  | 5824  | 2200 | 320              | 336              | 1475            | 76             | 3209            | 733                           | 244                           | 20                           | 0.78           |
| 26      | T-57      | Arokayipuram                  | 78.113    | 8.828    | 7.62 | 7200  | 4608  | 1120 | 192              | 154              | 977             | 61             | 1775            | 484                           | 366                           | 18                           | 0.92           |
| 27      | T-58      | Rajapallam                    | 78.143    | 8.831    | 8.00 | 2100  | 1344  | 72   | 13               | 9                | 247             | 10             | 128             | 72                            | 439                           | 5                            | 2.63           |
| 28      | T-60      | SBI Colony (St. Ann's School) | 78.126    | 8.815    | 7.72 | 2800  | 1792  | 448  | 90               | 54               | 373             | 16             | 248             | 240                           | 464                           | 2                            | 0.94           |
| 29      | T-64      | Chinakannupur                 | 78.112    | 8.813    | 7.34 | 17597 | 11262 | 3760 | 688              | 490              | 2443            | 179            | 5786            | 826                           | 317                           | 32                           | 1.22           |

pH:  $-\log_{10}H^+$  at 25°C; EC in  $\mu S/cm$ , All Ions in mg/l; TH total hardness as CaCO<sub>3</sub>; the samples were collected on April 2007, ND: Not detected.

(N = 22), 75.9% (N = 22), and 65.5% (N = 19) of the samples exceeded the upper limit for total dissolved solids (TDS=500 mg/l), magnesium (Mg<sup>2+</sup>=30 mg/l), chloride (Cl<sup>-</sup> =200 mg/l) and sodium (Na<sup>+</sup> = 200 mg/l), respectively. This indicates significant water quality deterioration in the study area.

To ascertain the suitability of groundwater for various purposes, it is essential to classify the groundwater based on their TDS values (Freeze and Cherry, 1979). The classification of groundwater based on the TDS shown that about 21% are fresh, 3% are saline and rest of the samples are moderately fresh (76%). It also indicates that only 17% of the samples falling below 500 mg/l of TDS which can be used for drinking purpose without any risk (Table 2).

The contour map of TDS (Figure 2) clearly shows that a higher value of TDS > 3000 mg/l was observed in the middle part covering more than 50% of the area, in particular, at the wells T-10, 19, 18, 14, 16, 56, 57, 54, 64, 47, and SIIL premises. Similarly, wells T-35 and 44 in the southern part and well T-5 in the north western part were also affected with higher TDS values (>3000 mg/l). This may indicate the possibility of a high rate of sea water intrusion in the middle, southern and north-western parts of the study area, where a high rate of withdrawal of groundwater was also observed (Mondal et al., 2009). It is noticed that the central and eastern parts are comparatively more populated, have larger industries and also have a large concentration of number of dug, tube, and bore wells (Singh

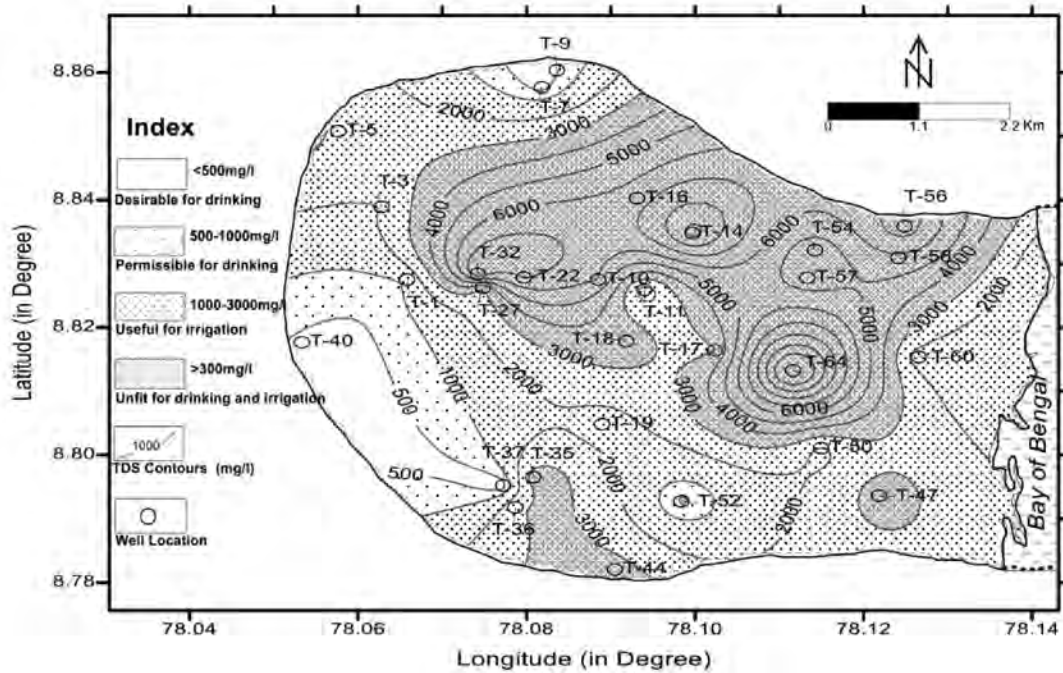


Figure 2. TDS contour map of the study area.

Table 2. Classification of the groundwater samples in the study area (Freeze and Cherry, 1979).

| Total dissolved solids (TDS) | Water type | Samples  | No. of samples | % of samples |
|------------------------------|------------|--|----------------|--------------|
| <1,000                       | Fresh      | T-7, 9, 37, 40, 52 and 58  | 6              | 21           |
| 1,000-10,000                 | Brackish   | T-1, 3, 5, 10, 11, 14, 16, 17, 18, 19, 22, 27, 32, 35, 36, 44, 47, 50, 54, 56, 57 and 60 | 22             | 76           |
| 10,000-1, 00, 000            | Saline     | T-64   | 1              | 3            |
| >1, 00, 000                  | Brine      | Nil  | Nil            | Nil          |
| Total                        |            |  | 29             | 100          |

et al., 2006). The TDS in groundwater was observed as low as 126 mg/l in the village of Kailashpuram well (no. T-37), which indicates the availability of fresh groundwater because of its proximity to tanks and recharge area.

### Cation chemistry

The concentration of  $Ca^{2+}$  in groundwater was found to be in the range of 10 to 832 mg/l, in the study area. Similarly, the concentrations of  $Mg^{2+}$  in 75% samples were found to be above the permissible limit of 50 mg/l (WHO, 1993). Sodium ( $Na^+$ ) is one of the important naturally occurring cation and its concentration in fresh waters is generally lower than that of  $Ca^{2+}$  and  $Mg^{2+}$ . The average concentration of  $Na^+$  comparatively is higher than that of  $Ca^{2+}$  and  $Mg^{2+}$  corroborating with earlier results

(Balasubramanian et al., 1993). The values of  $Na^+$  range between 6 and 2443 mg/l with average of 578 mg/l. It is observed that 65% of samples were above the permissible limit. The geological influence on the concentration of the cations is quite apparent as the study area is underlain by mainly granite gneisses. The concentration of potassium shows very low in the study area. Only 24% of samples are above permissible limit with an average of 45 mg/l in the groundwater samples. The total hardness (TH) varies from 72 to 4880 mg/l. The maximum allowable limit of TH for drinking purpose is 500 mg/l and the most desirable limit is 100 mg/l as per the WHO International standard. But the most desirable limit is 80–100 mg/l (Freeze and Cherry, 1979). Groundwater exceeding the limit of 300 mg/l (Table 3) is considered to be very hard (Sawyer and McMcarty, 1967).

**Table 3.** Groundwater classification based on total hardness (Sawyer and McMcarty, 1967).

| Total Hardness as CaCO <sub>3</sub> (in mg/l) | Type of water   | Sample numbers   | Number of samples | Percentage of samples |
|---|-----------------|--|-------------------|-----------------------|
| <75   | Soft            | T-58   | 1                 | 3                     |
| 75-150  | Moderately high | T-7,9,37 and 52  | 4                 | 14                    |
| 150-300                                       | Hard            | T-1 and 52   | 2                 | 7                     |
| >300  | Very hard       | T-3, 5,10, 14, 17, 18, 19, 22, 27, 32, 35, 36, 44, 47, 50, 54, 56, 57, 58, 60 and 64 | 22                | 76                    |
| Total   |                 |  | 29                | 100                   |

**Table 4.** Hydrogeochemical facies for the groundwater samples.

| Facies                       | Sample numbers                                     | No. of samples | % of samples |
|------------------------------|--|----------------|--------------|
| NaCl                         | T-1, 10, 22, 32, 44, 47, 50, 54, 56, 57, 60 and 64 | 12             | 42           |
| CaCl <sub>2</sub>            | T-5, 11, 14, 16, 17, 27, 35 and 36                 | 8              | 28           |
| Mixed Ca-Ma-Cl <sub>2</sub>  | T-3, 18 and 19                                     | 3              | 10           |
| Mixed Ca-Na-HCO <sub>3</sub> | T-9, 40 and 58                                     | 3              | 10           |
| Ca-HCO <sub>3</sub>          | T-37 and 52  | 2              | 7            |
| Na-HCO <sub>3</sub>          | T-7  | 1              | 3            |
| Total                        |  | 29             | 100          |

### Anion chemistry

The chloride (Cl<sup>-</sup>) content of samples varies between 7 to 5786 mg/l (an average: 1111 mg/l). Of the total samples, 22% of samples are exceeding the permissible limit. Similarly, 80% of the dug well samples show bicarbonate (HCO<sub>3</sub><sup>-</sup>) above the permissible limit with a wide variation in concentration between 98 and 854 mg/l with an average concentration of 327 mg/l. Sulphate concentration ranges from 5 to 4224 mg/l with about 79% of samples above the permissible limits. Only 10% of samples reveal nitrate concentration above permissible limit. Though the nitrate in the samples was ranging from 1 to 63 mg/l; the average shows slightly higher value (21 mg/l) as observed at the well no. T-22 (63 mg/l) and well T-10 (54 mg/l). Being loosely bound to soils, nitrate is expected to be more in runoff.

Fluoride values in the study area varies from 0.21 to 7.23 mg/l against the permissible limit of 1.50 mg/l (WHO, 1993) which can be attributed not only to mere presence of fluoride bearing minerals in rocks but also to the degree of weathering and leachable fluoride in the study area. The distribution of fluoride is quite sporadic and marked differences in concentrations are observed within very short distances with values less than 1.5mg/l in 24 samples and higher in only 5 samples. In the present case, the study area is underlain by crystalline formations such as charnockite and granitic gneiss which comprise quartz, feldspars (potash feldspars and albite), hornblende, biotite, etc. The acid charnockite of this area has quartz,

k-feldspars, hypersthene, and biotite minerals of coarse-grained nature, which are potential sources of fluoride.

### Hydro-geochemical facies

Chemical data of the groundwater samples are plotted on a Piper trilinear diagram (Piper, 1953). It provides a convenient way to classify and compare water types. The concentrations of major anions and cations were plotted in two trilinear diagrams and diamond shaped field of Piper diagram. On the basis of chemical analysis of water, it is divided into mainly six facies (Figure 3). The hydrogeochemical facies of water are summarized in Table 4. It is observed that Na-Cl type of water dominates the study area. The percentage of samples falling under the Na-Cl, Ca-Cl<sub>2</sub>, mixed Ca-Na-HCO<sub>3</sub> and Ca-Mg-Cl<sub>2</sub>, Ca-HCO<sub>3</sub> and Na-HCO<sub>3</sub> types are 42%, 28%, 10%, 10%, 7% and 3 %, respectively.

### Correlation analysis and cross plots

The correlation matrix indicates the degree of linear relationship between the independent and dependent variables (Nair et al., 2005). The EC strongly correlates with Na<sup>+</sup> (0.82), K<sup>+</sup> (0.81), TDS (0.77) and Cl<sup>-</sup> (0.69). Chloride (Cl<sup>-</sup>) shows high correlation with TDS (0.89), Mg<sup>2+</sup> (0.84), Ca<sup>2+</sup> (0.72), K<sup>+</sup> (0.71) and Na<sup>+</sup> (0.60). The results of correlation matrix show that the dissolved ions in the groundwater are responsible for EC. Likewise, NO<sub>3</sub><sup>-</sup> ions

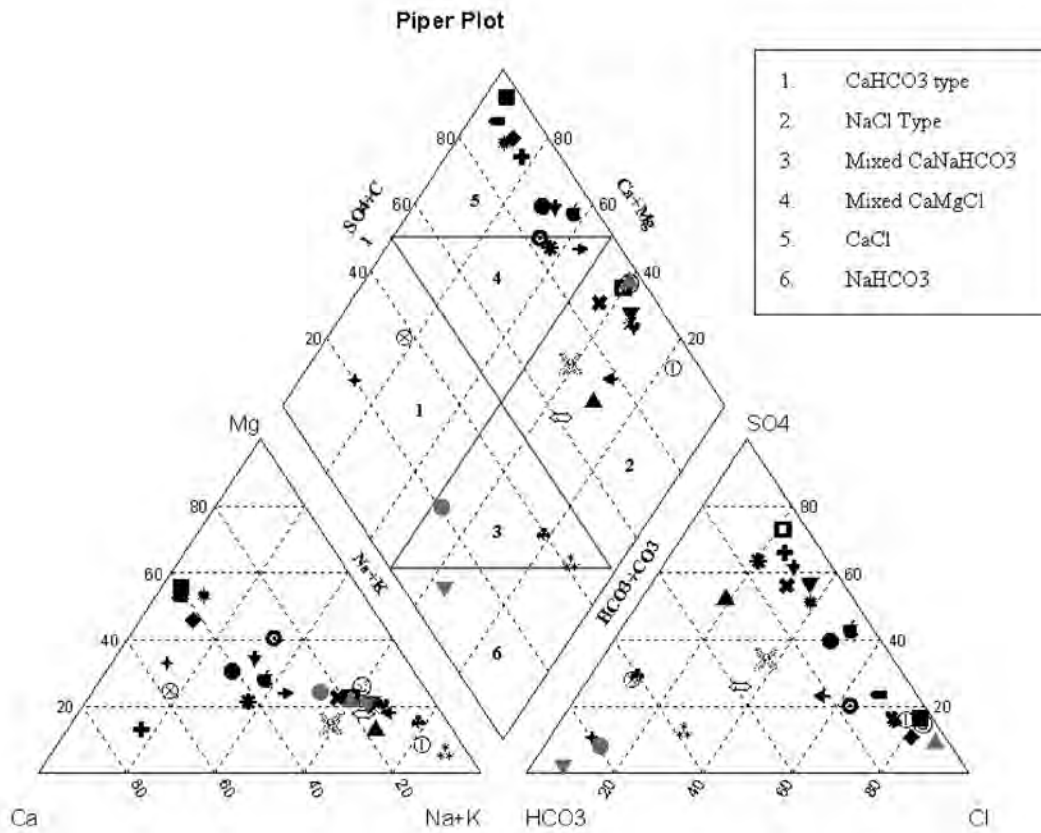


Figure 3. Piper diagram depicting hydrogeochemical facies of groundwater.

showed moderate to high correlation with  $\text{SO}_4^{2-}$  (0.82), TDS (0.65),  $\text{Ca}^{2+}$  (0.63) and  $\text{K}^+$  (0.63) during the study period. A significant correlation has been noticed between  $\text{K}^+$  with EC and TDS. The major exchangeable ions  $\text{Na}^+$  and  $\text{Ca}^{2+}$ ;  $\text{Na}^+$  and  $\text{Mg}^{2+}$  correlate positively as observed in the study area. It can therefore be postulated that the concurrent increase/decrease in the composition of ions in these waters is predominantly due to dissolution/precipitation reaction and concentration effects.

Sodium and chloride are the dominant ions of seawater/saline water, while calcium and bicarbonate are generally the major ions of fresh water (Hem, 1989). Thus, High levels of  $\text{Na}^+$  and  $\text{Cl}^-$  ions in coastal groundwater may indicate a significant effect of seawater mixing and occurrence of saline water (Mondal et al., 2008); while considerable amounts of  $\text{HCO}_3^-$  and  $\text{Ca}^{2+}$  mainly reflect the contribution from the water-rock interaction. A plot of  $\text{HCO}_3^-/\text{Cl}^-$  versus TDS (Figure 4) showed that the values of  $\text{HCO}_3^-/\text{Cl}^-$  (molar ratios) were  $<1.0$  in the high TDS concentration ( $>1,000$  mg/l) range of 72% analyzed samples, while its slope was steep negative in the low TDS concentration range ( $<1000$  mg/l). This result may indicate that groundwater with high TDS concentration is enriched with chloride due to seawater intrusion/saline

water occurrence, and that groundwater with low TDS concentration is not or less affected by seawater/saline water.

### Drinking water quality

The chemical parameters of groundwater samples are compared with the standard values of the World Health Organization (WHO, 1993) for drinking and public health standards. Based on the permissible limits of all aspects i.e., TDS (500 mg/l), TH (200 mg/l),  $\text{Ca}^{2+}$  (75 mg/l),  $\text{Mg}^{2+}$  (30 mg/l),  $\text{Na}^+$  (200 mg/l),  $\text{K}^+$  (100 mg/l),  $\text{Cl}^-$  (200 mg/l),  $\text{SO}_4^{2-}$  (200 mg/l),  $\text{HCO}_3^-$  (200 mg/l),  $\text{NO}_3^-$  (45 mg/l) and F (1.50 mg/l) in groundwater, the well no. 37 (village: Kailashpuram) is the only suitable one for drinking purpose.

### Irrigation water quality

Chemical data of groundwater sample in the area had been studied with respect to sodium hazards and are plotted in Wilcox diagram (Richards, 1954) as shown figure 5. In this diagram, Sodium Adsorption Ratio (SAR) vis-à-vis EC classifies the water according to sodium hazard (C1, C2, C3 and C4) and salinity hazard (S1, S2, S3 and S4) expressed as low, medium, high and very high, respectively (Piper,

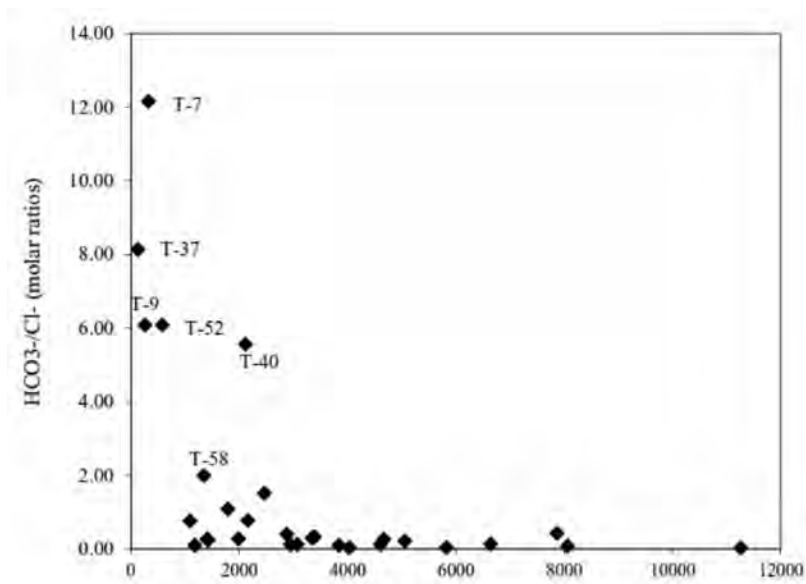


Figure 4. Cross plots of molar ratios of  $\text{HCO}_3^-/\text{Cl}^-$  with TDS.

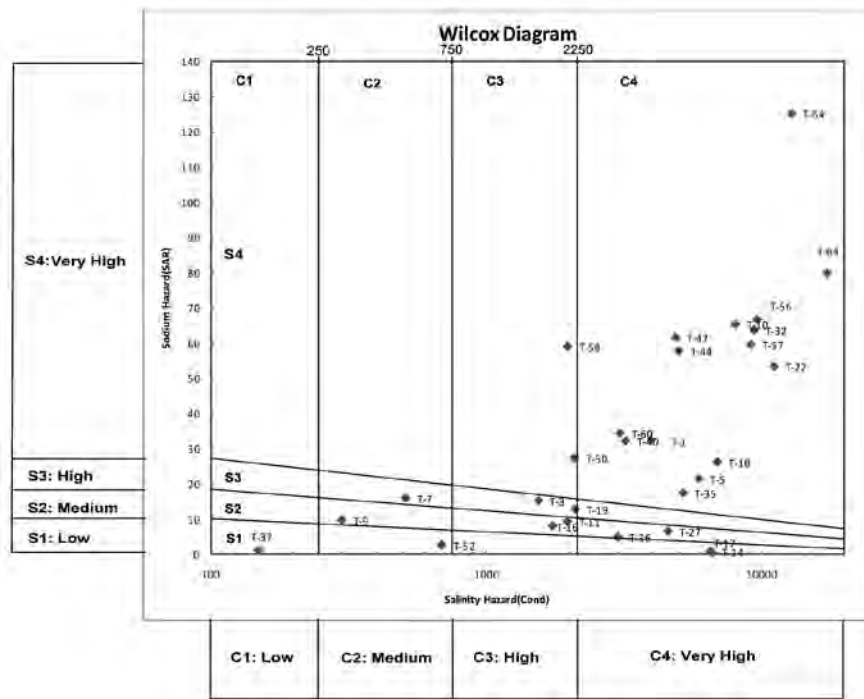


Figure 5. Wilcox diagram of the groundwater samples in the study area.

1953). Water from well nos. T-10 and T-11 are showing medium salinity and low sodium hazard and can be used for drinking purpose. The well nos. T-16, T-19 and T-52 are showing high salinity and low sodium hazard and this kind of water cannot be used for drinking purpose. The most important finding is from well nos. T-1, 3, 18, 36, 40 and T-60 which show very high salinity and medium sodium hazard and such type of waters cannot be used for

drinking purpose. The study reveals very high salinity and low sodium hazard at well nos. T-14, 17 and very high salinity and high sodium hazard at well T-35, medium salinity and sodium hazard at well T-9 and 27, medium salinity and high sodium hazard at well T-7. Wells T-50 and 58 are not suitable for irrigation purpose due to high salinity and very high sodium hazard. The sample no. T-37 is found only with low salinity and low sodium

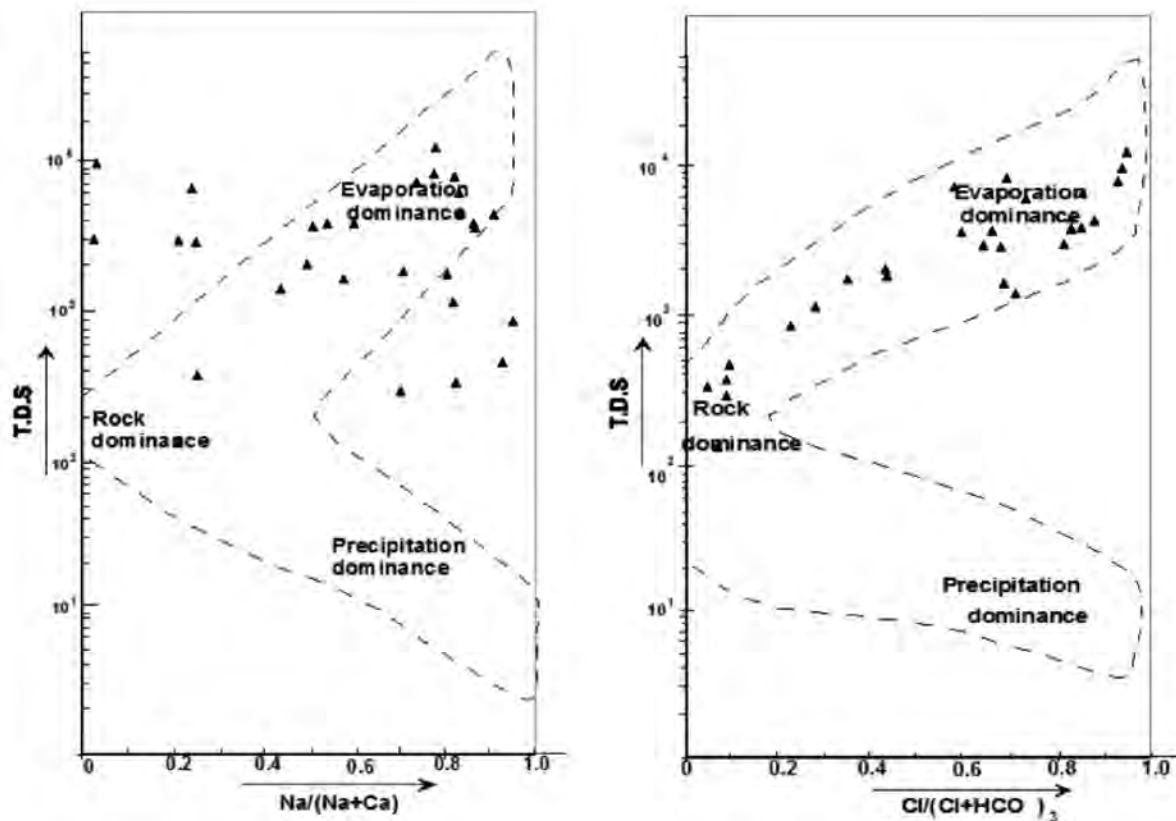


Figure 6. Gibbs diagram showing the rates of evaporation and rock dominance samples.

hazard, and this water can be used for both drinking and irrigation purposes. Water from well nos. T-5, 22, 32, 44, 47, 54, 56, 57 and T-64 are very high in both the classes and hence unsuitable for domestic as well as irrigation purpose. The study area nearby the coastal region covered by the well numbers T-44, 47, 54, 56, 57, 60, 64 (recent to sub-recent sediments) shows very high salinity due to sea water intrusion.

### Mechanism controlling groundwater chemistry

Lastly, to know the groundwater chemistry and relationship of the chemical components of groundwater from their respective aquifers such as chemistry of the rock types, chemistry of precipitated water and rate of evaporation, Gibbs (1970) has suggested a diagram in which ratios of dominant anions and cations are plotted against the values of total dissolved solids (TDS), representing the ratio-I for cations  $[(Na^+)/[Na^+ + Ca^{2+}]]$  and ratio-II for anions  $[Cl^- / (Cl^- + HCO_3^-)]$  as a function of TDS to assess the functional sources of dissolved chemical constituents, such as precipitation-dominance, rock-dominance and evaporation dominance. The chemical data of groundwater samples were plotted on the Gibbs diagram (Figure 6). It is found that about 38% of samples suggest chemical

weathering of rock-forming minerals and is influencing the groundwater quality by means of dissolution of rocks through which water is circulating. But 62% of samples represent evaporation dominance and most of the samples falling in the evaporation dominance are collected from dug wells in the close proximity to the sea. Evaporation makes salinity increase by increasing  $Na^+$  and  $Cl^-$  with relation to the increase of TDS. In addition, anthropogenic activities (agricultural fertilizers) and irrigation return flows also influence the evaporation by the increasing  $Na^+$  and  $Cl^-$ , and thus TDS.

### CONCLUSIONS

In order to assess the groundwater quality in Tuticorin area of Tamil Nadu, groundwater samples had been collected and analyzed. The pH values of groundwater, in general, are slightly basic in nature (average = 7.67). The TDS values of nearly 79% of the samples exceed the upper limit of drinking water as per WHO standards. About 83% of samples are hard and very hard types with majority cations showing values above permissible limits for drinking water. The order of abundance of cations is  $Na^+ > Mg^{2+} > Ca^{2+} > K^+$ . Among major anions,  $Cl^-$  and  $SO_4^{2-}$  are generally dominant representing of 90% and 80%, respectively. The

order of anionic abundance is in the order of  $\text{Cl}^- > \text{SO}_4^{2-} > \text{HCO}_3^- > \text{NO}_3^- > \text{F}^-$ . The irrigation water quality studies show that about 90% samples fall beyond permissible limits, hence are not suitable for agricultural purpose. Based on the relative dominance of major cations and anions, different hydrogeochemical facies have been identified and majority of the samples are represented by Na-Cl and Ca-Cl<sub>2</sub>-types of water. Quality of groundwater in the open well samples are mainly by evaporation while remaining samples are dominated by chemical weathering of rock forming minerals. The spatial variation of groundwater parameters shows increasing values of chemical parameters towards the sea in the study area.

### ACKNOWLEDGMENTS

The entire study is financed by SIIL, Tuticorin. The officials of SIIL have been always helpful during the field investigation. The authors have received valuable information from SIIL, CGWB, Chennai and Department of Geology, VOC Collage, Tuticorin, which have been useful for this investigation. Director, CSIR-NGRI, Hyderabad, Chairman, CGWB and Head of Office, UR, Dehradun have encouraged and provided all necessary facilities. We thank Dr. R. Rangarajan and Prof. B. Venkateswara Rao, for their constructive suggestions/comments to enhance the quality of the manuscript. We extend our thanks to Dr. M.R.K. Prabhakar Rao for detailed editing. We thank the Chief Editor for his support.

### Compliance with Ethical Standards

The authors declare that they have no conflict of interest and adhere to copyright norms.

### REFERENCES

- American Public Health Association (APHA) 1985. Standard methods for the examination of water and wastewater, 16th ed., Washington DC, USA., Am. Public Health Assoc, pp: 100.
- Antony Ravindran, A., and Mondal, N.C., 2015. Geotechnical investigation for resort construction using resistivity and granulometric studies in Pattinamaruthur coast, Southern India, *Geotechnical & Geological Engineering*, v.33, no.3, pp: 1-16.
- Balasubramanian, A.R., Thirugnana, S., Chellaswamy, R., and Radhakrishnan, V., 1993. Numerical modeling for prediction and control of saltwater encroachment in the coastal aquifers of Tuticorin, Tamil Nadu. Tech. Report, pp: 21.
- Batayneh, A.T., 2006. Use of electrical resistivity methods for detecting subsurface fresh and saline water and delineating their interfacial configuration: A case study of the eastern Dead Sea coastal aquifers, *Jordan. Hydrogeological Journal*, v.14, pp: 1277-1283.
- Brown, E., Skougstad, M.W., and Fishmen, M.J., 1983. Method for collection and analyzing of water samples for dissolved minerals and gases, Washington DC, USA: U.S. Govt. Printing Office, pp: 75.
- Edmunds, W.M., Shand, P., Hart, P., and Ward, R.S., 2003. The natural (baseline) quality of groundwater: a UK pilot study, *Sci Total Environ*, pp: 310:25-35
- Freeze, R.A., and Cherry, J.A., 1979. *Groundwater*, Printice-Hall, New Jersey.
- Gibbs, R.J., 1970. Mechanisms controlling world's water chemistry, *Science*, pp: 1089-1090.
- Hem, J. D., 1989. Study and interpretation of the chemical characteristics of natural water, U.S.G.S. Water-Supply Paper, US Government Printing Office, Washington DC., v.2254.
- Kim, K.Y., Park, Y.S., Kim, G.P., and Park, K.H., 2009. Dynamic freshwater-saline water interaction in the coastal zone of Jeju Island, South Korea, *Hydrogeol. J.*, v.17, pp: 617-629.
- Mondal, N.C., Singh, V. S., Puranik, S.C., and Singh, V.P., 2010b. Trace element concentration in groundwater of Pesarlanka Island, Krishna Delta, India, *Environ.Monit. Assess.*, v.163, pp: 215-227.
- Mondal, N. C., Singh, V. S., Saxena, V. K., and Prasad, R. K., 2008. Improvement of groundwater quality due to fresh water ingress in Potharlanka Island, Krishna delta, India, *Environ. Geol.*, v.55, no.3, pp: 595-603.
- Mondal, N.C., Singh, V. P., Singh, V. S., and Saxena, V. K., 2010a. Determining the interaction between groundwater and saline water through groundwater major ions chemistry. *J. Hydrol.*, v.388, no.1-2, pp: 100-111.
- Mondal, N.C., Singh, V. S., and Rangarajan, R., 2009. Aquifer characteristics and its modeling around an industrial complex, Tuticorin, Tamil Nadu, India: A case study, *J Earth Sys. Sci.*, v.188, no.3, pp: 231-244.
- Nair, R., Kalariya, T., and Chanda, S., 2005. Antibacterial activity of some selected Indian medicinal flora, *Turk. J. Biol.*, v.29, pp: 41-47.
- Piper, A.M., 1953. A Graphic Procedure in the Geochemical Interpretation of Water Analysis. Washington D.C.: United States Geological Survey. ISBN ASIN: B0007HRZ36, pp: 1475-1483.
- Rajmohan, N., Elango, L., Ramachandran, S., and Natarajan. M., 2000. Major ion correlation in groundwater of Kancheepuram Region, South India, *Indian J. Environ. Protection*, v.20, no.3, pp:188-193.
- Rangarajan, R., Mondal, N.C., Singh, V.S., and Singh, S. V., 2009. Estimation of natural recharge and its relation with aquifer parameters in and around Tuticorin town, Tamil Nadu, India, *Curr. Sci.*, v.97, no.2, pp: 217-226.
- Richard, L.A., 1954. Diagnosis and improvement of saline and alkali soils. Agriculture handbook 60. US Department of Agriculture, Washington DC.

- Richter, B.C., and Kreitler, C.W., 1993. *Geochemical techniques for identifying sources of groundwater salinization* (258), CRC Press.
- Sarwade, D.V., Nandakumar, M.V., Kesari, M.P., Mondal, N.C., Singh, V.S., and Singh, B., 2007. Evaluation of sea water ingress into an Indian Atoll, *Environ. Geol.*, v.52, no.2, pp: 1475–1483.
- Sawyer, G.N., and McCarty, D.L., 1967. *Chemistry of sanitary engineers*, 2nd edn. McGraw Hill, New York, pp: 518.
- Saxena, V. K., Mondal, N.C., and Singh, V.S., 2004. Identification of seawater ingress using Sr and B in Krishna delta, *Curr. Sci.*, v.86, no.4, pp: 586–590.
- Saxena, V. K., Singh, V. S., Mondal, N.C., and Jain, S.C., 2003. Use of chemical parameters to delineation fresh groundwater resources in Potharlanka Island, India. *Environ. Geol.*, v.44, no.5, pp: 516–521.
- Sherif, M., and Kacimov, A., 2007. Seawater intrusion in the coastal aquifer of Wadi Ham, UAE: A new focus on groundwater/seawater interactions. In *Proceedings of symposium HS 1001 at IUGG 2007, Perugia*. IAHS Publ. 312, IAHS, Wallingford, UK, pp: 315–325.
- Singh, V.S., Mondal, N.C., Singh, S., and Negi, B.C., 2006. Hydrogeological and geophysical investigations to delineate aquifer zone around SILL, Tuticorin, Tamilnadu, Tech. Rept. No. NGRI-2006-GW- 564, pp: 24.
- Singh, V.S., Sarwade, D.V., Mondal, N.C., Nanadakumar, M.V. and Singh, B., 2009. Evaluation of groundwater resources in a tiny Andrott Island, Union Territory of Lakshadweep, India, *Environ. Monit. Assess.t.*, v.158, no.1-4, pp: 145-154.
- Sukhija, B.S., Varma, V. N., Nagabhushanam, P, and Reddy, D.V., 1996. Differentiation of paleomarine and modern seawater intruded salinities in coastal groundwaters (of Karaikal and Tanjavur, India) based on inorganic chemistry, organic biomarker fingerprints and radiocarbon dating, *J. Hydrol.*, v.174, pp: 173–201.
- Todd, D.K., 1980. *Groundwater hydrology*, 2nd ed., New York: Wiley.
- Villholth, K.G., Manamperi, A.S.P., and Buergi, N., 2006. Chemical characteristics of Tsunami-affected groundwater and lagoon on the east coast of Sri Lanka. In: 32nd WEDC international conference, Colombo, Sri Lanka on “Sustainable development of water resources, water supply and environmental sanitation”, pp: 334–340.
- World Health Organization (WHO), 1993. *Guidelines for drinking water quality, recommendations*, 2nd edn. WHO, Geneva, v.1, pp: 130.

# Evaluation of shallow aquifers contamination along Cauvery River Basin using Electrical resistivity and hydro chemical investigations

K.V.Satyanarayana\*<sup>1</sup>, M.Pradeep Kumar<sup>1</sup>, M.S.Kumar<sup>1</sup>, B.Balakrishna<sup>2</sup> and Dinesh Gupta<sup>3</sup>

<sup>1</sup> Geological Survey of India, Southern Region, Hyderabad – 500 068

<sup>2</sup> Geological Survey of India, Central Region, Nagpur – 440 006

<sup>3</sup> Geological Survey of India, Eastern Region, Kolkata, 700 091

\*Corresponding Author: satyan0461@gmail.com

---

## ABSTRACT

The reasons for deterioration of quality of water in coastal aquifers are many. To investigate some of them, electrical resistivity surveys were carried out in the study area namely Cauvery sedimentary basin. A total of about 300 vertical electrical soundings (VES) using Schlumberger array was used for the study. Groundwater samples were also collected from shallow dug wells, hand pumps and ponds at sounding locations for chemical examination of TDS and chloride to correlate with the resistivity data for confirmation of quality of the groundwater. The sources of freshwater in the study area include the shallow unconfined aquifer below the dry unconsolidated layer as well as a series of confined aquifers below it.

The resistivity data was analyzed for true values by inverting the sounding data using partial curve matching as well as software methods. The interpretation of VES data reveal that the low resistivity regions corroborate with higher TDS and Chloride values mostly falling over areas occupied by rivers, canals and inlets which are connected to the sea. The seawater might be flowing into the mainland through these inter connected canals, rivers and inlets due to the action of waves and shore currents resulting in the infiltration of sea water into the shallow aquifers. The permeable zones occurring in proximity to backwater canals are most vulnerable for saline water intrusion and may further damage the deeper aquifers through seepage. The present surveys have clearly established regions of saltwater contamination and causes for deterioration of shallow aquifers. The present surveys helped in the classification of low resistivity regions, corroborating well with the high cut off values of TDS and chloride. This demarcates clearly saltwater contaminated areas. These results may possibly help in taking preventive measures to obstruct backwater flow through rivers and inlets due to tidal action by constructing barriers to safeguard the environmental disorders.

**Key words:** Coastal aquifers, Saltwater intrusion, Vertical electrical sounding, Water analysis and Cauvery basin.

---

## INTRODUCTION

Water requirements have increased manifold with the growing population and rising industrial and irrigation growth in India. With the growing living standards and health awareness of mankind, the demand for good quality of water is increasing day by day. Many coastal aquifers in the world, especially shallow aquifers experience an intensive saltwater intrusion caused by both natural and human induced processes. The study area is situated between Puducherry in the north and Chidambaram in the south (Figure 1), close to the Bay of Bengal coast in the East. Groundwater levels were deteriorating due to low rainfall and trapping of ground water through pumps for irrigation, industrial and drinking purposes. Consequently, the river system connected with the sea is experiencing reverse flow of sea water due to action of waves and shore currents. The flow of backwaters in Gingee, Mallattar, Gadilam, Uppenar and Vellar streams flowing in the study area are likely to aid recharge through infiltration and seepage of shallow layers where the permeable beds are exposed in the river bottom.

Excessive pumping of freshwater from an aquifer reduces the water pressure and intensifies the effect of drawing nearby sea water into permeable zones. Indiscriminate drilling of bore wells and hand pumps for discharge of groundwater at various depths may also causes the invasion of saltwater into freshwater aquifers by inward flow. This may causes the pollution of the underground water in the coastal area and hence, reduces the potability of such water for human use. In order to distinguish such polluted zones and causes for pollution of underground water along the coast, Geophysical investigations comprising of Vertical Electrical Resistivity soundings have been used.

## Geology and Hydrogeology

The area is occupied by Tertiary sediments, ranging in age from Eocene to Mio-Pliocene (Figure 2) with most part covered by Quaternary sediments. The Quaternary (Recent) formations in the region are represented by laterites and alluvium. Laterite occurs as thin cap over the Cuddalore formations. The alluvium in the area is composed of

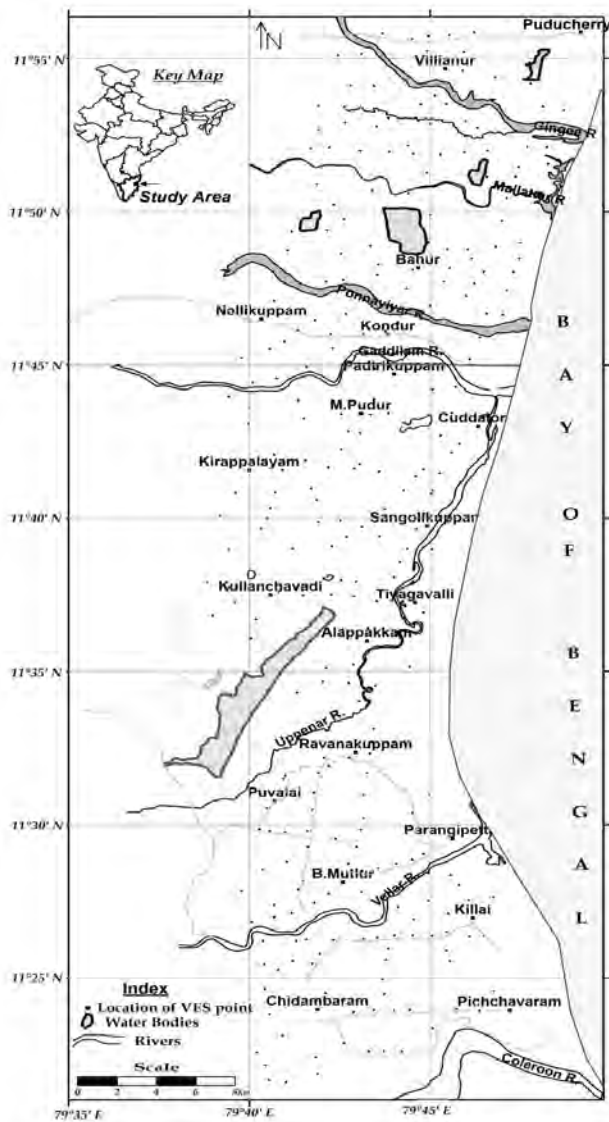


Figure 1. Location Map.

sands, clays, silts, gravels and kankar. Thick alluvial deposits are formed along the course of Rivers Ponnaiyar, Gadilam, Malattar and Gingee. The Tertiary formations are represented by the Kadapperikuppam, Manaveli and Cuddalore formations. The study area is covered by Cuddalore formation composed of thick succession of pebbly and gravelly, coarse-grained sandstones with minor clays, rarely with thin seams of lignite (Subramanyam, 1969). In the North western margin, the Cuddalore formation overlies the Ramanathapuram formation by completely concealing them and overlapping the Vanur sandstones. In the North eastern portion they overlie the Manaveli formation. The thickness of these formations varies from 30 m to 130 m at outcrop area and maximum thickness of 450 m is along the coast in the South eastern side (Subramanyam and Selvan, 2001).

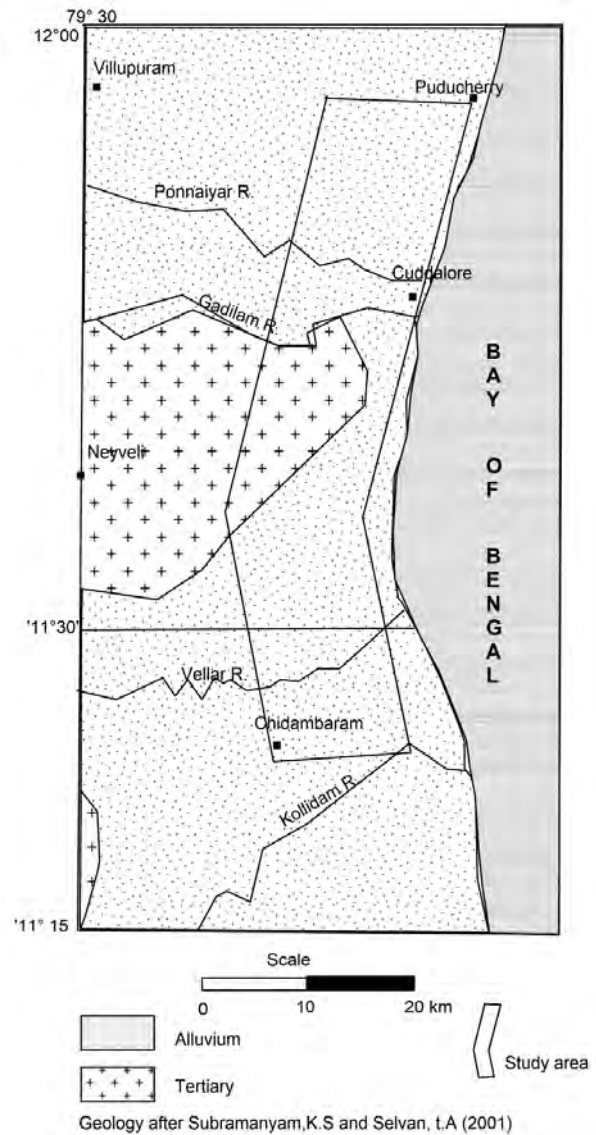


Figure 2. Regional Geology Map.

Groundwater occurs in Tertiary formations under un-confined to semi-confined condition. The depth of the tube wells tapping this aquifer ranges between 25 m and 50 m bgl.

The stratigraphy of the area has been established by the Oil and Natural Gas Commission (Varadarajan, 1969) by carrying out detailed geological, geophysical surveys and drilling 9 shallow boreholes. The area under study can broadly be classified into western high ground and eastern Gadilam-Ponnaiyar and Vellar alluvial plains. The drainage of the area is controlled by the Gingee, Malattar, Ponnaiyar, Gadilam, Uppenar and Vellar rivers and their tributaries. These rivers, though perennial, have only insignificant flows. The Bahur tank in the northern part and Perumal Eri in the south-central part of the area stores ample rain water and serves the needs of irrigation domain and may

**Table1.** Derived Resistivity ranges for different formations.

| S.No. | Resistivity ( $\Omega$ -m) | Lithology                                    |
|-------|----------------------------|--|
| 1     | 100-500                    | Laterite, Lateritic soil                     |
| 2     | 250-800                    | Dry Beach sand                               |
| 3     | 1-10                       | Clay/sand/gravel/sandstone with saline water |
| 4     | 10-30                      | Clay/sand/sandstone with brackish water      |
| 5     | 30-200                     | Sand/gravel/sandstone with freshwater        |

also recharge the shallow aquifers through seepage and infiltration. The observed water levels in the recent alluvial aquifers ranges between 2.18 to 20 m below ground level (Central Groundwater Board, 2012). Decline in water levels recorded on an average by 1 to 1.5 m annually due to excessive usage of groundwater for all purposes.

**Methodology and Instruments**

The electrical resistivity method is more commonly used for ground water exploration to demarcate an aquifer with freshwater and saltwater due to substantial resistivity contrast between them. Electrical resistivity soundings, using Schlumberger electrode configuration were carried out with half current electrode separations (AB/2) from 1 to 100m. A total of 300 electrical resistivity soundings were conducted, covering a total area of 770 km<sup>2</sup> (Figure 1) deploying high precision equipment consisting of Scintrex make square-wave TSQ-3 transmitter and RDC-10 receiver. Briggs and Stratton four stroke, 8 H.P generators was used for producing 230 V alternating current.

Groundwater samples collected from dug wells and tube wells at nearby sounding locations all over the study area were analysed for cations and anions respectively by Flame photometer and Spectrophotometry at NLC Chemical laboratory, Neyveli by adopting standard procedures (APHA, 1998).

**Analysis of Data**

The resistivity sounding data has brought out AH, HA, KH and HK type of field curves and majority of the soundings represented four layer model. The observed field curves are interpreted qualitatively with partial curve matching technique by using two layer master curves and auxiliary curves (Bhattacharya and Patra, 1968) initially and estimated the number of layers and their parameters. By taking these layer parameters, an initial model is generated using computer software (IX-1D, 2002) which is then iterated until a good match between the observed and the theoretical curve is found. Finally, an appropriate hydrogeological model was generated by overcoming the fundamental limits of the resistivity method.

Chemicals, which are strong electrolytes, such as potassium chloride and sodium chloride, can greatly reduce the resistivity of ground water to less than 1 ohm-m even at fairly low concentrations (Daniels and Alberty, 1966). In general, the ambiguity exists in discriminating clay or saline water zone by observing the range of resistivity values. The order of TDS and Chloride values in individual water sample will help to distinguish the clay or saltwater polluted zone. The higher order TDS and Chloride values in correlation with low resistivity values indicate the zone of contamination with saltwater (salinization).

**Discussion of Results**

Resistivity of an individual aquifer may vary depending on the quality of the water which in turn is controlled by the amount of dissolved solids in it. The resistivity method is an effective tool to detect any changes in quality of groundwater causing freshwater and saltwater imbalances in coastal aquifers (Urish, D.W. and Frohlich, R.K., 1990). Layer resistivities obtained by the inversion process are controlled by the quality of the water and host rock formation (Burger, 1992). This will help in easy conversion of various resistivity layers into subsurface geological formations with different hydrological conditions. The relationship between the fresh, brackish and saline water with their host media is derived from the analysis of resistivity data for the study area. The following table is prepared based on the resistivity variations for different subsurface formations in correlation with available borehole litholog data.

The water analysis results show that higher TDS and Chloride represent the contamination of saltwater with groundwater. However, the cut off values vary with the area. The cut off values for the contamination of salt water was determined as 1000 ppm for TDS and 250 ppm for Chloride (Balía Roberto et al., 2003). The Environmental Protection Agency (EPA) recommends against the consumption of water having TDS more than 500 ppm. Variations of TDS and Chloride components will readily recognize the areas of different water quality and higher than cut off values will help differentiating saltwater invaded areas very clearly. The drinking water

Evaluation of shallow aquifers contamination along Cauvery River Basin using Electrical resistivity and hydro chemical investigations

**Table 2.** Drinking water quality standards.

| S.No. | Parameter | BIS      | ICMR     | WHO      |
|-------|-----------|----------|----------|----------|
| 1     | TDS       | 500 mg/l | 500 mg/l | 500 mg/l |
| 2     | Chloride  | 250 mg/l | 200 mg/l | 200 mg/l |
| 3     | Sulphate  | 200 mg/l | 200 mg/l | 200 mg/l |

- BIS: Bureau of Indian Standards
- ICMR: Indian Council for Medical research
- WHO: World Health Organization

quality standards were tabulated below as per the different organizations.

Two different regions i.e VES stations falling within the 500 m radius from river (close to river path) and VES stations falling outside the 500 m radius (away from river path) were analyzed critically for the quality of the shallow aquifers and causes for change of water quality. The resistivity sounding curves located close to river path are characterized by descending curve showing steep fall and indicating unsaturated soil on top to saltwater saturated sediment below it. Figure 3 shows four typical sounding curves selected in the region of rivers characterized by steep fall of resistivity. The VES curve RS54 observed along Gingee River has four layers. The two consecutive layers below top layer have shown the resistivities of 10.3 and 3.6 Ohm-m respectively below a depth of 2 m. These are possibly corresponding to sand and sandy clay layers contaminated with saltwater. The VES curve RS67 has shown a very distinct low resistivity zone of 2.7 Ohm-m below a depth of 0.55m. This layer possibly represents saline sand or saline clay. The VES curves RS32 and RS34 observed near Malattar has also shown low resistivities for unconfined sand layer below top unsaturated soil. The low resistivity's for shallow layers indicate the infiltration of saltwater. The VES curves located close to the rivers Ponnaiyar, Gaddilam, Uppenar and Vellar has also shown low resistivities for shallow unconfined aquifer.

The sounding curves located away from the river path (backwater channels) have indicated a different subsurface resistivity picture as far as shallow layers are concerned. Figure 4 represent the typical sounding curves namely, RS106, RS121, RS206 and RS59 picked from the study area but away from the vicinity of backwater channels. The shallow layers below the top unsaturated soil cover have resistivities of more than 30 Ohm-m. The layers having higher order resistivities correspond to sand layer saturated with fresh water. From the above analysis, it can be inferred that the region occupied close to backwater channels is influenced by the saltwater infiltration in to the shallow layers

The resistivity contour maps prepared for two different depth segments i.e 5 m and 10 m reflecting the variations in resistivity's based on inverted values. The resistivity contour map (Figure 5) shows resistivity variations for depth segment of 5 m.

The resistivity contour map has indicated low contour values (light grey shades) along the river courses of Gingee, Malattar, Ponnaiyar, Gadilam, Uppenar and Vellar. The contact between low and higher resistivity contours is clearly seen at the passage of Gadilam River. The northern and southern parts, being low lying areas, is characterized with lower order resistivities indicating infiltration of saltwater whereas the central part dominated by high resistivity values is not affected much except the track of rivers. The area between Padirikuppam and B.Mutlur is not affected by seawater leaving a segment passing through Uppenar along northeast-southwest direction in the middle of the study area. The area in the west of Uppenar along Sangolikuppam and Ravanakuppam in the direction of river is characterized with lower order resistivity values suggesting saltwater infiltration. However, the areas close to bay in the east of Uppenar has indicated high resistivities, which may correspond to sand dunes. The area bounded by Vellar is also characterized with lower order resistivity values suggesting deterioration in the quality of water.

The resistivity contour map (Figure 6) for the depth segment of 10m depicts the resistivity variations indicating low resistivity values along the path of rivers. However, the higher range of resistivity values from more than 10 Ohm-m to less than 30 Ohm-m indicates the variation in water quality from saline to brackish in the shallow layers. The resistivity contour map (Figure 6) for 10m depth indicated improved resistivity values varying from 10 to 30 ohm-m compared to 5 m depth segment suggest the improvement in quality of water from saline to brackish. This will further suggests the contamination prevails at shallow levels only due to backwater infiltration. The lower order contour trends noticeably followed the direction of river, clearly indicating the infiltration of saltwater into the shallow aquifers through backwater channels.

The Total Dissolved Solids (TDS) contour map (Figure 7) for shallow levels ranging the depths from 4.5 to 10 m shows higher values along the river courses confirming the lower order resistivities.

The higher order TDS values having more than 1000 ppm were observed south of Devalakuppam between Gingee and Malattar rivers; near Bahur, Kondur along Ponnaiyar and Gadilam rivers; Burgespettai, Cuddalore and Kudikadu areas along Uppenar river and Tiyagavalli, B.Mutlur and Chidambaram areas along Vellar river. The contour map

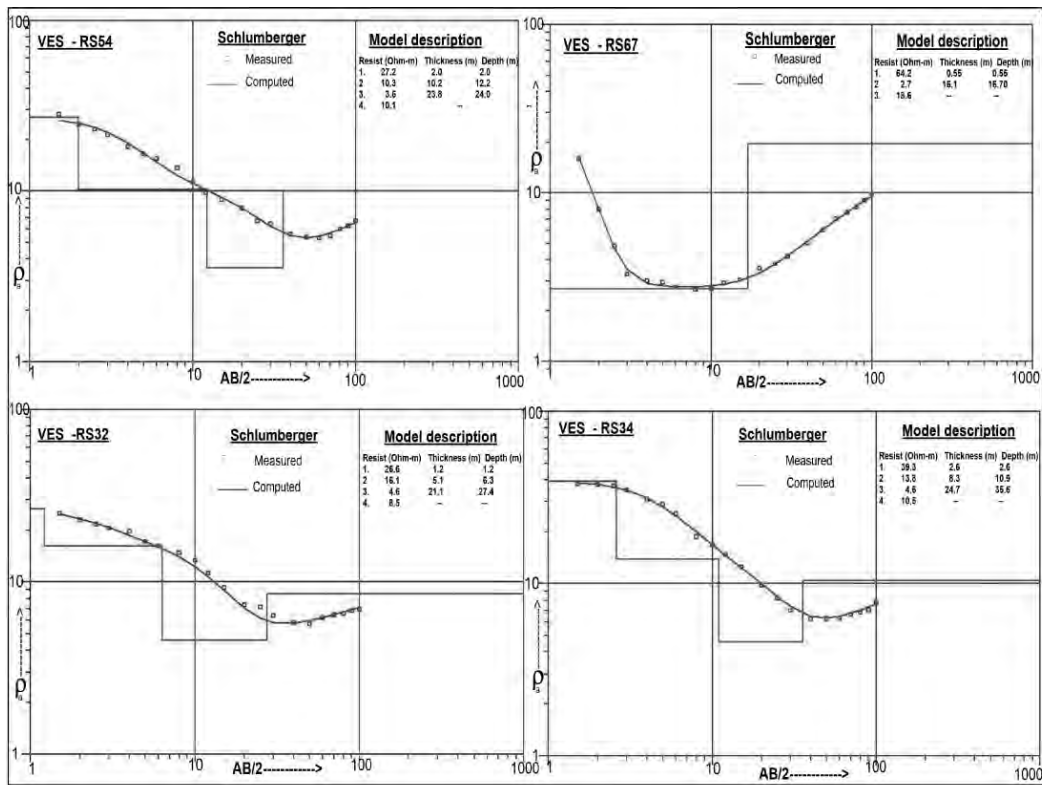


Figure 3. Interpretation of Typical VES Curves close to River path.

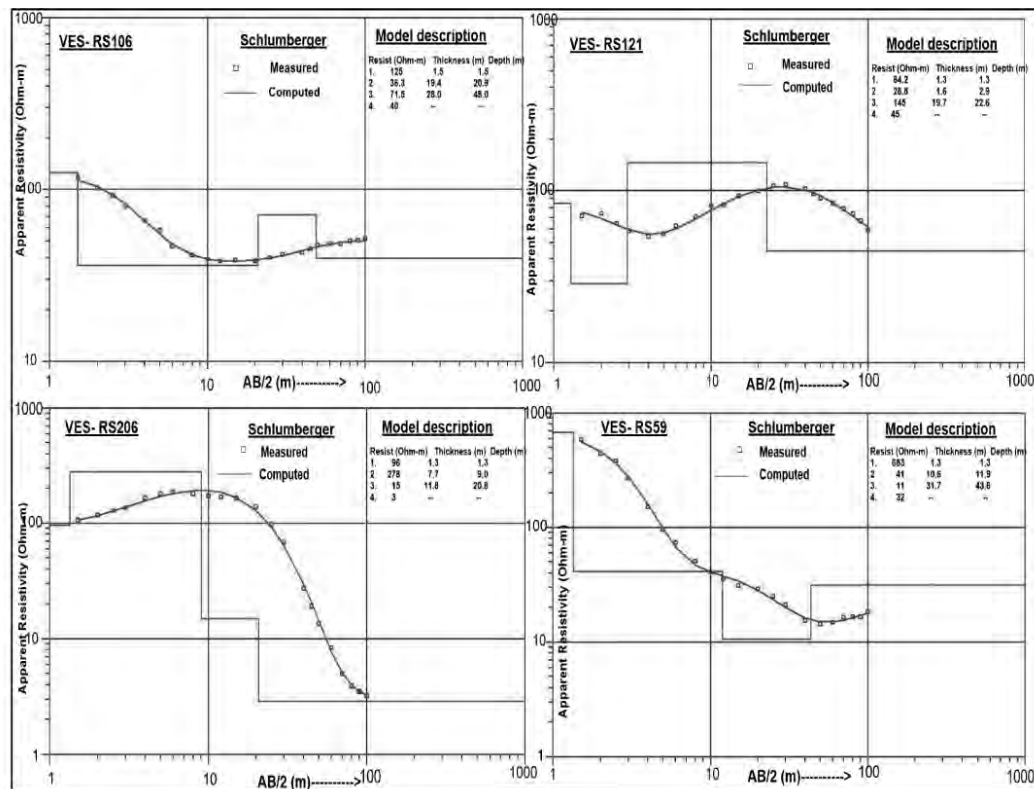


Figure 4. Interpretation of Typical VES Curves away from River path.

Evaluation of shallow aquifers contamination along Cauvery River Basin using Electrical resistivity and hydro chemical investigations

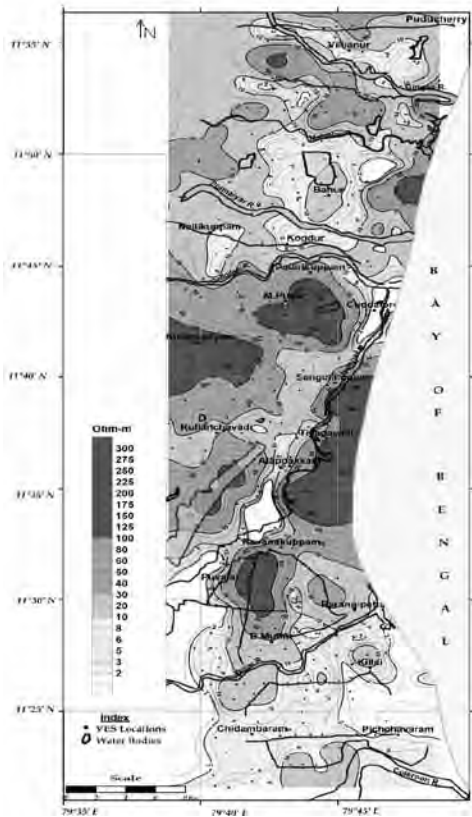


Figure 5. Resistivity contour map for 5m depth.

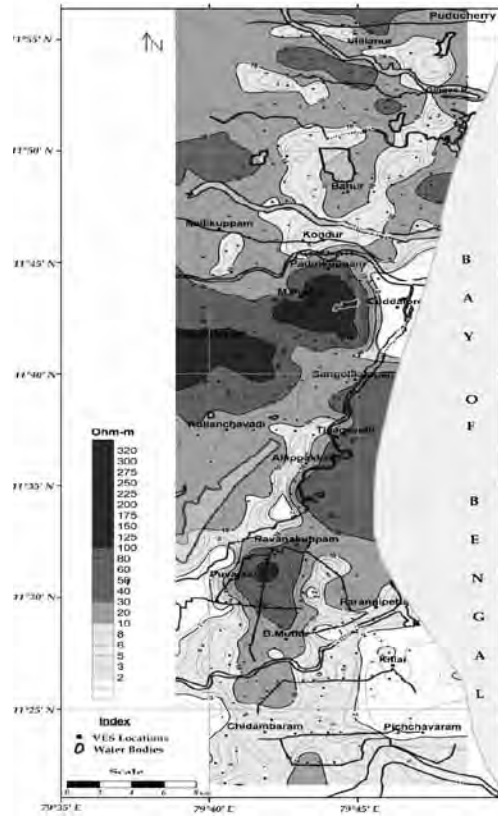


Figure 6. Resistivity contour map for 10m depth.

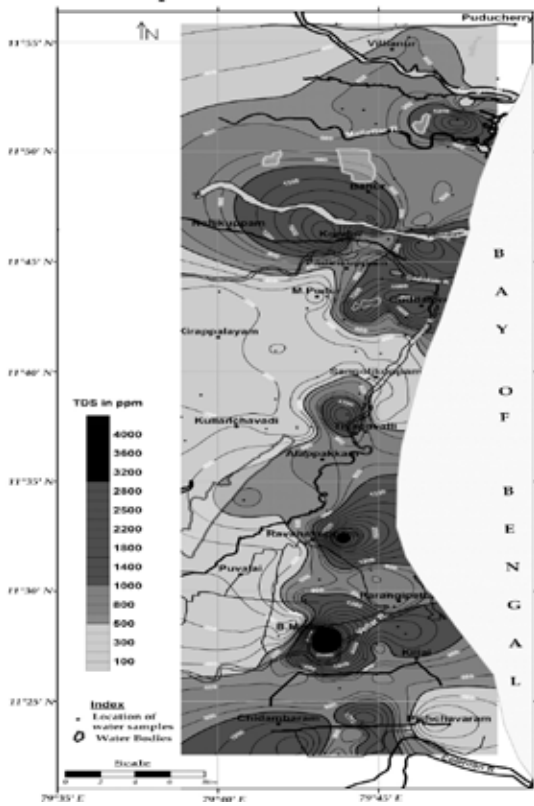


Figure 7. Total Dissolved Solids (TDS) Distribution Map.

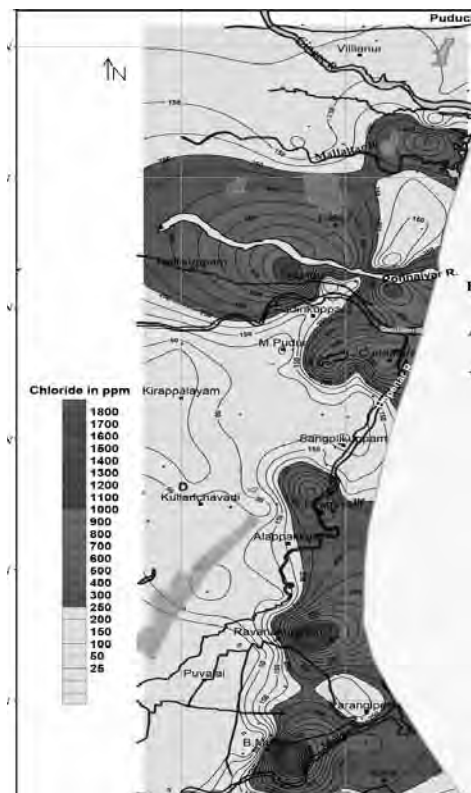


Figure 8. Chloride Distribution Map.

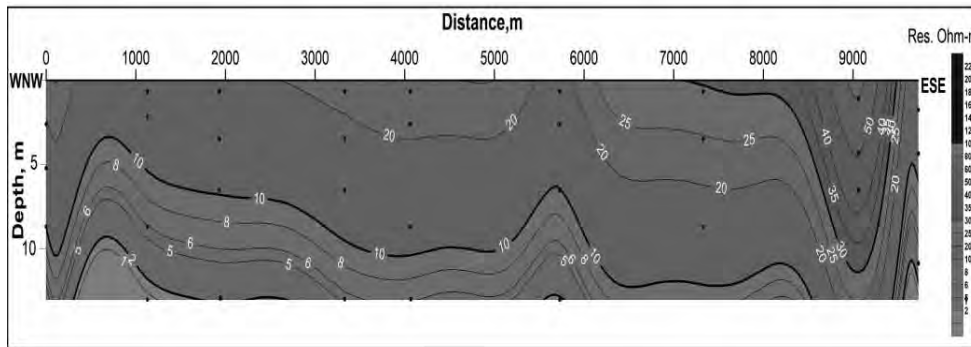


Figure 9. Resistivity Pseudosection along Gingee River.

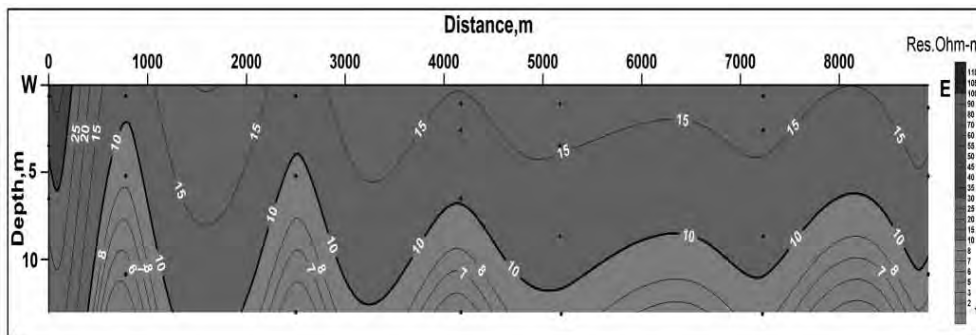


Figure 10. Resistivity Pseudosection along Malattar River.

(Figure 8) for Chloride has also reflected with higher order values having more than 250 ppm at all these locations corroborating with high TDS and low resistivity values. Therefore, it is evident from the above discussion that the water analysis results correlate well with resistivity results indicating contamination of saltwater along the area traversed by rivers, which carry the backwaters from the sea on tidal action.

Two resistivity pseudo sections were prepared using inverted data along the direction of Gingee and Malattar rivers from west to east to verify the subsurface resistivity distribution for classification of water quality. A total of nine VES stations were used for preparing Gingee section with light grey and black representing minimum and maximum values respectively. The Gingee section (Figure 9) shows low resistivity variations (1 to 10 Ohm-m) for the depths 4 to 12 m and 10 to 30 Ohm-m above this zone. These low resistivity values suggest the deterioration of quality of water. The high resistivity zone (> 30 Ohm-m) below station 8 corresponds to the sand dune with freshwater.

The resistivity pseudo section (Figure 10) along Malattar river covers seven resistivity sounding curves in east-west direction shows low resistivity variations (< 10 Ohm-m) below depth from 3 to 12 m and 10 to 20 Ohm-m above it. The lower order of resistivity distribution along the section indicates the contamination of freshwater aquifers with saline water.

## CONCLUSIONS

The resistivity investigation has clearly classified the variations in resistivities for different depths. The lower order resistivity values ranging from 1 to 10 ohm-m were demarcated mostly along the course of rivers and its peripheries. These low order resistivity values in correlation with water samples analysis data lead to the confirmation of subsurface formation without ambiguity. Water samples with TDS (more than 1000 ppm) and Chloride (more than 250 ppm) in low resistivity regions suggests the deterioration in quality of groundwater. The saltwater infiltration become maximum when highly permeable sediment formations make in contact with backwater carrier river path. The pseudo sections have also shown the low resistivity distribution at shallow depths suggesting the contamination of aquifers with saline water. It is observed from our present study that Contamination in unconfined shallow aquifers of the coastal regions is less in the regions where habitation is less. The analysis of resistivity and water analysis data was useful in precise determination of nature of shallow subsurface layers in the study area. The present study is also helpful to demarcate vulnerable areas of backwater flow in to the mainland for taking necessary measures to obstruct backwater flow by constructing barriers to safeguard the environmental degradation.

## Evaluation of shallow aquifers contamination along Cauvery River Basin using Electrical resistivity and hydro chemical investigations

### ACKNOWLEDGEMENTS

The authors thank Addl. Director General, Geological Survey of India, S.R., Hyderabad and General Manager, Neyveli Lignite Corporation Ltd. Neyveli for their kind approval to publish the data, (the data collected has been collected under sponsored category in 2009-2012, with terms and conditions). The authors are also grateful to geological team of NLC Ltd for useful discussions on hydrogeology of the area. Authors are thankful to Dr.M.R.K.Prabhakar Rao and Prof.B.Venkateswara Rao for constructive suggestions. We also thank Dr.M.R.K.Prabhakar Rao for editing the manuscript. We are grateful to Chief Editor for his support.

### Compliance with Ethical Standards

The authors declare that they have no conflict of interest and adhere to copyright norms.

### REFERENCES

APHA., 1998. Standard methods for the examination of water and waste water, 19<sup>th</sup> edition, APHA, Wasington DC, USASS.

- Balia Roberto, Enrico Gavaudo, Federica Ardaù and Giorgio Ghiglieri., 2003. Geophysical approach to the environmental study of a coastal plain. *Geophysics*, v.68, no.5, pp: 1446-1459.
- Bhattacharya, P.K., and Patra, H. P., 1968. Direct Current geoelectric sounding. Elsevier Science Publications.
- Burger, H.R., 1992. *Exploration Geophysics of the shallow surface*. Prentice Hall, NJ, pp: 485.
- Central Ground Water Board, 2012. *Aquifer systems of Tamil Nadu and Puducherry*, Govt. India, Ministry of Water Resources, Southeastern Coastal Region, Chennai.
- Daniels, F., and Alberty, R.A., 1966. *Physical Chemistry*, John Wiley and Sons Inc.
- IX-1D, 2002. *Resistivity Sounding Software, Version 2.06*. Interpex Limited, Golden Colorado, United States of America.
- Subramanyam, V., 1969. *Memoirs of GSI*, v.94, no.1.
- Subramanyam, K.S., and Selvan, T.A., 2001. *Geology of Tamilnadu and Pondicherry*, Geological Society of India, Bangalore.
- Urish, D.W., and Frohlich, R.K., 1990. Surface electrical resistivity in coastal groundwater exploration. *Geoexploration* v.26, pp: 267-289.
- Varadarajan, K., 1969. A report of Photo-geomorphological studies carried out in parts of Cauvery basin, ONGC, unpublished report, pp: 12.

# Co-Seismic Water Level Changes in Koyna – Warna Region - A Wavelet Analysis

D. V. Ramana\* and Ch. V. V. Eswari

National Geophysical Research Institute (CSIR), Hyderabad, India

\*Corresponding Author: [dvr@ngri.res.in](mailto:dvr@ngri.res.in)

---

## ABSTRACT

Koyna region in India is known to be the largest case of Reservoir Triggered Seismicity in the world and the region is seismically active till today. As wavelets are mathematical tools they can extract information from different kinds of time series. In this work the wavelet analysis has been used to see the seismic effects on the water level changes in the bore wells of the Koyna-Warna region. The 14<sup>th</sup> March 2005 earthquake with M5.1 of Koyna-Warna region has been studied for the induced co-seismic changes in bore wells. The Ukalu well has shown the maximum change in the water level since the epicenter is close to the well. The effect of epicenter distance to the wells is also studied. These results are useful in further analyzing the forecasting of the water level changes.

**Key words:** wavelet analysis, Co-seismic water level changes, Reservoir Triggered Seismicity, Koyna-Warna region

---

## INTRODUCTION

The Koyna region is located in the Western part of the Indian continental plate. The Koyna-Warna region has been prone to seismic activity. Earthquakes in this region were first noticed soon after the impoundment of the Koyna reservoir behind the Koyna dam. The seismicity in this region are believed to be a reservoir triggered (Gupta and Rastogi, 1976; Talwani 1976 and Gupta et al., 1980) and this area is unique for triggering activity since the earthquakes of magnitude greater than 5 occurs even after forty five years of impoundment. The seismicity in the Koyna-Warna region has been intensively studied by several researchers (Singh et al., 1975; Rastogi et al., 1997; Gupta, 1985, 1992; Talwani et al., 1996).

Anomalous changes in water level in the bore wells have been reported by several workers. Stress may create fractures and also may be the cause for heat emission and as a result rock becomes less dense. The hydrological properties in the porous media also get effected due to the stress changes in the region. The bore wells nearby these active zones may cause changes in the water level due to boundary stress. The water level variation could be pre- or co- or post- seismic effects of earthquakes and the pre-seismic changes are generally explained in terms of changes in the crustal volumetric strain prior to the earthquakes. The co-seismic water level changes in Izu Peninsula were reported by Koisumi et al., (1999) and in Indian peninsula by Chadha et al., (2003). Latter Chadha et al., (2004) studied the relation between the static deformation and the water level changes in the Koyna-Warna region.

The water level variations in some of the bore wells are very promptly seen directly, but some are not seen directly.

In this work, the wavelet transform method has been used for analyzing the time series of the bore well water level data to understand the response of the water table with the seismicity of the region.

## METHODOLOGY

The wavelet transform is being used widely in areas of Geosciences, astronomy, astrophysics engineering, medical sciences, economics etc. Wavelet transforms are integral transforms using integration kernels called wavelets. The general representation of a wave with its corresponding wavelet is shown in Figure 1. The wavelets are scaled and translated copies (known as "daughter wavelets") of a finite-length or fast-decaying oscillating waveform (known as the "mother wavelet"). Analysis using this transformation has advantages over traditional Fourier methods in analyzing physical situations where the signal contains discontinuities and sharp spikes. The wavelet transform can be used to analyze time series that contains non-stationary power at many different frequencies (Daubechies, 1990).

The morlet wavelet is applied here to analyze the local variations of power spectrum within a single non-stationary time series. The representation of morlet wavelet with its transformation is shown in Figure 2. To be 'admissible' as a wavelet, this function must have zero mean and be localized in both time and frequency space (Farge, 1992). Even though this wavelet is a complex function, it allows us to analyze the evolution in the time-space and to calculate the phase between two time series (Soon et al., 2011).

For the Morlet wavelet transform, where the mother wavelet is:

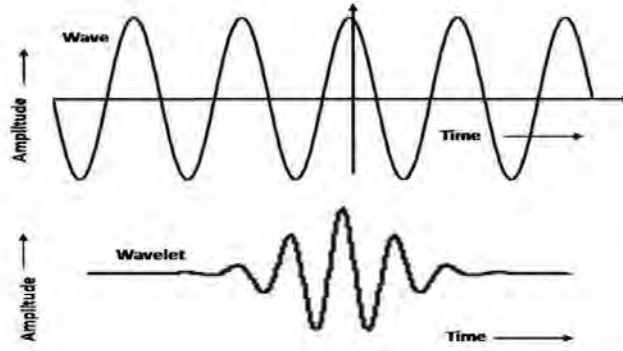


Figure 1. (a) General waves with time (b) General representation of wavelet with time.

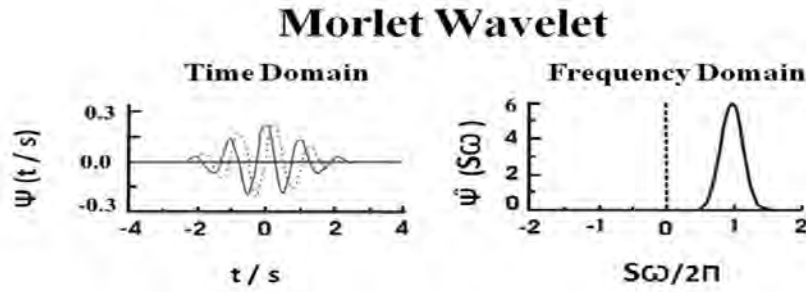


Figure 2. (a) Representation of the Morlet (mother) wavelet and (b) its transformation.

$$\Psi_o(\eta) = \pi^{-1/4} e^{i w_o \eta} e^{-\eta^2/2} \quad (1)$$

where,  $\Psi_o(\eta)$  is the wavelet value of non-dimensional time ( $\eta$ ). Here  $w_o$  is the nondimensional frequency, taken to be 6 to satisfy the admissibility condition. One condition of the wavelet transform is that the average of the wavelet itself must be zero. In practice, if we choose  $w_o = 6$ , then the error due to non-zero mean is smaller than the typical computer round-off errors (Farge, 1992). We are given a time series  $X$ , with values of  $x_n$ , at time index  $n$ . Each value is separated in time by a constant time interval  $\delta t$ . The wavelet transform  $W_n(s)$  is just the inner product (or convolution) of the wavelet function with our original time series:

$$W_n(s) = \sum_{n=0}^{N-1} x_n \Psi^* \left[ \frac{(n' - n) \delta t}{s} \right], \quad (2)$$

where, the asterisk (\*) denotes complex conjugate.

The above integral can be evaluated for various values of the scale  $s$  (usually taken to be multiples of the lowest possible frequency), as well as all values of  $n$  between the start and end time. A two-dimensional picture of the variability can then be constructed by plotting the wavelet amplitude and phase.

For set of scaling parameters  $s$ , first choose the smallest resolvable scale,  $s_o$ , as some multiple of the time resolution,  $\delta t$ . Thus  $\delta t = 0.25$  hours (i.e. 15 minutes). The smallest wavelet which can possibly be resolved is  $2\delta t$ , by choosing  $s_o = 2\delta t = 0.5$  hours. The larger scales (longer periods) are chosen as power-of-two multiples of this small scale,

$$s_j = s_o 2^{j\delta}, \quad j=0,1,\dots,J \quad (3)$$

$$J = \delta j^{-1} \log_2 \left( \frac{N \delta t}{s_o} \right) \quad (4)$$

Here  $j$  determines the largest scale and it is considered as 56,  $\delta j$  is 0.125 and  $N = 506$  respectively. The cone of influence (COI) is the region of the wavelet spectrum outside which the edge effects become important (Torrence and Compo, 1998). Wavelet Power Spectral Density (WPSD) is calculated for each parameter; the black thin lines in Wavelet Power Spectra of Figure 4 and Figure 5 mark the 95% confidence interval or boundaries of COI.

## RESULTS AND DISCUSSIONS

Twenty one bore wells were drilled during 1995 – 1998 in the Koyna-Warna region at depths ranging from 990 to 250 m to monitor the variation of pore pressure in and

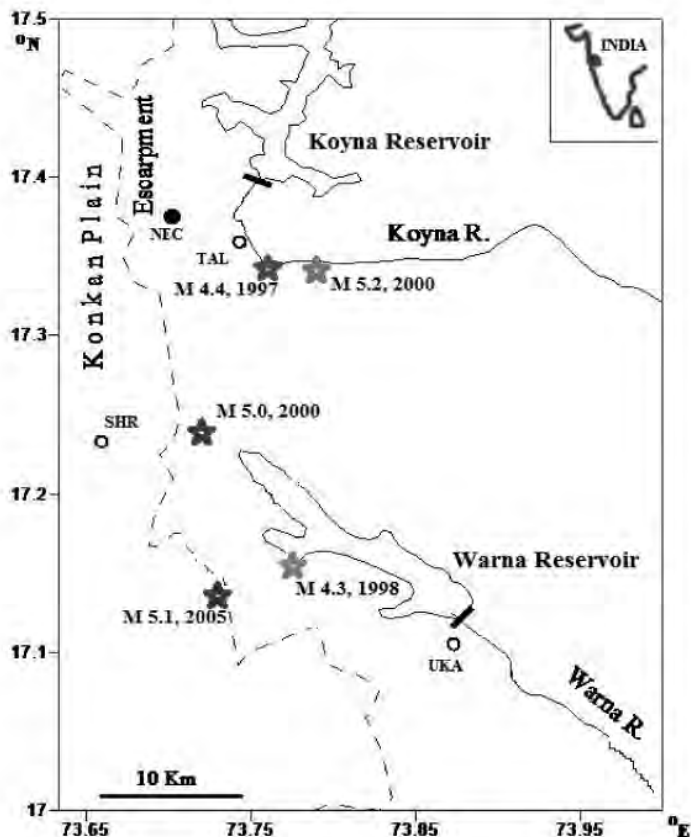


**Figure 3.** Location of the Koyna-Warna region. (Circles indicate the location of the bore wells, open circle is for open well and closed circle for closed well. Stars indicate the location of earthquake epicentres).

around the seismically active area of that region (Figure 3). The time series analysis on the water level data from some of these bore wells for the month of March 2005 was conducted, since on March 14, 2005 magnitude 5.1 earthquake had occurred in Koyna-Warna region and the epicenter of the event was close to the Warna reservoir. The focal mechanism was that due to a normal fault. The co-seismic effect of the event was observed in some of the bore wells. The sudden fall in the water level seen in Ukalu well close to the Warna reservoir is very significant. Time series analysis using the wavelet theory was carried out and the power spectrum of the water level data in some of the bore wells calculated. The Morlet wavelet transform was used for the bore well water level time series data from 1<sup>st</sup> March 2005 to 31<sup>st</sup> March 2005. Figure 4 shows the power spectrum of the bore well water level data. From Figure 4 it is very clear that the peaks in the transform domain and these peaks are correlated with the time of the earthquake of 14<sup>th</sup> March 2005 with magnitude 5.1. The variation in the water levels in the Shringarpur bore well is not significantly revealed in the original time series, but a small peak is seen in the power spectrum which correlates at 14<sup>th</sup> March.

In the original time series of Nechal well water level data a sudden rise in the water level was observed at the time of the event. The numerical results also show that there is a small variation in the original time series of Taloshi bore well water level data, but this is not reflected in the transformed power spectrum.

To see the importance of the wavelet transform method on the water level data time series the transformation has been applied to the bore well water level data at different times and also at different bore wells. The time series analysis was also taken up on the data from the earlier events reported in April 1997, Feb. 1998, June 1999, March 2000 and Sep. 2000 with magnitude greater than 4 in Koyna-Warna region. The spectrum has been calculated for the Ukalu well using the wavelet transform. The original data after removing the tidal effects (upper) and the spectrum (lower) is shown in Figure 5. Though the co seismic effects in the bore well water level data in the time domain are not noticeable in the figure (Figure 5) they appear prominently in the power spectrum of April 1997 data. The data of Feb. 1998, March 2000 and Sep. 2000 was also analysed in a similar way, the results of which are also shown in the same figure. It is clear from

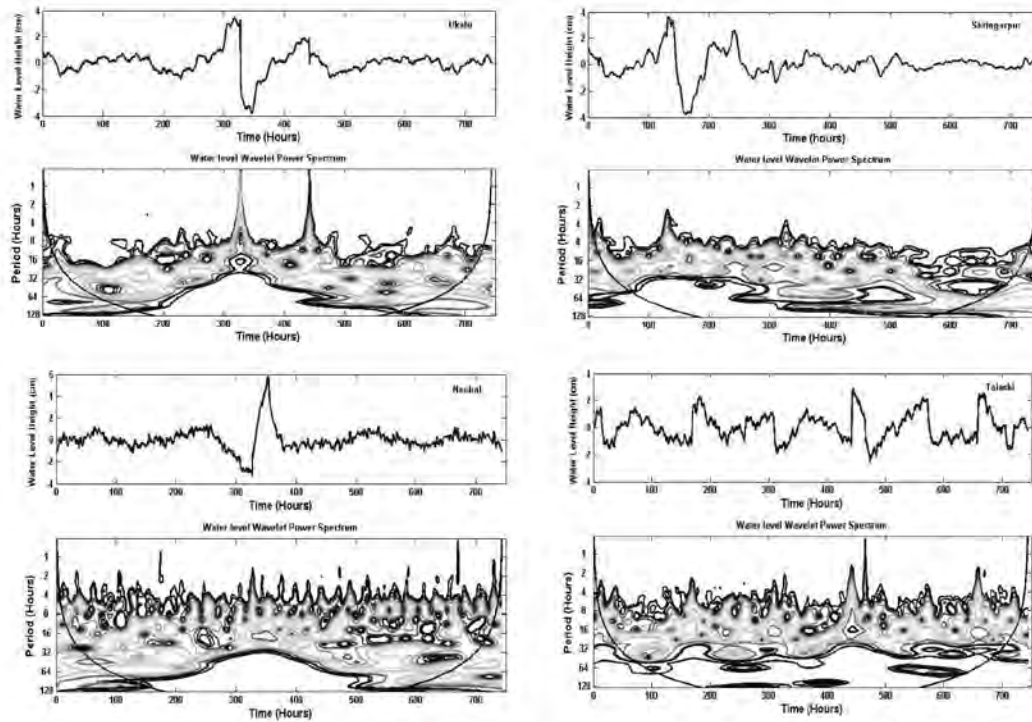


Figure 4. Water level variation (above), Power spectrum (below) in different bore wells from 1 March 2005 to 31 March 2005 (a) for Ukalu (b) Shringarpur (c) Nechal and (d) Taloshi.

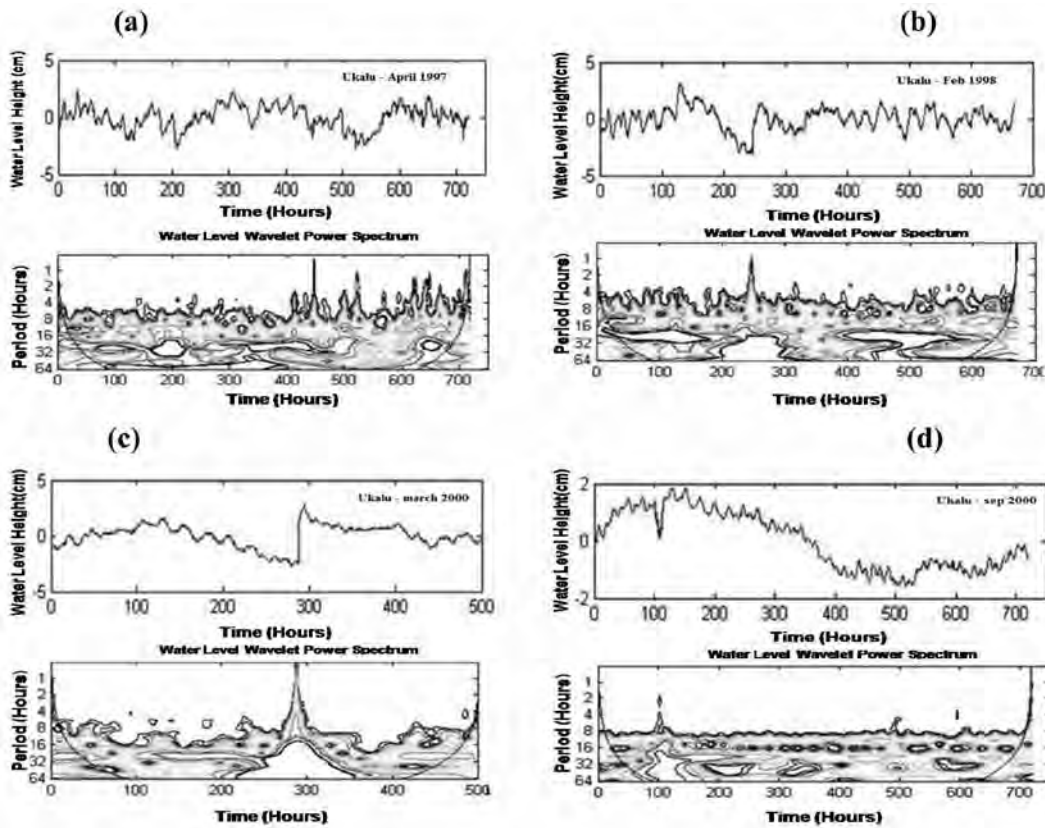
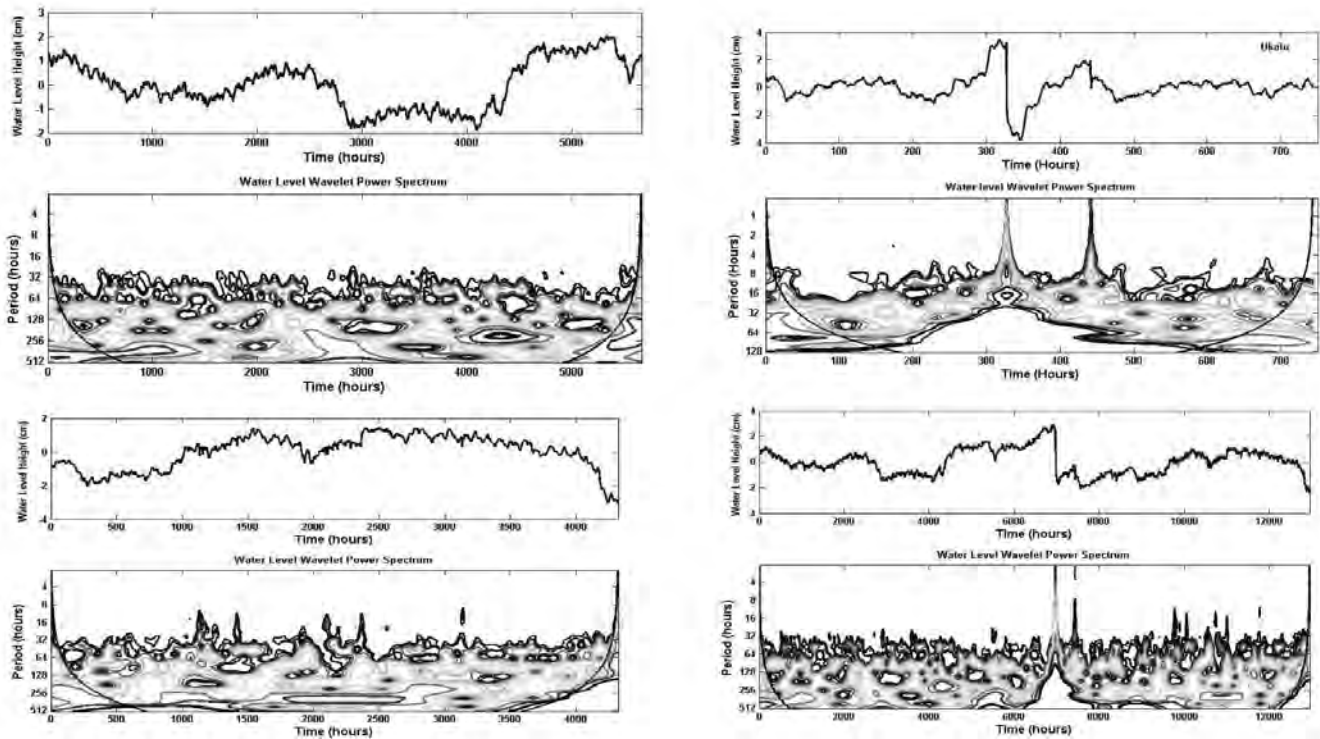


Figure 5. water level variation (above), Power spectrum (below) for Ukalu well data (a) April 1997 (b) Feb. 1998 (c) March 2000 and (d) Sep. 2000.



**Figure 6.** water level variation (above), Power spectrum (below) for Ukalu well data from January 1<sup>st</sup> 2005 to may 31<sup>st</sup> 2005: (a) January 1<sup>st</sup> 2005 to Feb 29<sup>th</sup> 2005 (b) march 2005 (c) march 31<sup>st</sup> 2005 to may 31<sup>st</sup> 2005 (d) January 1<sup>st</sup> 2005 to may 31<sup>st</sup> 2005.

**Table 1.** Water level variation in different wells due to 14th March 2005 event.

| Name of the Well  | Water Level Variation (cm) |
|-------------------|----------------------------|
| Ukalu (UKA)       | -14                        |
| Shringarpur (SHR) | -3                         |
| Nechal (NEC)      | 9                          |
| Taloshi (TAL)     | 3                          |

the figure that the co-seismic effects of the earthquakes in Koyna-Warna region are very distinctly revealed in the wavelet spectrum of the water level data.

Figure 6 shows the spectrum for different time periods; (a) shows the period from Jan. to Feb. 2005 i.e., before the event, (b) is for the month of March. 2005 i.e. at the time of event and (c) shows from April. 2005 to May. 2005 i.e. after the event. (d) Shows the time period from Jan. 2005 to May. 2005. From this Figure, it is very clear that a sudden peak in the spectrum which is well correlated with the time of event in Figure 6 (d) is more distinct when we consider the small window close to the time of the event (Figure 4 (a)).

In Table 1 are furnished the variation of water levels at different locations at the time of the event for 14<sup>th</sup> March 2005. Though no significant relationship could be established between variation in the bore well water levels and the distance between the epicenter and the bore well

it appears that the water level in the bore wells decreases when located in the zone of extension forces and the water level rises if located in the zone of compression forces.

## CONCLUSIONS

Analysis of water level data using wavelet transformation for some of the bore wells nearer to Koyna-Warna region has shown co-seismic variation due to 14<sup>th</sup> March 2005 Koyna earthquakes. The power spectrum calculated using the wavelet transform brought out the correlation between the water levels in bore wells and occurrence of an earthquake. In Ukalu the water level in the well nearer to an event showed prompt effect during earthquake. Analysis of the Ukalu well at different events of Koyna-Warna region show co-seismic water level change in the transformed domain very promptly but are not seen in the original time domain.

## ACKNOWLEDGEMENTS

The authors are grateful to the Director, National Geophysical Research Institute, for his kind permission to publish this work. Authors thank Prof. B.V.S.Murthy for apt editing and useful suggestions to enhance quality of the manuscript. We are grateful to Chief Editor for his support and timely help in completing review and editing process.

## Compliance with Ethical Standards

The authors declare that they have no conflict of interest and adhere to copyright norms.

## REFERENCES

- Chadha, R.K., Pandey, A.P., and Kuempel, H. J., 2003. Search for earthquake precursors in well water levels in a localized seismically active area of Reservoir Triggered Earthquakes in India, *Geophys. Res. Lett.*, v.30, pp: 69-1– 69-4.
- Chadha, R.K., Srivastava, K., and Kumpel, H.J., 2004. Earthquake-related changes in well water level and their relation to a static deformation model for the seismically active Koyna-Warna region, India. In: Rummel F (ed) *Rock mechanics with emphasis on stress*. Oxford & IBH Publ., New Delhi, pp: 135–150.
- Daubechies, I., 1990. The wavelet transforms time frequency localization and signal analysis, *IEEE Trans. Inf. Theory.*, v.36, pp: 961-1005.
- Farge, M., 1992. Wavelet transforms and their applications to turbulence, *Ann. Rev. Fluid Mech.*, v.24, pp: 395-457.
- Gupta, H.K., and Rastogi, B.K., 1976. *Dams and earthquake*, Elsevier, Amsterdam.
- Gupta, H.K., Ramakrishna Rao, C.V., Rastogi, B.K., and Bhatia, S.C., 1980. An investigation of earthquakes in Koyna region, Maharashtra for the period October 1973 through December 1976, *Bull. Seismol. Soc. Am.*, v.70, pp: 1838-1847.
- Gupta, H.K., 1985. *The Present Status of Reservoir Induced Seismicity Investigations with Special Emphasis on Koyna Earthquakes*, Elsevier Publishers, Amsterdam, *Tectonophysics*, v.118, pp: 257-279.
- Gupta, H.K., 1992. *Reservoir Induced Earthquakes*, Elsevier Scientific Publishing Company, Amsterdam, v.364.
- Koisumi, N., Tsukuda, E., Kamigaichi, O., Matsumoto, N., Takahashi, M., and Sato, T., 1999. Preseismic changes in groundwater level and volumetric strain associated with earthquake swarms off the east coast of the Izu peninsula, Japan, *Geophys. Res. Lett.*, v.26, pp: 3509–3512.
- Rastogi, B.K., Chadha, R.K., Sarma, C.S.P, Mandal, P, Satyanarayana, H.V, Raju, I.P, Kumar, N., Satyamurthy, C., and Nageswara Rao, A., 1997. Seismicity at Warna reservoir (near Koyna) through 1995, *Bull. Seismol. Soc. Am.*, v.87, pp: 1484–1494.
- Singh, D.D., Rastogi, B.K., and Gupta, H.K., 1975. Surface wave radiation pattern and source parameters of Koyna earthquake of December 10, 1967, *Bull. Seismol. Soc. Am.*, v.65, pp: 711-731.
- Soon, W., Dutta, K., Legates, D.R., Velasco V., and Zhang W.J., 2011. Variation in surface air temperature of China during the 20th century, *Journal of Atmospheric and Solar-Terrestrial Physics*, v.73, pp: 2331- 2344.
- Talwani, P, 1976. Earthquakes associated with Clark Hill Reservoir, South Carolina—a case of induced seismicity; Paper presented at the 1st Int. Symp. On Induced Seismicity. *Eng. Geol.*, v.10, pp: 239–253.
- Talwani, P, Kumar Swamy, S.V., and Sawalwade, C.B. 1996. The reevaluation of seismicity data in the Koyna-Warna area, 1963–1995, *Univ. S C Tech. Rept.*
- Torrence, C., and Compo, G. P., 1998. A Practical Guide to Wavelet Analysis, *Bulletin of the American Meteorological Society*, v.79, pp: 61-78.

# Simulation Results for Southern Indian Ocean (SIO) Using Ocean Model

A.P.Mishra<sup>1,2</sup> and A.C.Pandey<sup>1</sup>

<sup>1</sup>Department of Atmospheric and Ocean Studies, Faculty of Science, Nehru Science Centre,  
University of Allahabad, Allahabad-211002

<sup>2</sup>Central Water Commission, Sewa Bhawan, R.K.Puram, New Delhi-110066

\*Corresponding Author: anshu\_ms@yahoo.com

---

## ABSTRACT

A z-coordinate Modular Ocean Model (herein after referred as MOM3) has been implemented for global domain forced by NCEP/NCAR wind stress climatologies and executed for twenty five years. Several results of interest were analysed mainly for Southern Indian Ocean (SIO) (60°S-10°N, 30°E-120°E) including Antarctic Circumpolar Current (ACC) region of Southern Ocean (SO) from the output of the above model. The fidelity of the model is examined for varieties of phenomenon viz: surface elevation, horizontal circulations/vertical velocities at sub-surface, property transport including statistical estimation of Sea Surface Temperature (SST). The Results indicate that model produces strong variability of vertical velocity in the deeper ocean showing inability of z level model for bottom boundary layer correctly whereas the strength of the subsurface currents decays in comparison to the preceding depth circulation. It is noticed that in the upper ocean, the zonal transports are eastwards that may directly follow the surface currents. Statistical analyses include the estimation of model Error (ME), Correlation Coefficient (CC) denoted by R and Skill Score (SS) between model & observed SST data and result showing high correlation (R=0.94) with ME between 0 to 1°C. CC and SS suggests the success of model up to some extent. As seen from the R values, which are close to 1 over most of the model domain, is thought to be SST is simulated well.

**Key words:** Wind Stress, ACC, Sub surface horizontal circulation, Sea Surface Temperature, Vertical Velocity and Statistical Analyses.

---

## INTRODUCTION

The Southern Ocean (SO) plays a very important part in the general circulation of the world ocean and consequently the global climate system. Despite the recent advances in the understanding of SO, many questions remain unanswered. One reason is that the region is a particularly remote one with bad weather conditions and sea ice, which makes the collection of insitu data difficult (Best et al., 1999). Modelling SO is thus analytically somewhat intractable and resources must be had to be based on/ taken from numerical methods (Killworth and Nanneh, 1994). There has been a controversial issue on the choice of a vertical coordinate system for use in a numerical model like Modular Ocean Model (MOM) in the ocean modelling community. The geopotential or z-level coordinate is the simplest and has been widely used in the past. However, z-level models must represent the real bathymetry by a series of steps, which may lead to large truncation errors over steep topography (Gerdes 1993; Adcroft, Hill and Marshall 1997; Gnanadesikan and Pacanowski 1997; Sheng et al., 1998).

In this study, our interest is to see the performance of the above model and to see the improvements over the

existing studies/observation. In an attempt to reconcile some of the analyses/results from the present model for SIO/SO in response to wind forcing, we have examined horizontal circulation & vertical velocities (VV) at the sub-surface, property transport, SST using correlation and statistical measure from the output of the model and to possibly overcome the limitations of the observation based studies with the goal of obtaining a more complete physical understanding of the ocean dynamics and processes. Further, SST, being an important indicator of the state of the earth's climate system and its precise information, is very essential for climate monitoring, research and prediction (Reynolds et al., 2002) with focus on quantitative statistical measures between SST values of the model and observation. Moreover, VV diagnosed here is important as its measurements in the ocean are scarce (Thurnherr, 2011) and to study its variations, it is natural to quantify the VV variability and its distribution at the sub-surface and the processes responsible for such distribution. For instance, the equatorial upwelling that represents probably the largest mean VV is about 10<sup>-3</sup> cm/s (Wyrtki, 1981) and in the deep oceans, the mean value of VV is much smaller (about 10<sup>-5</sup>cm/s) (Munk, 1990). Spatial maps of different measures were shown/ generated to examine model performance.

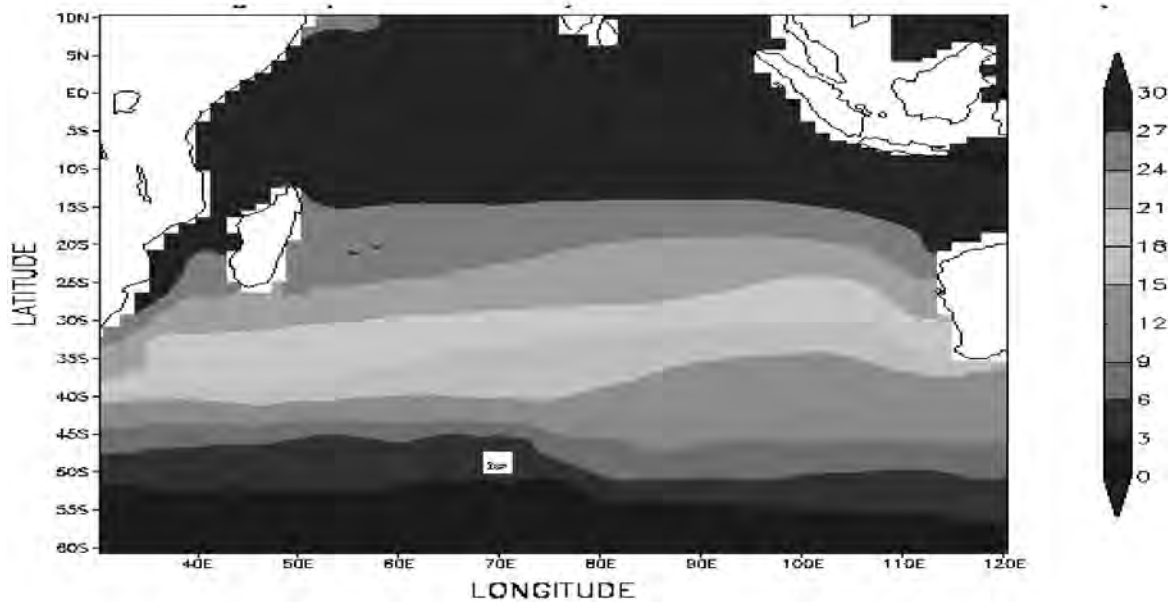


Figure 1. Six year average Model Surface Elevation Field (Units are in c.m.). The contour interval is 3 cm.

## METHODOLOGY AND MODEL SETUP

### Model and formulation

The version 3 of GFDL Modular Ocean Model [Pacanowski, Dixon and Rosati, 1993; Huang and Schneider 1995; Schneider et al., 1999] uses the Boussinesq and traditional approximations and allows the use of the rigid-lid and free-surface methods. It allows many types of mixing including horizontal mixing along surfaces of constant density and can be coupled to atmospheric models. The horizontal mixing of tracers and momentum is Laplacian. The momentum mixing uses the space-time dependent scheme of Smagorinsky (1963) and the tracer mixing uses Redi (1982) diffusion along with Gent and McWilliams (1990) quasi-adiabatic stirring. The zonal resolution is  $1.5^\circ$  while the meridional resolution is  $0.5^\circ$  between  $10^\circ\text{N}$  and  $10^\circ\text{S}$ , gradually increasing to  $1.5^\circ$  at  $20^\circ\text{N}$  and  $20^\circ\text{S}$ . There are 25 levels in the vertical with 17 levels in the upper 450 meters of the ocean. The model is forced by the long term mean surface wind stress from the National Center for Environmental Prediction (NCEP)-National Center for Atmospheric Research (NCAR reanalysis) (Kalnay et al., 1996). The original surface reanalysis is on an irregular grid with a zonal resolution of  $1.875^\circ$  and Gaussian latitudes of grid spacing less than  $2^\circ$ , and is linearly interpolated to the OGCM grids. The vertical mixing scheme is non-local K-Profile Parameterization (KPP) of Large, McWilliam and Doney 1994. The model surface salinity is relaxed to Levitus (1982) monthly climatology. Surface heat flux is also relaxed to Levitus (1982) climatology and relaxation time is 100 days. Model variables, set of equations, constants, coefficients and

depth to the grid point used in the model are described in an earlier study (Mishra et al., 2010). The four 3-D prognostic variables of the model are zonal and meridional components of velocity ( $u, v$ ), temperature ( $T$ ) and salinity ( $S$ ). The diagnostic variables are vertical velocity ( $\omega$ ) and density ( $\rho$ ). In order to suppress the fast moving surface gravity waves, the rigid lid approximation is employed (i.e.  $\omega=0$  at the surface  $z=0$ ).

### Experiment detail, Simulation domain and Study Region

The model is initialized from an ocean at rest with climatological temperature and salinity and then spun up for twenty five years under NCEP-NCAR climatological wind stress forcing. Initial condition is taken from annual mean temperature and salinity field without motion (Levitus, 1982). The monthly output of the model is saved and analyzed for SIO. Simulation domain of the model is that of the world oceans spanning from  $(74.25^\circ\text{S}$  to  $65^\circ\text{N}$ ,  $180^\circ\text{W}$ - $180^\circ\text{E}$ ) and the analysis region includes SIO region including SO spanning from  $30^\circ\text{E}$ - $120^\circ\text{E}$ ,  $60^\circ\text{S}$ - $10^\circ\text{N}$ .

## RESULTS AND DISCUSSIONS

### Surface Elevation, Horizontal Circulation and Vertical Velocities

Figure 1 shows the model climatology (last 6 year model run) of the surface elevation field in the Southern Indian Ocean region. We see that the surface elevation field shown in figure 1 is quite smooth and also the surface flow from the Indian Ocean into Madagascar near Somali

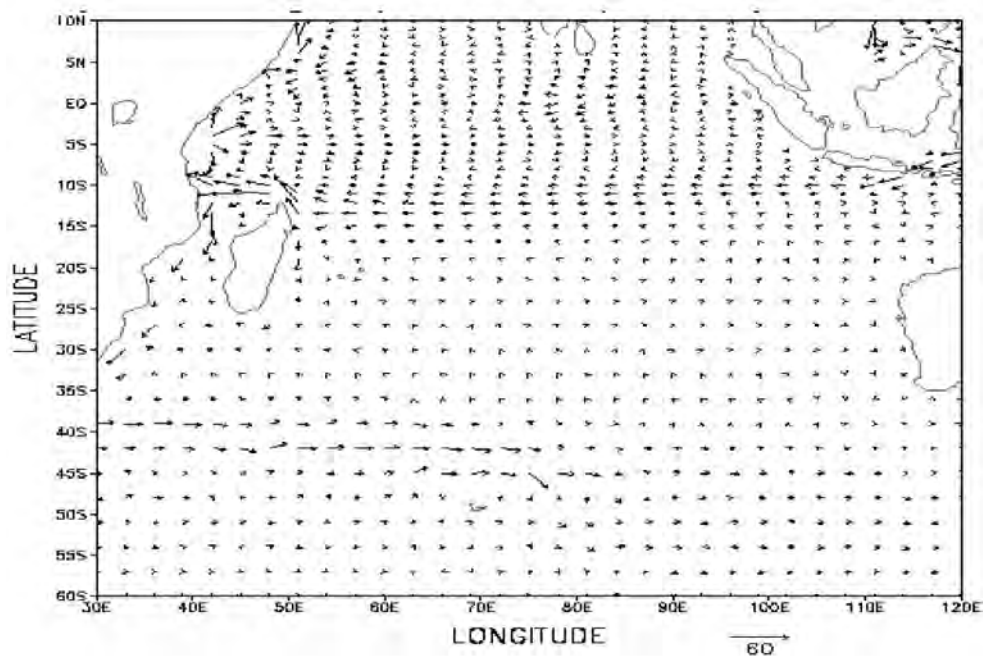


**Figure 2.** (a) Six year average horizontal circulation (cm/s) at 97.5 m. Arrow length of 0.5 cm represents current speed of 60 cm/s.

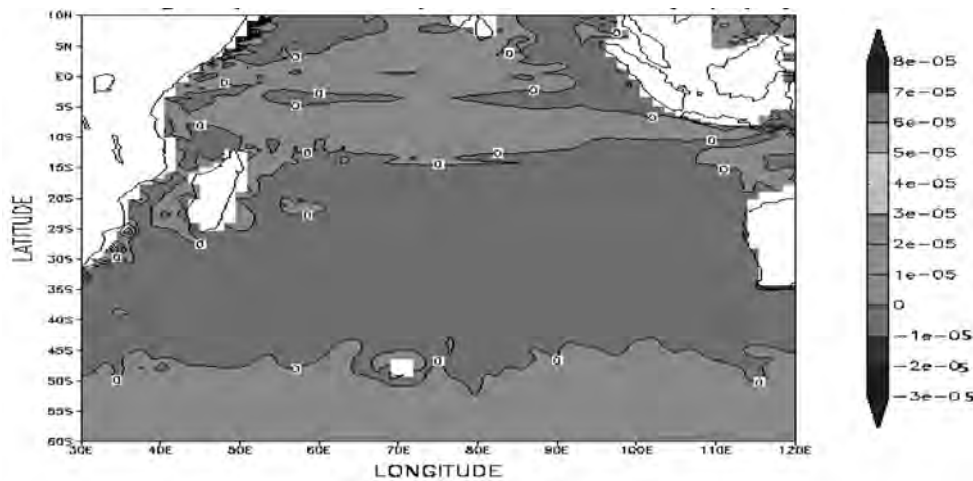


**Figure 2.** (b) Vertical velocity (m/s) at 97.5 m. The contour interval is  $1 \times 10^{-5}$  m/s in vertical velocity. Negative VV shows the downslope flows.

region. The high surface elevation field is associated with equatorial Indian Ocean/North Indian Ocean up to 25°S while the low elevation fields are seen near Antarctica Circumpolar Region (40°S-60°S). Moreover, the Sea level drop in Agulhas region is seen to be around 15-18 cm. In addition to such distribution, bump shaped frontal structure around Agulhas retroflexion area, 30°E (although area prior 30°E is not covered) can be understood and structure around the Antarctic Circumpolar Current (ACC) is well captured. Agulhas retroflexion is related to the Agulhas Current (27°S to 40°S, Gordon, 1985), a western boundary current of Southern Indian Ocean, since

as it reaches the Southern Ocean, the current retroflects or turns back on itself and flows eastward with part of the flow recirculating in the counter clockwise flowing subtropical gyre and part of the flow feeding the Antarctic Circumpolar Current as Agulhas return Current (Quarty and Srokosz, 1993).

Figures 2a, 3a and 4a show the velocity field at 97.5 m, 875.5m and near the bottom, respectively averaged over the last six years of the simulation. The vertical velocity is diagnosed through the continuity equation; horizontal velocities are driven by the Coriolis force, horizontal pressure gradient and advection terms.

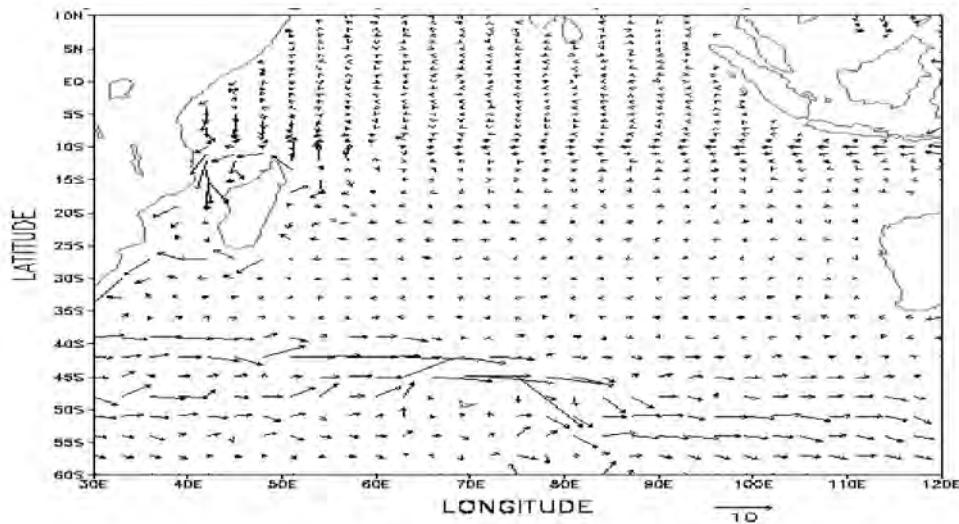


**Figure 3. (a)** Six year average horizontal circulation (cm/s) at 882m. In figure (a) arrow length of 0.5 cm represents current speed of 10 cm/s.

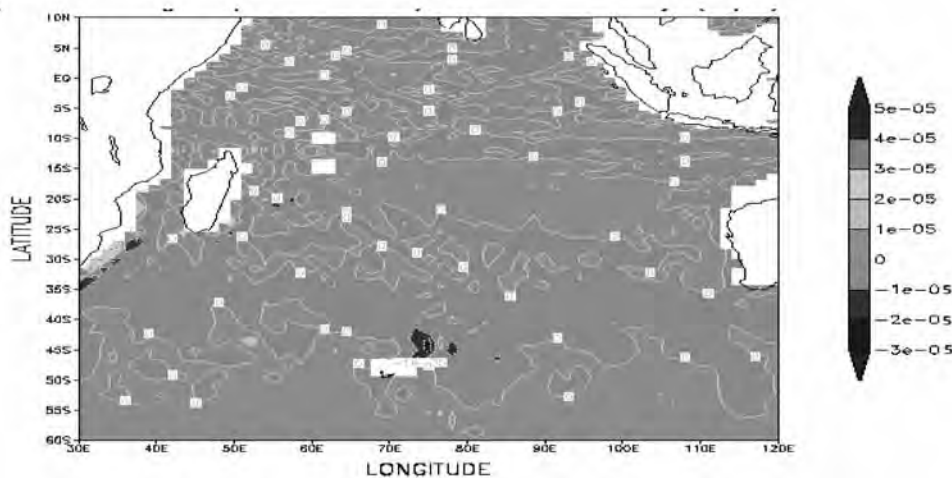


**Figure 3. (b)** Vertical velocity (m/s) at 882m. The contour interval is  $1 \times 10^{-5}$  m/s in vertical velocity. Negative VV shows the downslope flows.

At 97.5 m depth the dominant features are the westward and eastward flow of Southward Equatorial Current (SEC) and the Antarctic Circumpolar (ACC) flow respectively. Agulhas current is also revealed but various other currents viz; North Equatorial Current (NEC), Equatorial Counter Current (ECC) etc are not seen well and are too weak in the model (Figure 2a). The vertical velocity field shows the expected downward flow in the middle latitude from the wind driven Ekman pumping (Figure 2b). The horizontal flow field at 882m (Figure 3a) shows several small scale gyres in the Southern Ocean south of ACC. At this depth, SEC, NEC, ECC is not seen well while ACC is evident. We note entrainment of slope water west of the Madagascar into the subsurface water of ACC. Areas of strong downwelling are found along western boundaries, equatorial region etc. (Figure 3b).

The bottom flow field at 4882m (Figure 4a) generally follow the bottom topography contour (Olber and Volker 1996) and is the result of Ekman veering to the left (right) of the mean flow in the north (south) hemisphere, producing an upslope and downslope component. In the ACC, currents are very sparse and show few gyre structures (Figure 4a). The region of downslope near bottom flow in figure 4b indicates areas of possible deep water formation. For more clarity, we have plotted the overall feature of the model to find its fidelity. The very small vertical velocity ( $3 \times 10^{-21}$  m/s) shows that it is difficult to model bottom boundary layer correctly by z-level model, which is also suggested by Winton et al., 1998 in his studies. Overall, it is also evident in the figures 2a, 3a, 4a that strength of the subsurface currents at different depths is decaying monotonically down in comparison to the circulation in the preceding depths (e.g. 60cm/s at 97.5 m

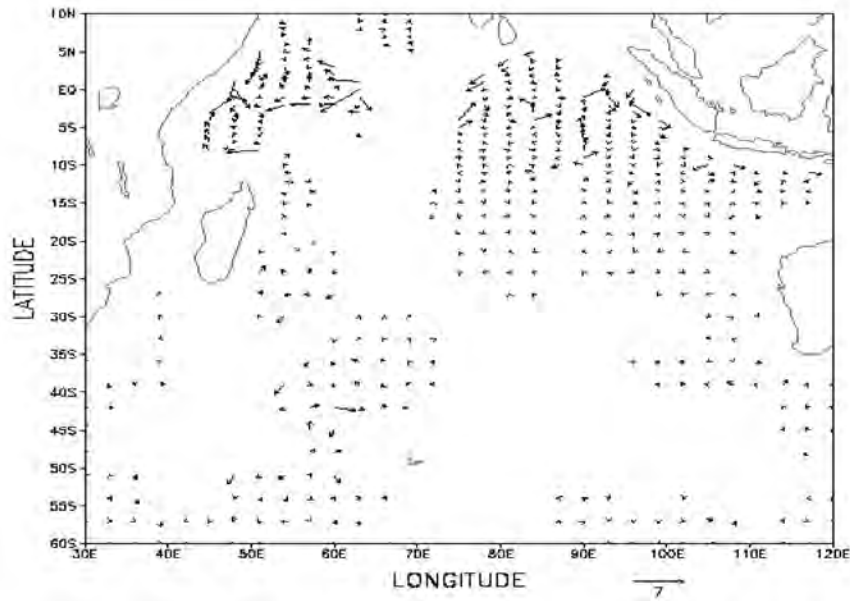


**Figure 4.** (a) Six year average horizontal circulation (cm/s) at 4482m. In figure (a) arrow length of 0.5 cm represents current speed of 7cm/s.

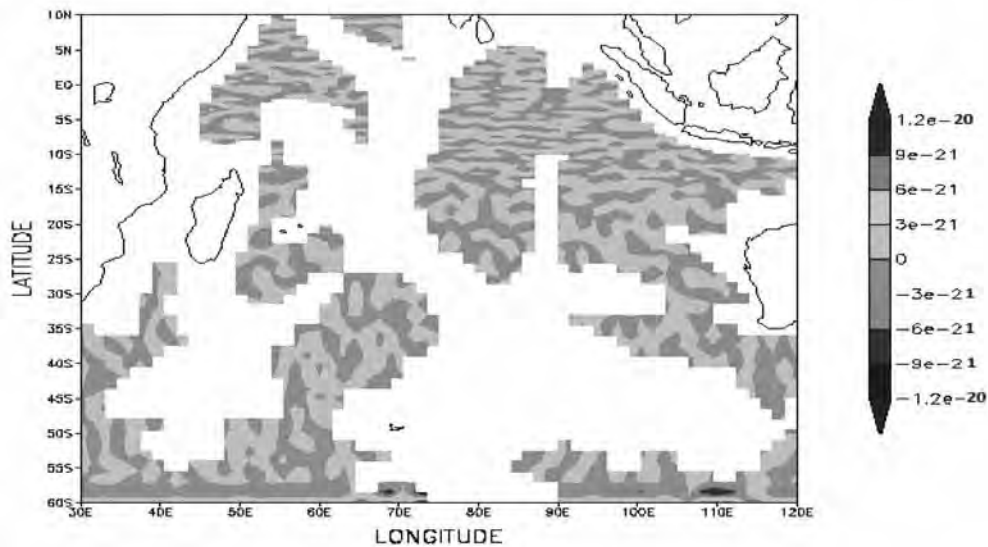


**Figure 4 (b).** Vertical velocity (m/s) at 4482 m. The contour interval is  $3 \times 10^{-21}$  m/s in vertical velocity. Negative VV shows the downslope flows.

depth, 10cm/s at 882m depth and 7cm/s at 4482 m depth) which shows that subsurface currents travel at a much slower speed when compared to surface flows. This is in accordance with the study suggested by Pidwirny, 2006 and owing to stratified ocean, velocities tend to be faster near to the surface (Gille, 1994).

### Upper Ocean Volume Transport

To examine the contribution of wind forcing, we have computed the upper ocean volume transport. The upper

ocean volume transport quantifies the flow patterns with water column of subtropical waters implied by the volume transport sections and is distributed at 60°S at about 250m depth, with magnitude lying between +5Sv to -1Sv ( $1 \text{ Sv} = 10^6 \text{ m}^3/\text{s}$ ). In the figure 5, the Agulhas current is marching swiftly towards north and the flow is weak with zero (0) Sv net transports at 30°E. These exterior flows significantly differ from the flows continuing up to 120°E. However, the energetics between +5/-1 Sv flows through Mozambique ridge at 35°E and Madagascar ridge at 44°E and there seems to be variable contribution of transport

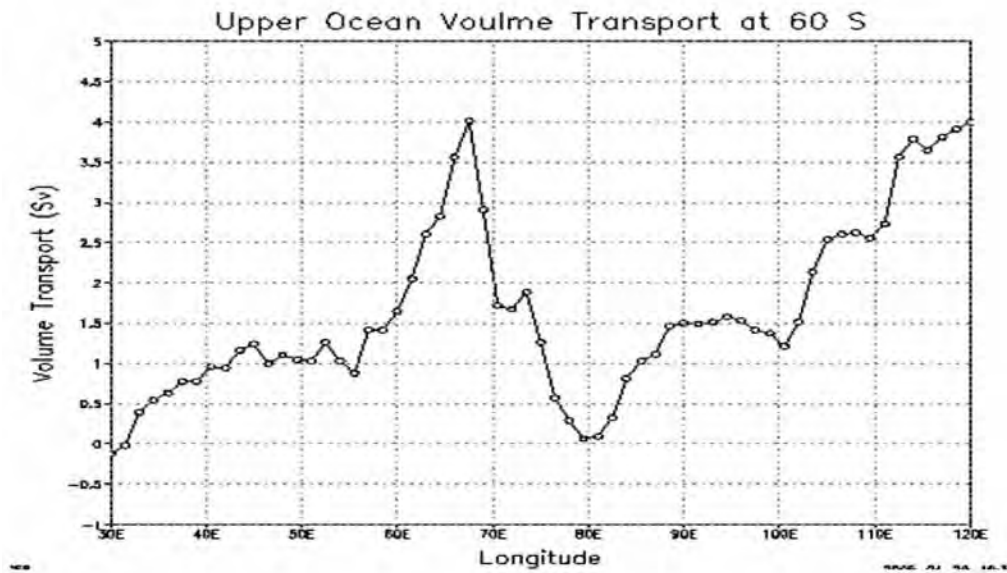


Figure 5. Upper ocean volume transport (Upper 250 meter depth) at 60°S in the region 30°E-120°E.

in feeding anticyclonic eddies on its left side as observed from incidence of different order (+5 Sv to -1 Sv). In the figure no 5, the fluctuations are confined to 250m depth, with a larger meridional scale width and in the upper ocean above the top of the thermocline, the zonal transports are eastward that may directly follow the surface currents. This result suggests that the vertically integrated, persistent eastward transport results largely from the layers in and below the thermocline (Weiying et al., 2004).

### Statistical Analysis between Model & Observed SST

#### Methodology and Formulation

For evaluation of the model results, monthly means are formed from January through December using the model years. These values are then compared to climatology at each grid point of the model domain. Several statistical measures are considered together to assess the comparisons between SST values predicted by the model and those predicted by the observed SST data (Levitus 1994). Here, we have taken the region of interest 60°S-20°N, 30°E-120°E to discuss SST analysis in detail.

Let  $X_i$  ( $i=1, 2, \dots, n$ ) be the set of  $n$  reference values (i.e. observed SST, Levitus, 1994) and let  $Y_i$  ( $i=1, 2, \dots, n$ ) be the set of estimates (i.e. Model SST). Also let  $\bar{X}$  and  $\bar{Y}$  and  $\sigma_x$  and  $\sigma_y$  be the mean and standard deviations of the reference (estimate) values respectively. For model data comparisons, we evaluate time series of monthly mean SST values from January to December at each grid point over the domain, so  $n$  is 12.

We have used the following statistical relationship between observed SST ( $X$ ) and Model SST( $Y$ ) [based on

Stewart (1990) and Murphy (1988) formula] as follows and also described by Kara, Wallcraft and Hurlburt 2003]:

$$ME = \bar{Y} - \bar{X} \quad (1)$$

$$RMS = \left[ \frac{1}{n} \sum_{i=1}^n (Y_i - X_i)^2 \right]^{1/2} \quad (2)$$

$$R = \frac{1}{n} \sum_{i=1}^n \frac{(X_i - \bar{X})(Y_i - \bar{Y})}{(\sigma_x \sigma_y)} \quad (3)$$

$$SS = 1 - \frac{RMS}{SD^2} \quad (4)$$

where ME is the bias or annual mean difference (in °C), RMS is the root mean square difference (in °C), R is the correlation coefficient, SS is the skill score (in degree C), SD is the standard deviation (in °C) and SS is dimensionless. The skill score is understood to be a very informative tool of model performance in predicting SST since it takes bias into account and often used to assess the accuracy of forecasts produced by numerical, statistical, and/or conceptual models relative to the accuracy of forecasts based on simple forecasting methods such as climatology or persistence (Murphy, 1996).

We have examined the model SST with respect to climatology for Model Error (Figure 7) i.e. departure of model SST from the observation using equation 1, RMS difference using equation 2, Correlation Coefficients denoted by R using equation 3 (Figure 6) and Skill Score (SS) over the model domain. The RMS difference between

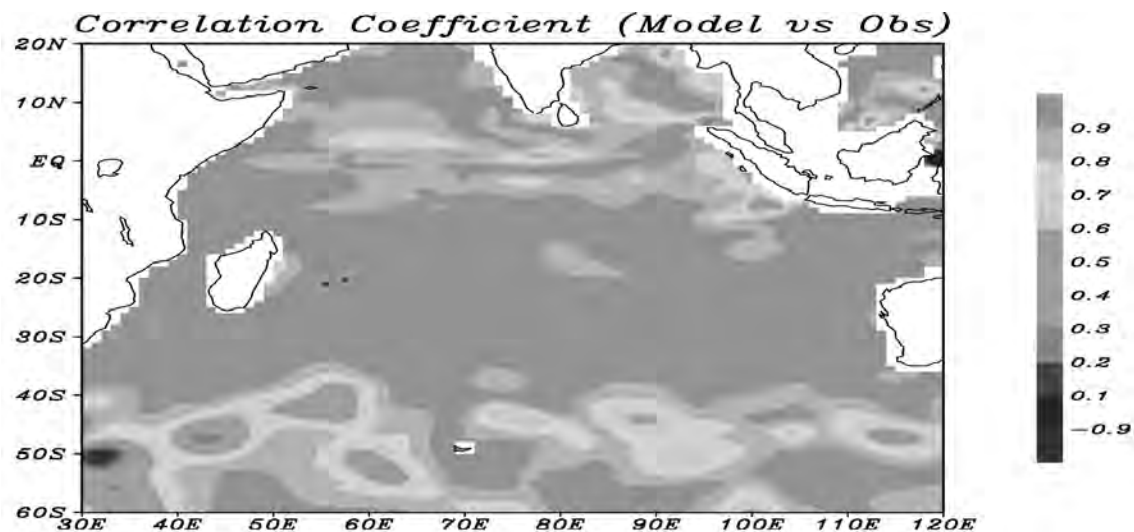


Figure 6. Correlation Coefficient (R) between model and observed SST.

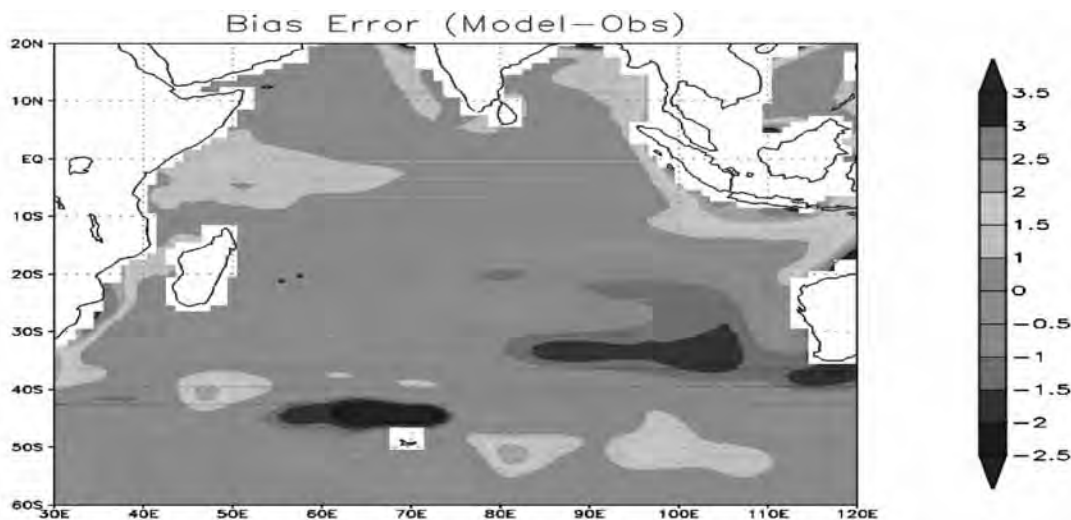


Figure 7. Annual mean error between model and observed SST. We note that mean error is between 0 to 1°C in the model domain.

model and observed SST is 1.34°C, Correlation Coefficients is 0.94, standard deviation between model and observed data is 1.15°C respectively. The domain average skill score is found to be 0.59, yet not very high, but suggests the success of model up to some extent. As seen from the R values, which are close to 1 over most of the model domain, is thought to be SST is simulated well.

Although the correlation is very high between model and observed SST in the most part of the southern ocean and equatorial warm pool, the model SST seems to be simulated well as evident from R values (Figure 6), especially in the ACC region, the correlation seems moderate to high. In general, SST bias (model error) in figure 7 looks within 0 to 1°C, when compared to the observations in most part of the study region, which may be because of advection of colder surface water by

upwelling processes. The SST errors in the open ocean are seen usually smaller than those along continental boundaries as well as upwelling regions. Cold SST biases are found in Southern Ocean around 20°S/40°S (Figure 7). Strong cooling by latent heat flux loss occurs in the central parts of the ocean (around 45°S/70°E) which may be due to strongness of the northeast trades and the weakness of south pacific convergence zone. In the present model study, the ocean temperature and salinity were restored to the observations, which could greatly improve the persistent bias. However, we would expect this bias to be improved in the high resolution model. In addition, it is also important to note that SST errors (Figure 7) along the continental boundaries may be due to steep structure of z-level models as suggested by Mellor et al., 2002; and Winton, Hallberg and Gnanadesikan, 1998).

## SUMMARY AND CONCLUSIONS

The primary motivation of this study is to evaluate the coarse resolution ocean model around SIO/SO. As far as modelling results are concerned, they are providing a good source of information on the model outputs viz; circulation, its energetic property transports, etc. including quantitative & statistical estimation of model SST against the observed data set. Success of the model SST is revealed well by the high correlation coefficient ( $R=0.94$ ) over the region of study, however, model is unable to predict/estimate VV for bottom boundary layer as the magnitude of VV is very small in the bottom. Its measurements are scarce because for, many years, velocity data in the ocean were collected primarily with mechanical current meters designed to measure the two horizontal component of velocity due to reasons of instrument cost and complexity (Thurnherr, 2011).

The model has always certain limitations and model provide its solution under a specified forcing under those limitations. However, forcing used in this Ocean General Circulation Model (OGCM) uses NCEP/NCAR climatological wind forcing which itself was regarded as less accurate forcing fields (Behra et al., 2000), due to which ocean modellers often relax ocean model simulation to the observed forcing. Hence, future step may be to use a coupled ocean atmosphere model to determine the implications on the finding presented here. Additionally, it is important to understand the uncertainty associated with the OGCM's simulation for statistical studies in respect of biases/error. In the modelling context, reproducing these results with OGCM's other than present set up with a coupled ocean-atmosphere model would be a valuable next step.

## ACKNOWLEDGEMENTS

We gratefully acknowledge Dr. Bohua Huang and Dr. Ben Kirtman of Center of Ocean Land Atmosphere Studies (COLA), Maryland, USA for providing the MOM source code and forcing fields for the model runs. We are very much thankful to COLA for providing the model source code. As, the work was funded by National Centre for Antarctic and Ocean Research, Goa (now under Ministry of Earth Sciences, Government of India) we would like to thank NCAOR for providing the assistance and valuable suggestions from time to time. The constructive comments and suggestions made by anonymous reviewers helped us to improve the manuscript. The authors are also thankful to Dr.M.R.K.Prabhakar Rao and Chief Editor for apt editing of the manuscript.

## Compliance with Ethical Standards

The authors declare that they have no conflict of interest and adhere to copyright norms.

## REFERENCES

- Adcroft, A., Hill C., and Marshall, J., 1997. Representation of topography by shaved cells in a height coordinate ocean model, *Mon. Wea. Rev.*, v.125, pp: 2293–2315.
- Best, S. E., Ivchenko V. O., Richards K. J., Smith R. D., and Malone, R. C., 1999. Eddies in Numerical Models of the Antarctic Circumpolar Current and their influence on the Mean flow, *J. Phys. Oceanogr.*, v.29, pp: 328-350.
- Behra, S. K., Salvekar, P. S., and Yamagata, T., 2000. Simulation of Interannual SST Variability in the Tropical Indian Ocean, *J. Clim.*, v.13, pp: 3487–3499.
- Gent, P. R., and McWilliams, J. C., 1990. Isopycnal mixing in ocean circulation models, *J. Phys. Oceanogr.*, v.20, pp: 150–155.
- Gerdes, R., 1993. A primitive equation ocean circulation model using a general vertical coordinate transformation. 1. Description and testing of the model; *J. Geophys. Res.*, v.98, pp: 14,683-14,701.
- Gille, S. T., 1994. Mean sea surface height of the Antarctic Circumpolar Current from Geosat data: Method and application, *J. Geophys. Res.*, v.99, pp: 18255-18273.
- Gnanadesikan, A., and Pacanowski, R., 1997. Improved representation of flow around topography in the GFDL Modular Ocean Model MOM2, *Int. WOCE Newsl.*, v.27, pp: 23–25.
- Gordon, A. L., 1985. Indian-Atlantic transfer of thermocline water at the Agulhas Retroflection, *Science*, v.227, pp: 1030-1033.
- Huang, B., and Schneider, E. K., 1995. The response of an ocean general circulation model to surface wind stress produced by an atmospheric general circulation model. *Mon. Wea. Rev.*, v.123, pp: 3059-3085.
- Kalnay, E., and Co-authors., 1996. The NCEP/NCAR 40 year Reanalysis Project, *Bull. Amer. Meteor. Soc.*, v.77, pp: 437-471.
- Kara, A. Briol., Wallcraft A. J., and Hurlburt, H. E., 2003. Climatological SST and MLD Prediction from a Global Layered Ocean Model with an Embedded Mixed Layer, *J. Atmos. and Ocean Technol.*, v.20, pp: 1616-1632.
- Killworth, P. D., and Nanneh, M. M., 1994. Isopycnal Momentum Budget of the Antarctic Circumpolar Current in the FRAM, *J. Phys. Oceanogr.*, v.24, pp: 1201-1223.
- Large, W. G., McWilliams J. C., and Doney, S., 1994. Oceanic vertical mixing: A review and a model with nonlocal boundary layer parameterization, *Rev. of Geophys.*, v.32, pp: 363-404.
- Levitus, S., 1982. Climatological Atlas of the World Ocean 1982, NOAA (US Government Printing Office, Washington D C), Report No. 13, pp: 173.
- Levitus, S., and Boyer, T. P., 1994a. World Ocean Atlas 1994, Oxygen. NOAA Atlas NESDIS 2, U.S. Department of Commerce, NOAA, NESDIS., v.2.
- Levitus, S., Burgett R., and Boyer, T. P., 1994b. World Ocean Atlas 1994, Salinity. NOAA Atlas NESDIS 3, U.S. Department of Commerce, NOAA, NESDIS., v.3.

- Mellor, G. L., Hakkinen, S., Ezer, T., and Patchen, R., 2002. A generalization of a sigma coordinate ocean model and an intercomparison of model vertical grids, In: *Ocean Forecasting: Conceptual Basis and Applications*, N. Pinardi and J. D. Woods (Eds.), Springer, pp: 55-72.
- Mishra, A. P., Rai S., and Pandey, A. C., 2010. Ocean Model derived global surface circulation and vertical velocity, *J. of Geolog. Soc. India*, v.76, pp: 468-478.
- Munk, W., 1990. The Heard Island Experiment *Naval Research Reviews*, v.42, pp: 326-369.
- Murphy, A. H., 1996. General decompositions of MSE-Based Skill Scores: Measures of some basic aspects of Forecast quality, *Mon. Wea. Rev.*, v.124, pp: 2353-2369.
- Murphy, A. H., 1988. Skill scores based on the mean square error and their relationships to the correlation coefficient, *Mon. Wea. Rev.*, v.116, pp: 2417-2424.
- Olber, D., and C. Völker, 1996. Steady states and variability in oceanic zonal flows. *Decadal Climate Variability: Dynamics and Predictability*, D. L. T. Anderson and J. Willebrand, Eds., Springer-Verlag, pp: 407-443.
- Pacanowski, R. C., Dixon, K., and Rosati, A., 1993. The GFDL Modular Ocean Model user guide, version 1.0, Technical Report 2, Geophys. Fluid Dyn. Lab., National Oceanic and Atmospheric Administration, Princeton, New Jersey, pp: 16.
- Pidwirny, M., 2006. Surface & subsurface Ocean Currents *Fundamentals of Physical Geography*, 2<sup>nd</sup> edition. (<http://www.physicalgeography.net/fundamentals/8q.html>).
- Quarty, G. D., and Srokosz, M. A., 1993. Seasonal variations in the region of the Agulhas retroflection: Studies with Geosat and FRAM, *J. Phys. Oceanogr*, v.23, pp: 2107-2124.
- Redi, M. H., 1982. Oceanic isopycnal mixing by coordinate rotation, *J. Phys. Oceanogr*, v.12, pp: 1154-1158.
- Reynolds, W. R., Rayne, N. A., Smith T. M., Stokes, D. C. and Wang, W., 2002. An improved In Situ and Satellite SST Analysis for Climate, *J. Climate*, v.15, pp: 1609-1625.
- Schneider, E. K., Huang B., Zhu Z., DeWitt D. G., Kinter III J. L., Kirtman, B., and Shukla, J., 1999. Ocean data assimilation, initialization, and predictions of ENSO with a coupled GCM, *Mon. Wea. Rev.*, v.127, pp: 1187-1207.
- Sheng, J., Wright D. G., Greatbatch, R. J., and Dietrich, D. E., 1998. CANDIE: A New Version of the DieCAST Ocean Circulation Model, *J. Atmospheric and Ocean Technology*, v.15, pp: 1414-1432.
- Smagorinsky, J., 1963. General circulation experiments with the primitive equations: I. The basic experiment, *Mon. Weather Rev.*, v.91, pp: 99-164.
- Stewart, T. R., 1990. A decomposition of the correlation coefficient and its use in analyzing forecasting skill, *Wea. Forecasting*, v.5, pp: 661-666.
- Thurnherr, A. M., 2011. Vertical Velocity from LADCP Data. Division of Ocean and Climate Physics, *Journal of Atmosphere and Ocean Technology*, 28:6, Lamont-Doherty Earth Observatory, Palisades, NY 10964.
- Winton, M., Hallberg, R., and Gnanadesikan, A., 1998. Simulation of density driven frictional downslope flow in z-coordinate ocean model, *J. Phys. Oceanogr*, v.28, pp: 2163-2174.
- Weiqing, Han., Webster P, Lukas, R., and Hacker, Hu. Aixue., 2004. Impact of Atmospheric Intraseasonal Variability in the Indian Ocean: Low-Frequency Rectification in Equatorial Surface Current and Transport, *J. Phys. Oceano.*, v.34, pp: 1350-1372.
- Wyrtki, K., 1981. An estimate of equatorial upwelling in the Pacific. *J. Phys. Oceanography*, v.11, no.9, pp: 1205-1214.

## NEWS AT A GLANCE

---



### FORTHCOMING EVENTS:

- 1) First International Conference on the Material Point Method for Modelling Large Deformation and Soil-Water-Structure Interaction  
  
10 Jan 2017 - 13 Jan 2017; Delft, Netherlands  
<http://www.mpm2017.eu>
- 2) EAGE Workshop on Naturally Fractured Reservoirs  
  
05 Feb 2017 - 08 Feb 2017;  
Dubai, United Arab Emirates  
Seismic attributes, 3D fracture statistics, rock matrix, well logs, Petrochemistry  
<http://www.eage.org/event/index.php?eventid=1266>
- 3) Third AAPG/EAGE/MGS Myanmar Oil and Gas Conference Exciting Evolution : Myanmar's petroleum systems, plays and field developments  
  
22 Feb 2017 - 24 Feb 2017; Yangon, Myanmar  
<http://www.eage.org/event/index.php?eventid=1497&Opendivs=s3>

### AWARDS AND RECOGNITION

- 1) ISRO Young Scientist award has been received by Ms.Jenita Mary
- 2) Dr. Abhey Ram Bansal, Principal Scientist working at CSIR – NGRI, Hyderabad has been elected as a Fellow of the National Academy of Sciences, India (FNASc)
- 3) Prof G. Parthasarathy, Chief Scientist of CSIR-NGRI has been honoured with "Best Reviewer Award" for the year 2015 by the Journal "Geoscience Frontiers".

- 4) The prestigious 'India Gaurav Award' has been conferred on Dr. T.K. Chand, CMD, NALCO, for his significant contributions and achievements in the field of Industry, on 18<sup>th</sup> Sep.2016.

### IGU Awards for the year 2016

- 1) Dr.Hari Narain LifeTime Achievement Award- Prof.O.P. Varma
- 2) Decennial Award- Dr.Kalachand Sain
- 3) Krishnan Medal- Dr.Uma Shankar
- 4) Anni Talwani Memorial Prize- Dr.Prakash Kumar

### Memorial/Endowment Lectures:

- 1) Prof.K.R.Rannathan Memorial Lecture- Prof.Harsh K Gupta
- 2) Sri LN Kailasam Memorial Lecture – Sri Sudhakar Mahapatra
- 3) Prince Mukarram Jah Endowment Lecture- Prof.D.C.Panigrahi
- 4) Dr.H.N.Siddique Memorial Lecture- Sri.G.C.Katiyar
- 5) Electrotek & Geometric Endowment Lecture- Prof.Mrinal Sen

### Prof.D.Lal Best Paper Award

- 1) M.S.Chaudhari, M.Majumdar, V.Bagade and S.Ranga
- 2) Uma Vadapalli and N.Vedanti

## SCIENCE NEWS

### **\*Historical records may underestimate global sea level rise**

New research published in *Geophysical Research Letters* shows that the longest and highest-quality records of historical ocean water levels may underestimate the amount of global average sea level rise that occurred during the 20th century. Dr. Philip Thompson, associate director of the University of Hawai'i Sea Level Centre in the School of Ocean and Earth Science and Technology (SOEST), led the study.

The investigation concludes that it is highly unlikely that global average sea level rose less than 14 cm during the 20th century, while the most likely amount was closer to 17 cm.

**Source:** P. R. Thompson, B. D. Hamlington, F. W. Landerer, S. Adhikari. Are long tide gauge records in the wrong place to measure global mean sea level rise? *Geophysical Research Letters*, 2016; DOI: 10.1002/2016GL070552

### **\* Magma movements foretell future eruptions**

Geologists have traced magma movement beneath Mt. Cameroon volcano, which will help monitoring for future volcanic eruptions. The researchers revealed a complex magma plumbing system beneath Mt. Cameroon volcano by analyzing crystals from the two most recent eruptions in 1999 and 2000. The results further suggest that between eruptions magma batches migrate to shallower depths where they evolve and increase their explosive potential. Hence a longer time between eruptions increases the likelihood of the next eruption being more explosive in style, similar to the Eyjafjallajökull eruption on Iceland in 2010.

**Source:** Harri Geiger, Abigail K. Barker, Valentin R. Troll. Locating the depth of magma supply

for volcanic eruptions, insights from Mt. Cameroon. *Scientific Reports*, 2016; 6: 33629 DOI: 10.1038/srep33629

### **\* Exhaling Earth: Scientists closer to forecasting volcanic eruptions**

On average, 40 volcanoes on land erupt into the atmosphere each month, while scores of others on the seafloor erupt into the ocean. A new time-lapse animation uniting volcanoes, earthquakes, and gaseous emissions reveals unforgettably the large, rigid plates that make the outermost shell of Earth and suggests the immense heat and energy beneath them seeking to escape.

Recent discoveries by Deep Carbon Observatory (DCO) scientists in the Deep Earth Carbon Degassing (DECADE) initiative are laying the foundation for improved volcanic eruption forecasts. These hard-won advances required expensive, dangerous expeditions to sniff gas emissions for clues. By 2019, DECADE scientists hope to have gas monitoring stations on 15 of the world's 150 most active volcanoes. This will add to the eight stations currently operated by other entities such as the USGS and the University of Palermo (Italy). Data collected at these monitoring stations are feeding a new database of volcanic carbon emissions, making potentially life-saving information available to many more scientists around the world.

DCO volcanologists are also advancing basic knowledge about how different volcanoes work, which is further advancing eruption forecasting.

**Source:** J. Maarten de Moor, A. Aiuppa, G. Avar, H. Wehrmann, N. Dunbar, C. Muller, G. Tamburello, G. Giudice, M. Liuzzo, R. Moretti, V. Conde, B. Galle. Turmoil at Turrialba Volcano (Costa Rica): Degassing and eruptive processes inferred from high-frequency gas monitoring. *Journal of Geophysical Research: Solid Earth*, 2016; 121 (8): 5761 DOI: 10.1002/2016JB013150

## TECHNICAL NEWS

\*\* Ocean Bottom Seismometer: Compiled by **Raja Acharya**, IMD, Regional Meteorological Centre, Kolkata

An ocean-bottom seismometer (OBS) is a seismometer designed to record natural and manmade vibrations under oceans and lakes. Data analysis yields information about structure and composition of the sea floor and the deeper crust. In a typical seismic survey, the instruments should be operational for several days (deployments can exceed 12 months), which requires a data storage capacity of more than 500 Mbyte.

The OBS consists of an aluminium sphere which contains sensors, electronics, enough alkaline batteries to last 10 days on the ocean bottom, and an acoustic release. The two sphere halves are put together with an O-ring and a metal clamp to hold the halves together. A slight vacuum is placed on the sphere to better ensure a seal. The sphere by itself floats, so an anchor is needed to sink the instrument to the bottom. The instrument is designed to deploy and recover by any vessel. All that is needed (for deployment and recovery) is enough deck space to hold the instruments and their anchors and a boom capable of lifting an OBS off the deck and swing it over to lower it into the water. The OBS is bolted to the anchor and then dropped (gently) over the side.

Seismometers work using the principle of inertia. The seismometer body rests securely on the sea floor. Inside, a heavy mass hangs on a spring between two magnets. When the earth moves, so does the seismometer and its magnets, but the mass briefly stays where it is. As the mass oscillates through the magnetic field it produces an electrical current, which the instrument measures. The seismometer itself is a small metal cylinder; the rest of the footlocker-sized OBS consists of equipment to run the seismometer (a data logger and batteries), weight to sink it to the sea floor, a remote-controlled acoustic release and flotation to bring the instrument back to the surface.

Prior to deployment, the data logger is programmed with the number of sensors to record the sample rate for data acquisition and the start time. At the designated time, information from the selected sensors is recorded on the data logger's 810 Megabyte hard disk. This information is recorded contiguously for all selected sensors until either the hard disk is filled or the OBS is recovered and the data collection stopped.

The OBS is recovered with an acoustic release. Once the OBS's location is confirmed, a coded transmitted pulse is sent from the surface to initiate the release. Once the OBS has reached the surface, the instrument is retrieved and stored until a later time when the data can be downloaded. Turning the instrument around for the next deployment requires downloading the data onto another computer, replacing the batteries, testing the system, and programming in new parameters.

The sensors used in the OBS consists one vertical 4.5 Hertz seismometer, two horizontal 4.5 Hertz seismometers, and one hydrophone. The horizontal seismometers are mounted 90 degrees to the vertical and 90 degrees to each other. The hydrophone provides information that is similar to the vertical seismometer, and under certain conditions can have a better signal/noise ratio. To keep the design of the USGS OBS simple and compact, the seismometers are indirectly coupled to the earth via the sphere, release hardware, the anchor, and the spring used to hold the OBS to its anchor (the spring is needed to pull the attachment bolt away from the OBS during release).

The ground motion caused by earthquakes can be extremely small (less than a millimetre) or large (several meters). Small motions have high frequencies, so monitoring them requires measuring movement many times per second and produces huge amounts of data. Large motions are much rarer, so instruments need to record data less frequently, to save memory space and battery power for longer deployments. Because of this variability, engineers have designed two basic kinds of seismometers: 1) Short-period OBSs and 2) Long-period OBSs.



**Source:** 1) [https://en.wikipedia.org/wiki/Ocean-bottom\\_seismometer](https://en.wikipedia.org/wiki/Ocean-bottom_seismometer)

2) <http://woodshole.er.usgs.gov/operations/obs/whatobs.html>

### **Outstanding Contribution to Atomic Energy and India's Nuclear Weapons Program**



**Rajagopala Chidambaram**

Dr. Chidambaram was born on 12 November 1936 in Madras, India. Chidambaram completed his early education in Meerut and Chennai, completing his B.Sc. with honours in physics, having stood first rank at the departmental and the University level of the Madras University in 1956. After enrolling in master's program, Chidambaram taught introductory physics laboratory courses and obtained M.Sc. in physics, writing a fundamental thesis on analog computers from the same institution, in 1958. He was accepted for the doctoral programme of the Indian Institute of Science (IISc), and was awarded the PhD in 1962. His thesis contained the research work on the development of Nuclear Magnetic Resonance, and was conferred with the Martin Forster Medal

for the best doctoral thesis submitted to the Indian Institute of Science. His contribution to the enhancement of condensed matter physics and material science led him to be conferred with a D.Sc., in physics by the IISc after submitting his doctoral thesis on experiments which he conducted at IISc. He has been conferred doctoral degrees in physics by eight Indian universities.

After receiving his doctorate in physics, Chidambaram joined the Bhabha Atomic Research Centre (BARC). He served as the director of the physics group initiating research on physical aspects of nuclear weapons. At BARC, he rose to become one of the senior nuclear scientists involved in various classified projects, and was one of the central figures building the nuclear programme. In 1967, Chidambaram joined the nuclear weapon designing effort along with his fellow scientists in constructing and building the metallurgical and physical aspects of the nuclear weapons. He and his colleagues worked out the equation of state of plutonium, which is still classified by all nuclear weapon states. He chose the implosion method and initiated research at BARC in very close interaction with the Terminal Ballistics Research Laboratory (TBRL) of the Defence Research and Development Organisation (DRDO). Chidambaram also assisted the Indian Army to construct a nuclear test site at long-constructed Indian Army base, Pokhran Test Range in Rajasthan.

He served as the principal scientific adviser to the federal Government of India. Some of his initiatives as Principal Scientific Adviser, including the setting up of the Core Advisory Group for R&D in the Automotive Sector (CAR) to increase academia-industry interaction, the creation of RuTAGs

(Rural Technology Action Groups) for effective need based technology delivery in rural areas and the establishment of SETS (Society for Electronic Transactions and Security). All of them are making significant impact. During the last few years, he helped conceptualise and supervised, along with National Informatic Center, the setting up of the high-speed 'National Knowledge Network' to connect about 1,500 educational and research institutions in India. He has emphasised the need for 'Coherent Synergy' (a phrase he has coined) in India's Science & Technology (S&T) efforts to take India on a sustained fast-growth path. He has also focused on the importance of 'Directed Basic Research' as an addition to (not a substitute for) self-directed basic research.

Chidambaram is the recipient of number of awards and honours. The Indian Government acknowledged his contribution to the successful nuclear tests by awarding the Padma Shri, the fourth highest Civilian honour of the nation, in 1975 and the Padma Vibushan, the second highest civilian honour, in 1999. His other prominent awards are the Distinguished Alumnus Award of the Indian Institute of Science (1991), the C.V. Raman Birth Centenary Award of the Indian Science Congress Association (1995), the Distinguished

Materials Scientist of the Year Award of the Materials Research Society of India (1996), the R.D. Birla Award of the Indian Physics Association (1996), the H. K. Forodia Award for Excellence in S & T (1998), the Hari Om Prerit Senior Scientist Award (2000), the Meghnad Saha Medal of the Indian National Science Academy (2002), the INS Homi Bhabha Lifetime Achievement Award of the Indian Nuclear Society (2006), the Life Time Contribution Award in Engineering (2009) from Indian National Academy of Engineering, the C.V. Raman Medal of the Indian National Science Academy. He has been awarded D.Sc. degrees (Honoris Causa) by more than twenty universities in India and abroad. Chidambaram is a Fellow of all the science Academies in India and the Third World Academy of Science (TWAS), Trieste (Italy). He has also served as a member, chairman and president of a number of organizations which, among others, include IIT-Madras, IIT-Bombay, the Materials Research Society of India, the Council of Scientific and Industrial Research (CSIR), and the International Union of Crystallography. In early 2008, the IAEA invited Chidambaram to be a member of the "Commission of Eminent Persons", for making recommendations to the Board of Governors, regarding long-term priorities and funding.

**P.R.Reddy**

## Can we have an organised Sustainable agriculture System that can ensure our food security?

P.R.Reddy

Director Grade Scientist (Retd), CSIR-NGRI, Hyderabad-500 007, Telangana State  
E-mail: parvatarreddy@gmail.com

---

### ABSTRACT

Agriculture practices vary from place to place. Even concepts and methodologies need to be changed, taking in to consideration a region`s ecosystem peculiarities and socio-economic aspects. From time to time decisions are taken by the concerned focusing on the problem on hand, ignoring or not worrying about repercussions of any decisions taken to overcome the problem on hand. At a later stage when setbacks of significant nature crop up critics pounce on the decisions taken earlier, forgetting decisions and execution mechanisms change with time and our focus should be to take steps that can improve the situation, instead of wasting our energies in finding reasons for spilled milk.

Green Revolution was hailed for bailing us out of a tricky situation in 1960s and 1970s. In the process the introduction of chemical fertilizers, chemical pesticides led to deterioration of soil fertility and overall environmental degradation. While there is a definite necessity to improve our soil fertility and proper usage of depleted water resources, it is essential to take up any steps that can help our country as a single entity and not a disjointed forty and odd independent segments.

**Key words:** Food Security, Green Revolution, Sustainability, chemical fertilizers & pesticides, soil fertility, organic farming.

---

### PREAMBLE

It is the intellect of an individual that makes his way of logical analysis more impressive, rather than the merits and demerits of the subject during a debate. Majority of the present day problems faced by us needs an in depth understanding of the problem before taking up apt preventive and curative measures. In the absence of such a measure the intellect can hoodwink a routine planning, administrative and execution mechanism and makes his business choices get the needed support compared to more useful sustainable measures. These intellectuals have been invariably responsible for setbacks noticed in the present day local, regional and global food production and environmental degradation. Overcoming these manipulations at different levels can we ensure an organised sustainable agriculture system in the foreseeable future amidst various setbacks? To have an in depth analysis of the problem let us look in to various aspects. Agriculture practices vary from place to place. Even concepts and methodologies need to be changed, taking in to consideration a region`s ecosystem peculiarities and socio-economic aspects. Ecological or sustainable agriculture, as the name suggests, is a kind of farming that is sensitive to local conditions. It makes judicious use of available resources and tries to bind locally available plants, trees, birds, animals, insects and micro-organisms to interplay in a mutually beneficial fashion - one that results

in nutritious, rich and chemical-free crops. An organised approach pays attention to soil fertility, agricultural biodiversity, climate mitigation and adaptation, green knowledge development, a decent living for farmers and gender inclusiveness. Sustainable agriculture can essentially be described as the practice of farming ecologically. Rather than focusing only on the economic viability of the crops, sustainable agriculture also involves using non-renewable resources effectively, growing nutritious foods and enhancing the quality of life of the farmers. Besides the obvious benefits, sustainable farming also allows farmers to transform their farms into giant recycling centres. They can turn crop waste and animal manure into fertilizers, use crop rotation to enrich the soil and reroute rainwater to fuel the irrigation system. Not only does this save money, but it also conserves natural resources. Sustainable farming also lowers the need for chemicals and pesticides, and it makes the transition to a more organic, clean farming process a lot more feasible. It is basically aimed at stimulating green and rewarding small holder farming by supporting and scaling up promising approaches. With the above criteria gaining importance we come across a significant number of articles supporting or opposing " Green Revolution" measures introduced in 1960s that bailed us out from food deficient country in to a self sufficient one by 1970s. The resultant adverse effect on soil productivity capacity and overall negative impact on our ecosystem adversely affected our food production by 2000. Various remedial measures

## Can we have an organised Sustainable agriculture System that can ensure our food security?

have been suggested by learned scientists for ensuring sustainability of agriculture .

As per one school of experts it is advisable to re-introduce the traditional agriculture to make our agriculture sustainable. As stated by a highly respected agriculture and Climate expert "The traditional agriculture was soil and climate driven farming system that encompasses the animal husbandry. It provided socio-economic, food and nutrient security with the healthy food. Those were the "Golden Days" in the history of farming. It was an environment-friendly system and was highly successful & sustainable. No pollution, no worry about seeds and fertilizer adulteration as they used good grain as seed and compost of farmyard manure and green manure as fertilizer. Following growth in population the food production balance got disrupted and in order to find a solution to ever-growing problem, 1960s saw the chemical inputs technology and genetically modified seed technology entering India in the form of much eulogised "Green Revolution Technology". With the help of those technologies, food security was achieved to a considerable extent. But, it came at huge costs with negative impact on environment. The Green Revolution increased the production substantially in terms of quantity but could not achieve the quality of traditional agriculture in terms of food and fodder. The technology includes high yielding seeds, chemical inputs (fertilizers & pesticides, insecticides, herbicides, etc) and irrigation; all of them increased the cost of agriculture. To reduce the burden on farming community the government introduced input subsidy, a huge component. Studies on paddy/rice production figures of 1970s & 1980s in Andhra Pradesh revealed that the traditional paddy under irrigation yielded 1300 kg/ha; by adding high yielding seed this increased by 500 kg/ha; and by adding chemical fertilizers the yield level rose further by 2000 kg/ha. That means total yield achieved was 3800 kg/ha under farmers' fields. This was far less than research station yields of 5000 to 6000 kg/ha. The present average yields of farmers' field are 2600 – 2800 kg/ha as the yield curve flattened since 1984-85. Only increase in area under irrigation contributed to additional increase in production after 1984-85. Studies clearly reflect that high yielding seeds were tailored to chemical fertilizers under irrigation. This severely affected dry-land agriculture that constituted around 60% of the cultivated land. This forced dry-land farmers migrating to urban areas as the dry-land agriculture with high input costs became unsustainable and non-remunerative".

Even though what has been stated above was true, to meet our ever increasing demand for quantity of food products the steps taken during "Green Revolution" were to a large extent necessary at that phase . As we look in to various negative impacts due to chemical fertilisers, chemical pesticides, high yielding seeds it is clear that none took in to cognizance the negative impacts, as the

focus at that time was on higher production to cater to the needs of ever increasing population. Lack of co-ordinated monitoring system that brings in to light area specific soil and water role in our food production resulted in depletion of soil fertility and non-availability of sufficient water for irrigation. Even though the increase in production, as stated above, after 1984-85 was attributed to increase in cultivable land we are alarmed by conversion of fertile lands in to urban conglomerations from Kashmir to Kanya Kumari shrinking the cultivable land steadily from around 2005. To ensure re-emergence of free pollution environment and sufficiently good agriculture land with fertile soil it has become necessary for a proper co-operation between farmers of different segments of our country; a necessity. Instead of assuming our country is made up of 40 isolated segments with conflicting interests it is essential to bring together all the states in developing a beneficial sustainable food security package that can help every Indian. Such a development alone can help us to survive and grow amidst number of hurdles faced by our agriculture based economy.

\*\*\*A sustainable approach to farming is economically viable, environmentally sound, and socially beneficial: it works for the farmer, the land, and the community. Sustainable agriculture is grounded in the idea of stewardship: preserving the resources that allow us to meet our own needs, so that future generations can meet theirs too. This idea might seem too obvious to need stating, but its implications are far-reaching. If we are serious about sustainability, we cannot continue to farm in ways that deplete soil, pollute water, reduce biodiversity, and impoverish rural communities. We need a new agricultural toolkit. And farmers across America, with the help of science, are developing that toolkit. Crops require fertile soil and protection from weeds and insect pests in order to produce the food we need. Sustainable agriculture meets these requirements with sophisticated management practices grounded in the science of agro-ecology, which views farms as ecosystems made up of interacting elements—soil, water, plants, and animals—that can be modified to solve problems, maximize yields, and conserve resources.

Research has shown that agro-ecologically based methods—such as organic fertilizers, crop rotation, and cover crops—can succeed in meeting our food needs while avoiding the harmful impacts of industrial agriculture. As farmers incorporate these practices into their work, many benefits emerge: Less pollution, healthier and more fertile soil that is less vulnerable to drought and flooding. Also it can result in a lighter impact on surrounding ecosystems and greater biodiversity, reduced global warming impact and less antibiotic and pesticide resistance. This checklist of benefits adds up to more than the sum of its parts. The ultimate benefit of adopting sustainable agriculture is that in doing so, we make it more likely that our farms will remain

healthy and productive for future generations. Ultimately, it is farmers themselves, by adopting sustainable practices, who will turn sustainable agriculture from a movement of forward-thinking innovators into standard operating procedure for U.S. food production. But consumers and policy makers have a role to play as well. The current system in practice in different parts of the world is the result of policy choices—and we will need to make better policy choices to move that system in a new direction.

Even though what is pointed out above is the right path, we find difficult to switch over to pure organic cultivation, as farmers from different segments of the country are more interested in producing more to gain financially at the expense of quality. Soil fertility and depletion of ground water are going to adversely affect our food production, in the near future, unless the experts convince the farmer the necessity to change the age old cultivation practices.

#### **What we need to make our initiatives sustainable?**

Take the roads of Punjab during the monsoon and you will find most fields turned into pools of water. It's mainly the water pulled out from the underground vault to support the kharif crop of paddy (rice). Neither a native plant nor suited to the agro-climatic region, paddy has pushed out maize and cotton, which were common in the pre-green revolution era. From 2,27,000 hectares in 1960, the area under paddy rose to 26,12000 hectares by the year 2000; a growth rate of 1,050 percent. In fact, estimates by the Commission for Agricultural Costs and Prices suggest that to grow one kilogram of rice, 5337 litres of water is required, which is double the figure for West Bengal (2605 litres), a natural habitat for the crop. The conventional method of rice cultivation requires flood irrigation (730 mm per hectare) as it helps check the growth of weeds. This is why paddy was traditionally grown mostly on floodplains of rivers and around drains, even in Punjab. Expansion of irrigation canals and accessibility to groundwater through pump sets meant more area could be brought under this crop. The DSR rice cultivation technique, which involves sowing the seeds instead of transplanting saplings, is practiced in central Punjab district of Moga to save on labour and fuel used to power pumpsets when power supply is erratic. It is noticed that introduction of a machine that drills the seeds in the soil can be profitable, but one has to take extra care for one and a half months as weeds may flourish due to less water. In addition, DSR does not work everywhere. It needs good loamy soil. Also, farmers are wary of this technique as they are more in groove with the conventional practice. Infestation of weeds requiring regular monitoring is another reason that DSR got restricted to few pockets. Most of the Punjab farmers now practise system of rice (or root) intensification (SRI), which has many takers

across the world. SRI involves plantation of saplings 10-12 days old instead of three weeks in a grid pattern with space of eight inch on all sides. The idea is to get better nourishment for the roots which can support a strong plant. The soil moisture is maintained through irrigation every four to five days instead of keeping the fields flooded all the time. If better water availability pushed paddy, assured procurement made it stay. The green revolution, introduced in India in 1960s, came with high-yielding varieties of wheat and paddy meant to make the country self-sustaining in food production. Assured procurement of these two crops by government agencies for distribution to other states fetched better prices for farmers. Over time, paddy dovetailed well with wheat, a major winter crop of Punjab. Consequently, machinery was also specifically designed for wheat-paddy cycle, which further pushed the combination. Even though the economics reveals paddy cultivation in Punjab is flourishing it has pushed back Maize, Cotton and other irrigated dry crops leading to an imbalance in the agriculture output. No one is ready to convince the Punjab farmer the need to grow the nutritious Maize and other ID crops along with Paddy. A time may come when a Punjab farmer while ready to import his favourite staple food of Makki ki roti and Sarson Ka Saag, would be competing with the conventional rice growing farmers of W.Bengal, Orissa, Andhra Pradesh, Tamil Nadu and other states, leading to unhealthy competition. In areas where one can grow rice due to presence of thick loamy soils, as all along the east and west coastal belts, in major river basins these techniques can be used by gaining needed knowledge through proper interaction between Punjab and other farmers, especially when monsoon aberrations have resulted no assured water supply to practice conventional flow irrigation.

Any planned initiative aimed at in ensuring food security should be termed as an Indian initiative and not x.y and z state initiative. This aspect assumes importance if we go through the recent study on "Virtual water trade". Due to lack of a properly planned export and import of food products we are running India dry, while China is conserving its water supply by importing water intensive crops such as soya. Concerns over looming water scarcity in large tracts of Asia and Africa, especially due to climate change, have led researchers to develop new analytical approaches to quantify expected water losses. One such concept is 'virtual water trade', which refers to the water embedded in commodities. A country that exports wheat, for example India, is in effect exporting the water needed to grow it. When states like West Bengal and other states along the coast, as stated earlier, use half the quantity of water for growing one kg of rice compared to Punjab our agriculture scientists encourage rice cultivation in Punjab, setting aside clear warnings that India will be deprived of precious water much faster compared to China. If such

## Can we have an organised Sustainable agriculture System that can ensure our food security?

short sighted approaches are allowed to continue we would face many setbacks in ensuring food security.

In nutshell it is essential to take proper care of our water, soil and other essential components for achieving sustainable agriculture amidst monsoon vagaries. Everyone needs to focus on this important approach. To a considerable extent our dedicated experts tried to introduce the state of the art technology, hoping the steps introduced would meet our food needs. They succeeded to a considerable extent but failed to visualise the negative impact of the production enhancement chemicals on soil fertility and quality of the product. Instead of criticising their initiatives, as now we know what ails our food production, let all the experts

pool in their energies and expertise to take immediate and long standing preventive and curative measures to ensure food security. As explicitly explained in the previous paragraph our food export and import trade policies should be periodically monitored introducing apt mid course corrections.

### **Web-links:**

1) [http://www.ucsus.org/our-work/food-agriculture/solutions/advance-sustainable-agriculture#.VLUX\\_CuUcik](http://www.ucsus.org/our-work/food-agriculture/solutions/advance-sustainable-agriculture#.VLUX_CuUcik)

2) <https://www.thethirdpole.net/2015/07/08/india-loses-and-china-gains-water-through-food-trade/>

## GUIDE LINES TO AUTHORS

The Journal of Indian Geophysical Union (J-IGU), published quarterly by the Indian Geophysical Union (IGU), is an interdisciplinary journal from India that publishes high-quality research in earth sciences with special emphasis on the topics pertaining to the Indian subcontinent and the surrounding Indian Ocean region. The journal covers several disciplines of earth sciences such as the Geosphere, its watery and gaseous envelopes (the Hydrosphere, the Cryosphere and the Atmosphere), and life (the Biosphere). It also publishes articles on Space and Planetary sciences. J-IGU welcomes contributions under the following categories:

- Research papers reporting new findings, results, etc.
- Review articles providing comprehensive overview of a significant research field related to earth sciences

In addition, J-IGU also welcomes short communications on opinion and report on scientific activity, personal information, book reviews, news and views, etc.

The manuscript should be submitted electronically as a single pdf file including the main text, figures, tables, and any other supplementary information along with the signed "Declaration Letter". The manuscript should be submitted by email ([jigu1963@gmail.com](mailto:jigu1963@gmail.com)) to the Editor.

After acceptance of the manuscript the corresponding author would be required to submit all source files (text and Tables in word format) and figures in high resolution standard (\*.jpg, \*.tiff, \*.bmp) format. These files may be submitted to the Editor as a single \*.zip file along with the "Copyright Transfer Statement".

### IMPORTANT INFORMATION

#### **Ethics in publishing**

J-IGU is committed to ensuring ethics in publication and takes a serious view of plagiarism including self-plagiarism in manuscripts submitted to the journal. Authors are advised to ensure ethical values by submitting only their original work and due acknowledgement to the work of others in case used the manuscript. Authors must also refrain from submitting the same manuscript to more than one journal concurrently or publish the same piece of research work in more than one journal which is unethical and unacceptable. Editor of J-IGU is committed to make every reasonable effort to investigate any allegations of plagiarism brought to his attention, as well as instances that come up during the peer review process and has full authority to retract any plagiarized publication from the journal and take appropriate action against such authors if it is proven that such a misconduct was intentional.

Similarly, Editor and Reviewers are also expected to follow ethical norms of publishing by ensuring that they don't use any unpublished information, communicated to them for editorial or review purpose, in their own research without the explicit written consent of the author. They are also expected to keep manuscript/ data/ observations/ any other information related to the peer review confidential to protect the interest of the authors. Reviewers should refrain from reviewing the manuscripts in which they have conflicts of interest resulting from competitive, collaborative, or other relationships or connections with any of the authors, companies, or institutions connected to the manuscript.

#### **Conflict of interest**

All authors are requested to disclose any actual or potential conflict of interest including any financial, personal or other relationships with other people or organizations within three years of beginning the submitted work that could inappropriately influence, or be perceived to influence, their work.

#### **Submission declaration**

Submission of a manuscript implies that the work has not been published previously and it is not under consideration for publication elsewhere, and that if accepted it will not be published elsewhere in the same or any other form, in English or in any other language, without the written consent of the publisher. It also implies that the authors have taken necessary approval from the competent authority of the institute/organization where the work was carried out.

#### **Copyright**

After acceptance of the manuscript the corresponding author would be required to sign and submit the "Copyright Transfer Statement".

### MANUSCRIPT PREPARATION

The corresponding author should be identified (include E-mail address, Phone/Mobile number). Full affiliation and postal address must be given for all co-authors.

#### **Abstract:**

An abstract of not more than 300 words must be included.

#### **Text:**

The manuscript should be structured to include a front page containing the title, Author(s) name, affiliation and address of the institute where the work was carried out, a short title, and 5-to-6 index terms/Key words. Author(s) present address, if different from the above mentioned address, may be given in the footnote. The corresponding author should be identified with an asterisk and his/her email ID should be provided. This page should be followed by the main text consisting of Abstract, Introduction, Methods/ Techniques/ Area description, Results, Discussion, Conclusions, Acknowledgements, and References. Tables and Figures with captions should be inserted in the main text of the manuscript at appropriate places.

#### **Figures/ Illustrations:**

All figures should be provided in camera-ready form, suitable for reproduction (which may include reduction) without retouching. Figures in high-resolution (at least 300 dpi) standard formats (\*.jpg, \*.tiff, \*.bmp) are acceptable. Figures should be numbered according to their sequence in the text. References should be made in the text to each figure. Each figure should have a suitable caption.

#### **Tables:**

Authors should take note of the limitations set by the size and layout of the journal. Table should not exceed the printed area of the page. They should be typed on separate sheets and details about the tables should be given in the text. Heading should be brief. Large tables should be avoided and may be provided as supplementary information, if required.

#### **Equations:**

Equations should be numbered sequentially with Arabic numerals and cited in the text. Subscripts and Superscripts should be set off clearly. Equation writing software that presents each equation as an object in MS Word will be accepted. Style and convention adopted for the equations should be uniform throughout the paper.

#### **References:**

All references to publications cited in the main text should be presented as a list of references following the text and all references in the list must be cited in the text. References should be arranged chronologically, in the text. The list of references should be arranged alphabetically at the end of the paper.

References should be given in the following form:

Kaila, K.L., Reddy P.R., Mall D.M., Venkateswarlu, N., Krishna V.G. and Prasad, A.S.S.R.S., 1992. Crustal structure of the west Bengal Basin from deep seismic sounding investigations, *Geophys. J. Int.*, v.111, no., pp:45-66.

### REVIEW PROCESS:

All manuscripts submitted to the journal are peer-reviewed. It is advisable to send the contact details of **4 potential reviewers** along with the manuscript to expedite the review process. Editor has the option to select reviewers from the list or choose different reviewers. The review process usually takes about 3 months. All enquiries regarding the manuscript may be addressed to the Editor.

#### **GALLEY PROOF:**

Technical editing of manuscripts is performed by the editorial board. The author is asked to check the galley proof for typographical errors and to answer queries from the editor. Authors are requested to return the corrected proof **within two days** of its receipt to ensure uninterrupted processing. The editor will not accept new material in proof unless permission from the editorial board has been obtained for the addition of a "note added in proof". Authors are liable for the cost of excessive alterations to galley proof.

### PUBLICATION CHARGES:

There are no page charges for publication and printing charges for b/w figures. However, in view of substantial cost involved in printing of color figures, author will be charged for printing of pages containing color figures @ Rs. 2,500/- per page. The charges may be revised at any time based on cost of printing and production. Author will receive an estimate/ invoice of the color figures reproduction cost along with the galley proof. It is the responsibility of the author to remit the color figures reproduction cost **within one month** of the receipt of the estimate/invoice.

The corresponding author will receive a soft copy (pdf format) of his/her published article. Should the author desire to purchase reprints of his/her publication, he/she must send the duly signed Reprint Order Form (accompanies the galley proof and contains price details) along with the corrected galley proof to the Editor. The reprint charges must be paid **within one month** of sending the Reprint Order Form.

Any payment related to printing of color figures and/or purchase of reprints should be made in the form of a Demand Draft in the name of **Treasurer, Indian Geophysical Union**, payable at **Hyderabad**.

You may download the pdf file here: [Guide for Authors](#)